Summer 2016

Seismic anisotropy and mantle dynamics beneath the central and western United States

Bin Yang

Department: Geosciences and Geological and Petroleum Engineering

SEISMIC ANISOTROPY AND MANTLE DYNAMICS BENEATH THE CENTRAL AND WESTERN UNITED STATES

by

BIN YANG

A DISSERTATION

Presented to the Faculty of the Graduate School of the

MISSOURI UNIVERSITY OF SCIENCE AND TECHNOLOGY

In Partial Fulfillment of the Requirements for the Degree

DOCTOR OF PHILOSOPHY

In

GEOLOGY AND GEOPHYSICS

2016

Approved by:

Kelly Liu, Advisor

Stephen Gao, Co-Advisor

Ralph E. Flori

J. David Rogers

Leslie S. Gertsch

PUBLICATION DISSERTATION OPTION

This dissertation has been prepared in the style utilized by the Journal of Geophysical Research: Solid Earth and Seismological Research Letters, respectively. Paper I, Pages 3-32 have been published in the Journal of Geophysical Research: Solid Earth; Paper II, pages 33-127 have been published in Seismological Research Letters.

ABSTRACT

Various tectonic features and the recent availability of high-quality broadband seismic data from the USArray and other seismic stations in the central and western United States (CWUS) provide a distinct opportunity to test different anisotropy-forming mechanisms. For the first part of the study, a total of 4138 pairs of well-defined shear wave splitting (SWS) parameters observed at 445 stations on the northern Great Plains show systematic spatial variations of anisotropic characteristics. Azimuthally invariant fast orientations subparallel to the absolute plate motion (APM) direction are observed at most of the stations on the Superior Craton and the southern Yavapai province, indicating that a single layer of anisotropy with a horizontal axis of symmetry is sufficient to explain the anisotropic structure. Based on the splitting measurements and previous results from seismic tomography and geodynamic modeling, we propose a model involving deflecting of asthenosphere flow by the bottom of the lithosphere and channeling flow by a zone of thinned lithosphere approximately along the northern boundary of the Yavapai province.

The second part of the study created an up-to-date SWS database for CWUS in the area of 125^{o} W to 90^{o} W, 26^{o} N to 52^{o} N to upgrade a previous database [Liu et al., 2014]. A total of 7452 pairs of high-quality measurements recorded by 1202 digital broadband seismic stations (both permanent and portable seismic networks) over the period of 1989-2014 is obtained. The current version includes 23448 pairs of well-defined splitting parameters in three phases, i.e. PKS, SKKS and SKS.

The dissertation is a combination of two journal papers published in 2014 and 2016, respectively.

ACKNOWLEDGMENTS

I would like to express my deep appreciation and gratitude to my advisor, Dr Kelly Liu, and co-advisor, Dr. Stephen Gao for the patient guidance and mentorship they provided to me. Dr. Liu and Dr. Gao show me how to be an outstanding research scientist in terms of skills on critical thinking, writing, speaking, and teaching. Moreover, I also learnt what a perfect work should be and the spirit of working hard and carefully, which will benefit my future career.

I would like to thank my committee members, Dr. Ralph Flori, Dr. David Rogers, and Dr. Lesile Gertsch for being my PhD committee members and their constructive suggestions. I also appreciate the help of Dr. Allen Chapman. I want to express my thanks to all my friends and colleagues of the geophysics group.

Special thanks to my family for their unwavering support and unceasing encouragement. I would also to express my deep love to family and my girlfriend, thanks so much for their great support. I love you all.

TABLE OF CONTENTS

LIST OF ILLUSTRATIONS

Figure Page

PAPER I

LIST OF TABLES

NOMENCLATURE

Symbol	Description
PAPER I	
A_0	Amplitude
α	Decay factor
δt	Splitting time
f	Frequency
ϕ	Fast polarization orientation
F_v	Spatial variation factor
PAPER II	
ϕ	Fast polarization orientation
δt	Splitting time

SECTION

1. INTRODUCTION

Intensive geological and geophysical research over the past several decades has demonstrated that mechanical anisotropy is a ubiquitous property of the Earth's crust and upper mantle [Silver, 1996; Savage, 1999]. Measurements of the strength and direction of seismic anisotropy from splitting of teleseismic P-to-S converted phases at the core-mantle boundary on the receiver side, such as SKS, SKKS, and PKS (hereinafter are collectively called XKS) have provided the geoscientific community with important information on the structure and deformation of the Earth's deep interior [Silver, 1996; Savage, 1999; Fouch and Rondenay, 2006; Long and Silver, 2009].

The dissertation is mainly composed of two parts. The first part demonstrates the studies of seismic anisotropy and mantle flow beneath the Northern Great Plains of North America. We propose a model involving deflecting of asthenosphere flow by the bottom of the lithosphere and channeling of flow by a zone of thinned lithosphere approximately along the northern boundary of the Yavapai province by analyzing the results from shear wave splitting.

The second part presents a new version of a shear wave splitting database for the western and central United States (WCUS) using broadband seismic data recorded up to the end of 2014 to update a previous version that used data recorded prior to the end of 2012. A total of 7452 pairs of additional measurements recorded by 1202 digital broadband seismic stations are obtained, and all the measurements in the previous database are re-checked. The resulting uniform SWS database contains a total of 23448 pairs of well-defined SKS, SKKS, and PKS splitting parameters. Relative to the previous version of the

database, the additional measurements notably improved the spatial and azimuthal coverages of the measurements, providing an improved dataset for constraining geodynamic models related to lithospheric deformation and asthenospheric flow, as well as for complex anisotropy recognition and characterization.

PAPER

I. SEISMIC ANISOTROPY AND MANTLE FLOW BENEATH THE NORTHERN GREAT PLAINS OF NORTH AMERICA

ABSTRACT

A diverse set of tectonic features and the recent availability of high-quality broadband seismic data from the USArray and other stations on the northern Great Plains of North America provide a distinct opportunity to test different anisotropy-forming mechanisms. A total of 4138 pairs of well-defined splitting parameters observed at 445 stations show systematic spatial variations of anisotropic characteristics. Azimuthally invariant fast orientations subparallel to the absolute plate motion (APM) direction are observed at most of the stations on the Superior Craton and the southern Yavapai province, indicating that a single layer of anisotropy with a horizontal axis of symmetry is sufficient to explain the anisotropic structure. For areas with simple anisotropy, the application of a procedure for estimating the depth of anisotropy results in a depth of 200–250 km, suggesting that the observed anisotropy mostly resides in the upper asthenosphere. In the vicinity of the northern boundary of the Yavapai province and the Wyoming Craton, the splitting parameters can be adequately explained by a two-horizontal layer model. The lower layer has an APM-parallel fast orientation, and the upper layer has a fast orientation that is mostly consistent with the regional strike of the boundary. We propose a model involving deflecting of asthenosphere flow by the bottom of the lithosphere and channeling of flow by a zone of thinned lithosphere approximately along the northern boundary of the Yavapai province.

1. INTRODUCTION

Intensive geological and geophysical research over the past several decades has demonstrated that mechanical anisotropy is a pervasive characteristic of the Earth's crust and upper mantle. Measurements of the strength and orientation of seismic anisotropy from splitting of teleseismic P-to-S converted phases at the core-mantle boundary on the receiver side, such as SKS, SKKS, and PKS (hereinafter are collectively called XKS) have provided the geoscientific community with important information on the structure and deformation of the Earth's deep interior [Silver, 1996; Savage, 1999; Fouch and Rondenay, 2006; Long and Silver, 2009]. The splitting parameters, the fast orientation (ϕ) and the splitting time between the fast and slow split shear waves (δt), are measurements of the orientation and strength of the anisotropy, respectively, and have been increasingly used by a wide range of geoscientists to understand crustal and mantle structure and dynamics [Silver and Holt, 2002; Maupin et al., 2005; Becker et al., 2006; Fouch and Rondenay, 2006; Marone and Romanowicz, 2007; Kreemer, 2009; Gao et al., 2010; Yuan and Romanowicz, 2010; Conrad and Behn, 2010; Satsukawa et al., 2011; Huang et al., 2011; Li et al., 2011].

In spite of the numerous studies, the origin of the observed seismic anisotropy is still a topic of much debate. While the lattice preferred orientation (LPO) of the crystallographic axis of olivine is believed to be the main cause of anisotropy, whether the LPO mostly takes place in the lithosphere or the asthenosphere is still not certain [Silver, 1996; Frederiksen et al., 2007]. In the lithosphere, most studies proposed that the LPO associated with past tectonic events was responsible for the observed anisotropy with a fast orientation parallel to the strike of the orogenic zones [Silver, 1996; Fouch and Rondenay, 2006], and in the asthenosphere, the LPO could result from simple shear originated from

flow gradient [Vinnik et al., 1992; Bormann et al., 1996; Tommasi et al., 1996]. Another possible mechanism that can form anisotropy in the mantle is preferably oriented magmatic dikes in the lithosphere [Gao et al., 1997, 2010; Kendall et al., 2005].

The northern Great Plains of North America (Figure 1.1) is well sampled by the USArray stations with outstanding data quality and has experienced various of deformational and magmatic events from the Precambrian to the Cenozoic [Karlstrom and Bowring, 1988; Whitmeyer and Karlstrom, 2007]. Major tectonic provinces include the Archean Superior Craton (>2.5 Ga), Penokean orogeny (2.45–1.75 Ga), Trans-Hudson orogeny (THO, 2.0–1.8 Ga), Wyoming Craton (>2.5 Ga), Yavapai province (1.9–1.7 Ga), Proterozoic Midcontinent rift (MCR, >1.1 Ga), and the Cenozoic Rio Grande rift [Whitmeyer and Karlstrom, 2007]. Precambrian accretion of Archean microcontinents formed most of the basement in the area [Hoffman, 1989; Davidson, 1995; Holm, 1999]. The Cenozoic widespread extension created a series of magmatic episodes and formed the Rio Grande rift [Morgan et al., 1986; Coward et al., 1987; Baldridge et al., 1991; Balch et al., 1997; Mosher, 1998; Lawton and McMillan, 1999; McMillan et al., 2000].

Seismic body wave tomographic models suggested a high-velocity feature beneath the western Superior Craton, probably associated with elevated lithospheric anisotropy [Grand and Helmberger, 1984; Frederiksen et al., 2013a, 2013b]. Beneath the Superior Craton, the thickness of the lithosphere varies between 200 and 250 km [Darbyshire et al., 2007; Darbyshire and Lebedev, 2009]. A low-velocity channel-shaped feature was proposed toward the southeast through the southern extreme of the THO and Superior Craton into the Penokean orogeny [Frederiksen et al., 2013a], approximately along the northern edge of the Yavapai province.

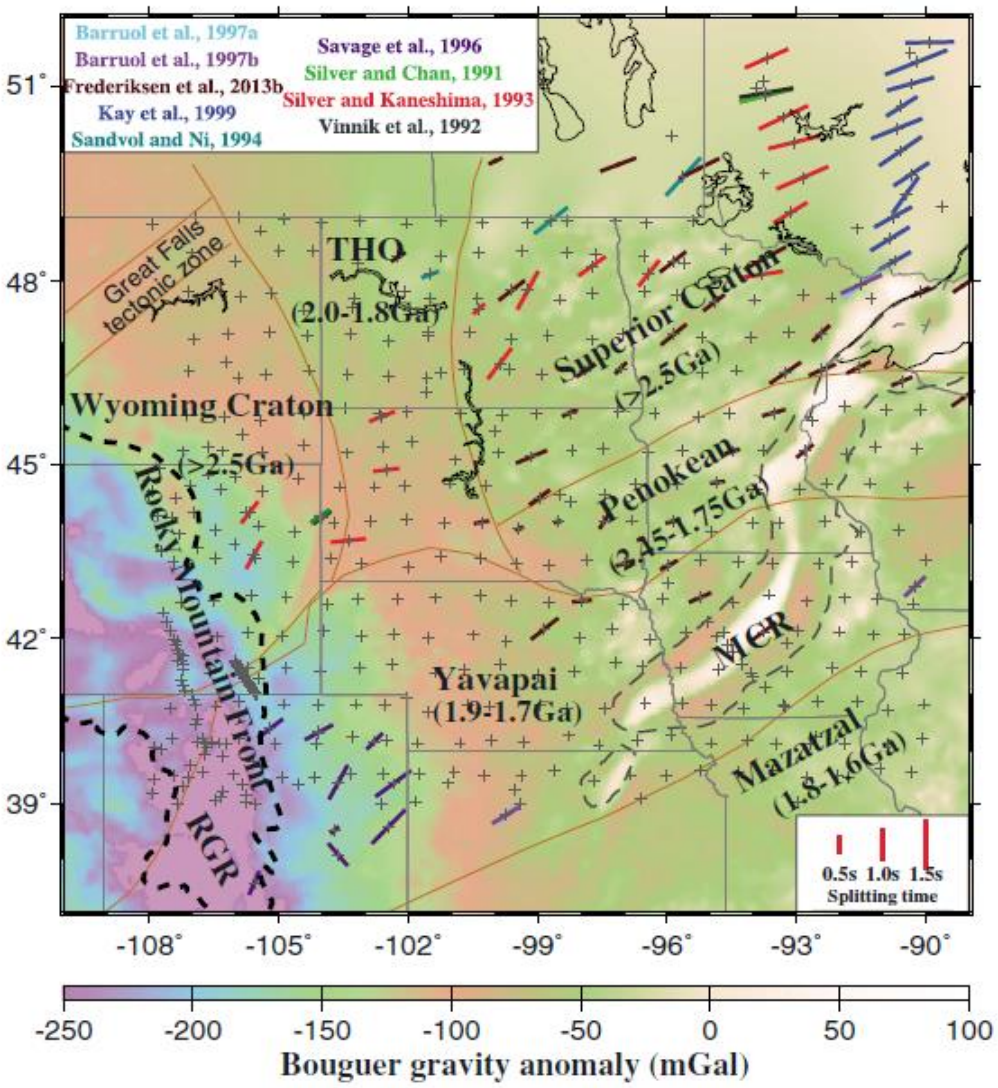

Figure 1.1. Bouguer gravity anomaly map of the study area showing seismic stations used in the study (pluses) and major tectonic provinces. The solid brown lines separate Precambrian basement terranes [Hoffman, 1988; Zhao et al., 2002]. Also shown are previous shear wave splitting measurements in the study area [Silver and Chan, 1991; Vinnik et al., 1992; Silver and Kaneshima, 1993; Sandvol and Ni, 1994; Savage et al., 1996; Barruol et al., 1997a, 1997b; Kay et al., 1999; Frederiksen et al., 2013b]. For a given study, the same color is used for the citation in the legend and the bars in the map. THO: Trans-Hudson orogeny; MCR: Midcontinent rift; RGR: Rio Grande rift.

Three possibilities, including a mantle plume, a failed branch of the MCR, and an older feature from the Superior accretion, were proposed for the origin of the channel [Frederiksen et al., 2013a]. The thickness of the lithosphere beneath the Great Plains is

about 200–250 km and reduces to about 125 km beneath the western U.S. orogenic zone [van der Lee and Frederiksen, 2005; Darbyshire et al., 2007; Bedle and van der Lee, 2009; Darbyshire and Lebedev, 2009; Yuan and Romanowicz, 2010].

The vast majority of the previous shear wave splitting (SWS) investigations in the study area (Figure 1.1) assumed a single layer of anisotropy with a horizontal axis of symmetry. A study conducted by Silver and Chan [1991] involved two stations on the Superior Craton. Large splitting times (>1.7 s) and NE-E fast orientations were observed. A lithospheric deformation model was proposed to explain the obtained splitting parameters. The same stations were used by Vinnik et al. [1992] to suggest that there was a positive correlation between the absolute plate motion (APM) direction and the fast orientation of anisotropy. Silver and Kaneshima [1993] found that the fast orientations displayed good geologic coherence in the western Superior Craton and the THO, and the delay times (0.40–1.75 s) showed systematic variations across the transition zone of the two areas. They concluded that Precambrian fossil fabrics preserved in the subcontinental lithosphere dominated the observed anisotropy. Savage et al. [1996] reported variable splitting parameters and implied a single-layer anisotropy structure across the Rocky Mountain Front. They proposed that the fast orientations were consistent within small geographic regions and that weak anisotropy with a horizontal symmetry axis was present beneath the study area. A model of asthenospheric flow converging on or diverging from the central uplifted region of the Rocky Mountain Front was postulated. Barruol et al. [1997a] suggested the existence of an asthenosphere flow channeled around the North American cratonic root. Frederiksen et al. [2007] proposed a lithospheric anisotropy and reported splitting parameters as ENE-WSW and 1.34 s at stations west of 86◦W and E-W

and 0.67 s on the eastern Superior Craton. SKS splitting measurements at 40 stations in the U.S. and five in Canada on the Superior Craton and surrounding areas were attributed to lithospheric fabrics (Figure 1.1.) [Frederiksen et al., 2013b].

Complex anisotropy was proposed by recent studies for portions of the study area. Yuan and Romanowicz [2010] used a three-layer anisotropy model beneath central North America to interpret the results of surface wave inversion. The top layer resides in the lithosphere and the fast orientation is mostly consistent with the geological trends, indicating ancient orogenic collisional activities. The middle layer, which is also in the lithosphere, has a N-S fast orientation, while the bottom layer, which is in the asthenosphere, is dominated by NE-SW fast orientations which are subparallel to the APM direction of the North American Plate. Beneath the southwestern edge of the North American continent, Refayee et al. [2013] suggested a single layer of anisotropy in the majority of the areas. They proposed that shearing between the partially coupled lithosphere and asthenosphere was the origin of the observed anisotropy, with small contributions from the lithosphere beneath areas with two-layer anisotropy. A model involving deflecting of asthenospheric flow along the western and southern edges of the North American continent was used to interpret the observed edge-parallel fast orientations and large splitting times.

The northern Great Plains is an ideal locale for distinguishing different anisotropy models (lithospheric, asthenospheric, or both) and for investigating the degree of coupling of lithosphere and asthenosphere, for the following reasons: (1) There are several major Precambrian tectonic provinces such as the Superior Craton, THO, Wyoming Craton, and the MCR with spatially varying lithospheric thickness and tectonic trends; (2) There is an

excellent spatial coverage by the USArray stations from which numerous splitting parameters can be obtained; (3) A number of recent seismic tomographic [Yuan and Romanowicz, 2010; Frederiksen et al., 2013a, 2013b] and geodynamic modeling studies [Forte et al., 2007; Conrad and Behn, 2010] in the area provided additional constraints on anisotropy-forming mechanisms.

2. DATA AND METHODS

The broadband seismic data used in the project were recorded by 388 stations of the USArray, 19 permanent and 38 portable stations from 1992 to 2012 within the area of 108◦W–90◦W and 39◦N–51◦N. We requested data from the IRIS (Incorporated Research Institutions for Seismology) DMC (Data Management Center) based on the criteria that the epicentral distance for PKS, SKKS, and SKS is 120◦–180◦, 95◦–180◦, and 84◦–180◦, respectively [Gao and Liu, 2009], and that the minimum magnitude is 5.6 for all the events with the focal depths less than 100 km. For deeper events, the corresponding magnitude is reduced by 0.1 in order to make better use of the sharper waveform.

Based on the method of minimizing energy on the corrected transverse component [Silver and Chan, 1991], Liu [2009] produced a set of robust procedures to obtain reliable SWS parameters. A band-pass filter with corner frequencies of 0.04–0.5 Hz was applied to the seismograms. An automatic data selection procedure was used to reject XKS waveforms with low signal-to-noise ratio on the original radial component [Gao and Liu, 2009; Liu and Gao, 2013]. Visual inspections were made to all the measurements, and manual adjustments were applied when necessary, on the start and end times of the XKS window, on the quality ranking determined automatically, and on the band-pass filtering frequencies [Liu and Gao, 2013]. A total of 445 stations (Figure 1.1.) were found to have at least one quality A or B [Liu et al., 2008] XKS measurement. The number of events used in the study is 492 (Figure 2.1.).

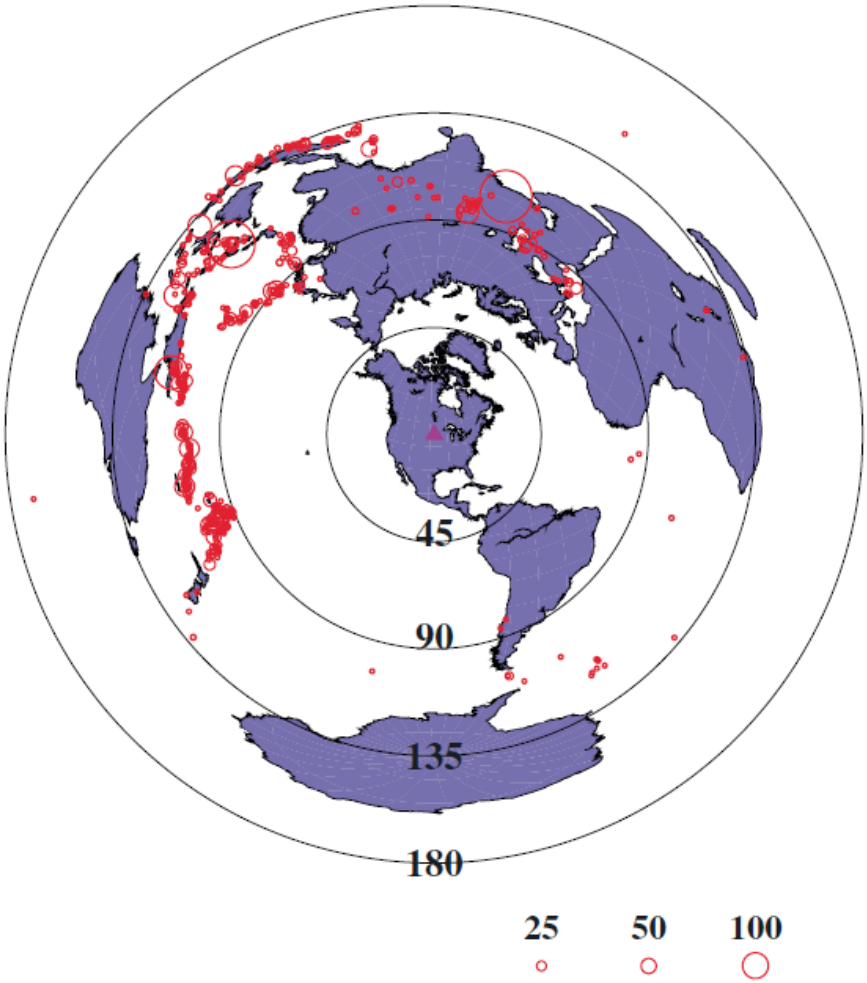

Figure 2.1. Azimuthal equidistant projection map showing earthquakes used in the study (open dots). The radius of the dots is proportional to the number of resulting well-defined splitting measurements from the events.

3. RESULTS

A total of 4138 pairs of well-defined (quality A and B, see Liu et al. [2008] for ranking criteria) splitting parameters are obtained, including 447 for PKS, 749 for SKKS, and 2942 for SKS measurements (Figure 3.1.). The mean value of the splitting times (Figure 3.2.) over all the measurements is 0.98±0.32 s which is almost the same as the global average of 1.0 s for continents [Silver, 1996] and corresponds to a 110±30 km thick layer with a 4% anisotropy [Mainprice et al., 2000].

The Superior Craton contains 1079 pairs of measurements from 63 stations and shows large splitting times (1.12±0.31 s). The mean fast orientation is 47.8±17.5°. Fast orientations in the THO show three general patterns: NE in the north, W-E in the center, and SE in the south. The 414 measurements from 38 stations have a mean fast orientation of 67.8±32.0° and a mean splitting time of 0.93±0.30 s. The Wyoming Craton contains 314 measurements from 38 stations. The fast orientations, which are spatially inconsistent, have a mean of 65.0±41.0°. The mean splitting time for this area is 0.92±0.33 s. The Rio Grande rift contains 394 measurements from 31 stations. The mean splitting parameters are 82.0±26.8° and 0.98±0.32 s. The 1073 measurements from 115 stations in the Yavapai province have a mean fast orientation of 74.7±27.5° and a mean splitting time of 0.89±0.28 s. The mean splitting parameters of the 310 measurements from 26 stations in the MCR are 56.6±21.8° and 0.95±0.27 s, respectively. The 36 stations located in the Penokean province resulted in 312 measurements with mean splitting parameters 59.9±30.8° and 0.90±0.29 s.

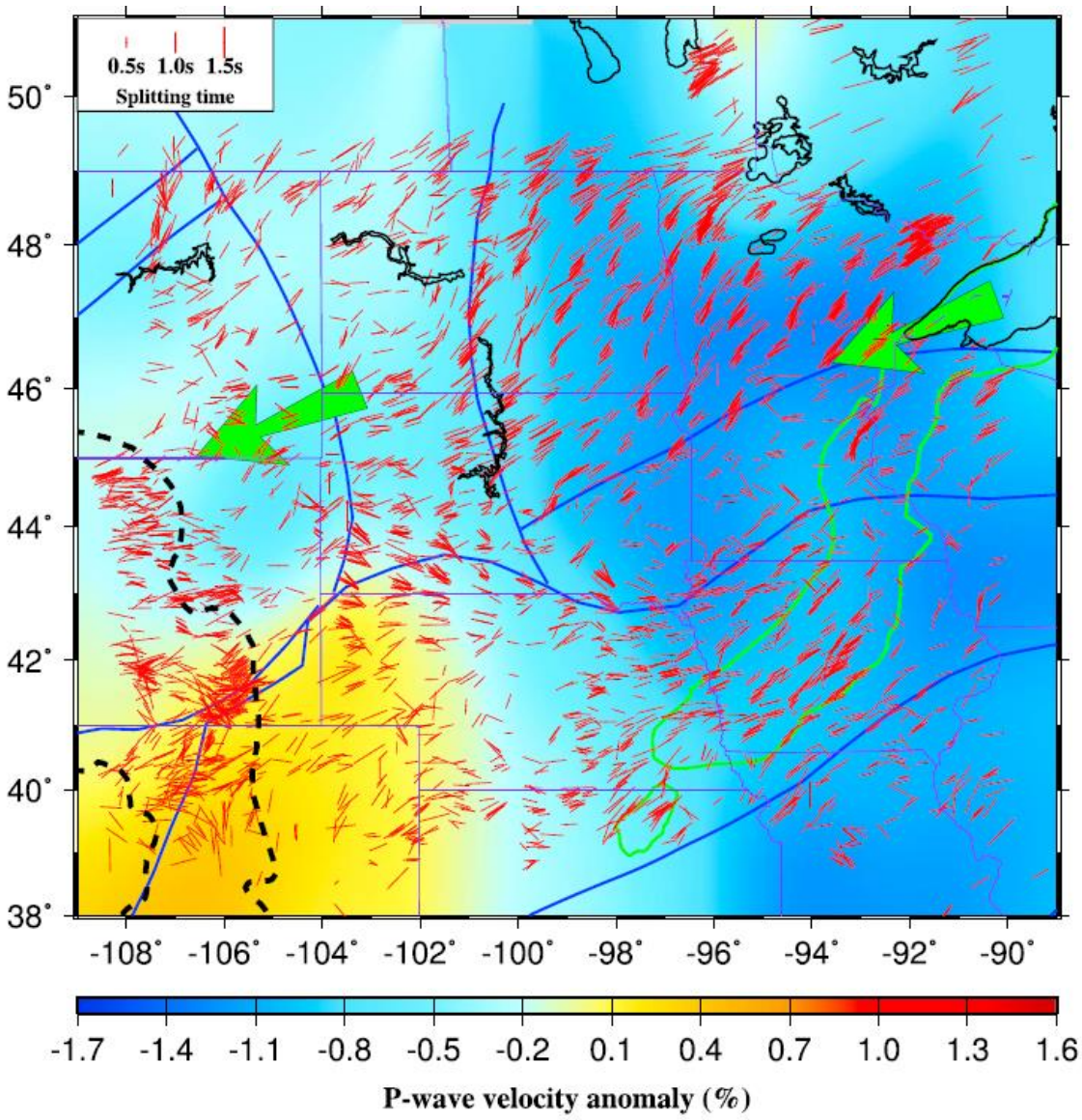

Figure 3.1. Shear wave splitting measurements plotted above 200 km ray-piercing points. The background image shows P wave velocity anomalies at the depth of 200 km [Burdick et al., 2014]. The orientation of the red bars represents the fast orientation, and the length is proportional to the splitting time. The arrows indicate the APM direction.

3.1 RELATIONSHIP BETWEEN THE FAST ORIENTATIONS AND THE APM

We calculate the absolute differences between the APM and the observed fast orientations in the range of 0° to 90° for each of the 4210 ray-piercing points (including results of previous studies from Figure 1.1.) at the depth of 200 km to illustrate the spatial

variation of the fast orientations. The APM direction was determined using the model of Gripp and Gordon [2002] in a fixed hot spot frame. We obtained the absolute difference between the two directions and resampled the results in $1^\circ \times 1^\circ$ overlaying blocks with a moving step of 0.05° (Figure 3.3). The results indicate that the fast orientations are about 30°–50° away from the APM in the THO and the Penokean orogeny and that the fast orientations in the Superior Craton generally correlate well with the APM direction. Fast orientations in the central Yavapai province vary spatially, leading to apparent deviations from the APM. Large deviations are observed in two areas: the Great Falls tectonic zone (centered at 109°W, 49°N) in which the fast orientations are mostly N-S and the Rio Grande rift (centered at 106°W, 38°N) in which the splitting parameters are spatially varying. For most other parts of the study area, the fast orientations and the APM are less than 30° apart (Figure 3.3.).

3.2 SPATIAL DISTRIBUTION OF SPLITTING TIMES

The spatial distribution of splitting times (Figure 3.2.) are investigated using the mean value of individual splitting times in overlapping $0.1^\circ \times 0.1^\circ$ blocks with a moving step of 0.01°. The results (Figure 3.2.) show that the splitting times decrease generally from north to south and the largest ones (>1.5 s) are located on the southwest part of the Superior Craton. Small splitting times ($\leqslant$ 0.8 s) are located along the contact between the Yavapai and the Penokean provinces and in the central Yavapai province (Figure 3.2.).

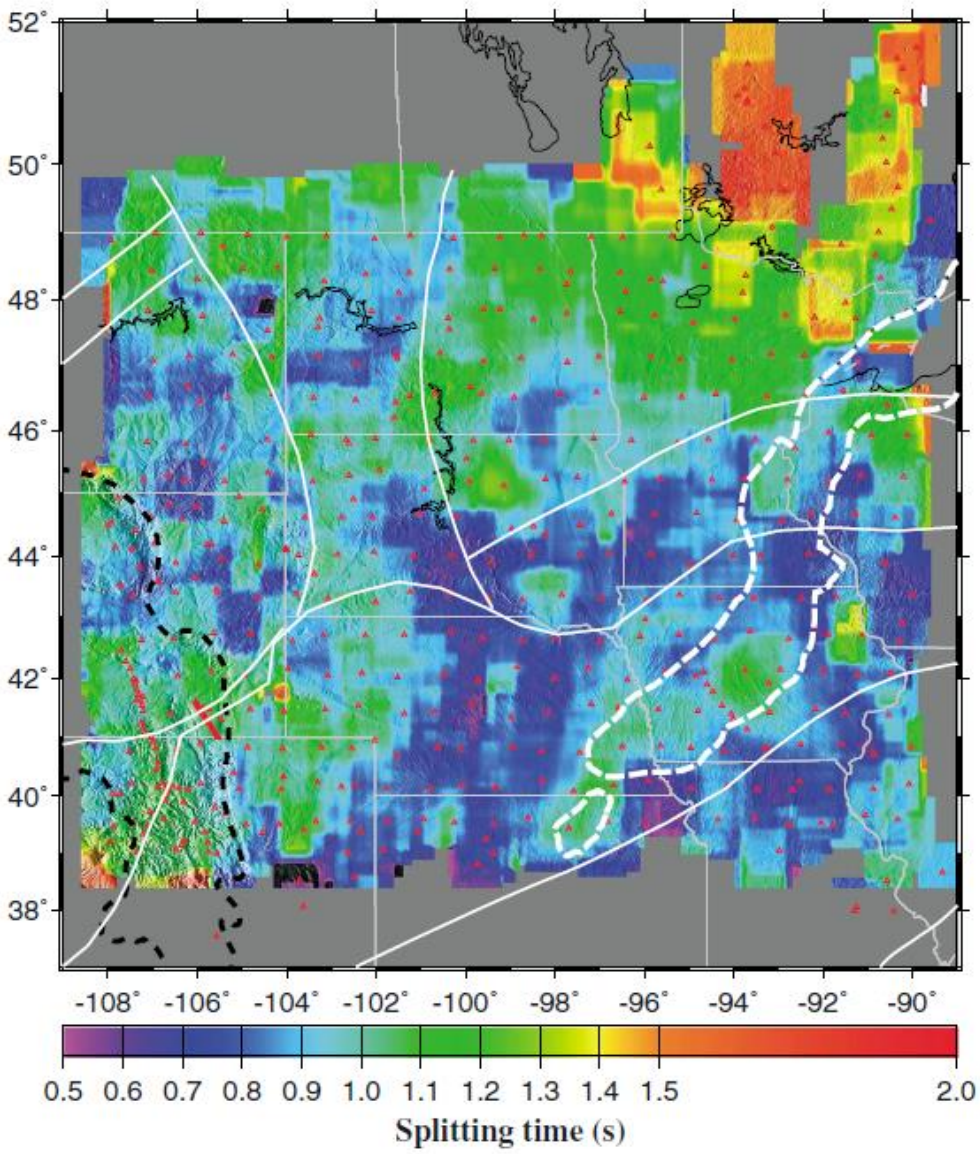

Figure 3.2. Spatial distribution of splitting times. Red triangles represent seismic stations used in the study.

The area covered by the MCR in the Yavapai province has larger splitting times than the surrounding areas. The THO and Wyoming Craton are characterized by splitting times of 0.7–1.0 s. Splitting times in the Rio Grande rift are about 1.0 s; this region generally shows the largest deviations between fast splitting orientations and APM direction.

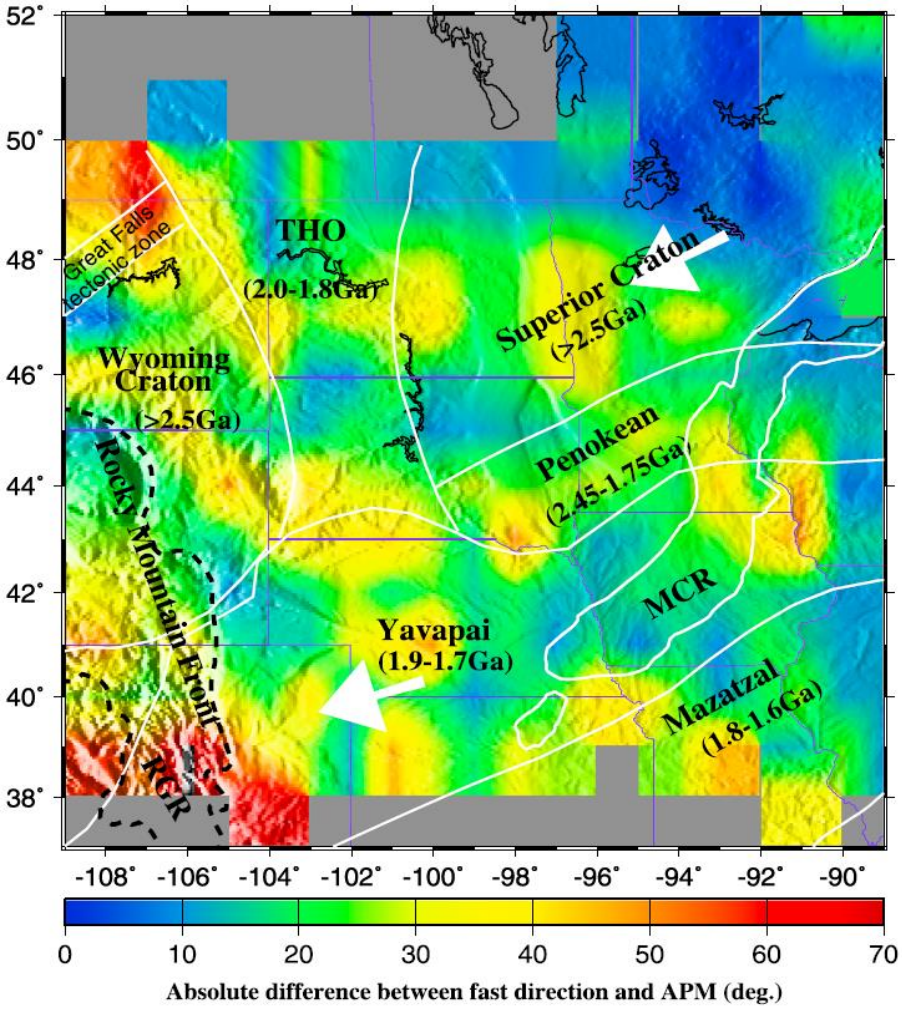

Figure 3.3. Absolute difference between the observed fast orientations and the APM direction (white arrows).

4. DISCUSSION

4.1 SPATIAL DISTRIBUTION OF COMPLEX ANISOTROPY

Identification of complex anisotropy is essential for making reasonable interpretations of the SWS measurements and for understanding the XKS waveforms and the particle motion patterns, because complex anisotropy usually leads to an incomplete removal of XKS energy on the corrected transverse component [Silver and Savage, 1994; Liu and Gao, 2013]. The most common forms of complex anisotropy are characterized by systematic azimuthal variations of the splitting parameters [Silver and Savage, 1994]. On the other hand, for simple anisotropy, the apparent splitting parameters are invariant with the back azimuth.

We visually examine the observed splitting parameters for all of the 445 stations to identify the ones with systematic azimuthal variations. To quantitatively represent the spatial distribution of complex anisotropy, we divide the stations into three types. For stations with no systematically varying splitting parameters, we assign a complex anisotropy index value of 0 to describe one-layer anisotropy (Figure 4.1.a). We give an index value of 2 to stations with systematic azimuthal variations (Figures 4.1.c and 4.1.d), and a value of 1 to stations with poor azimuthal coverage (Figure 4.1.b), at which the existence of complex anisotropy cannot be determined. We spatially average the assigned index values using a cosine arch filter with a radius of 2° and moving step of 0.05°. The results (Figure 4.2.) suggest that one-layer anisotropy is mostly located in the Superior craton (Area A) and the eastern part of the Yavapai province (Area B) in the study area. The area with complex anisotropy is mainly along the Yavapai-Penokean suture zone, on the Wyoming Craton, and along the Rio Grande rift (Figure 4.2., Area C).

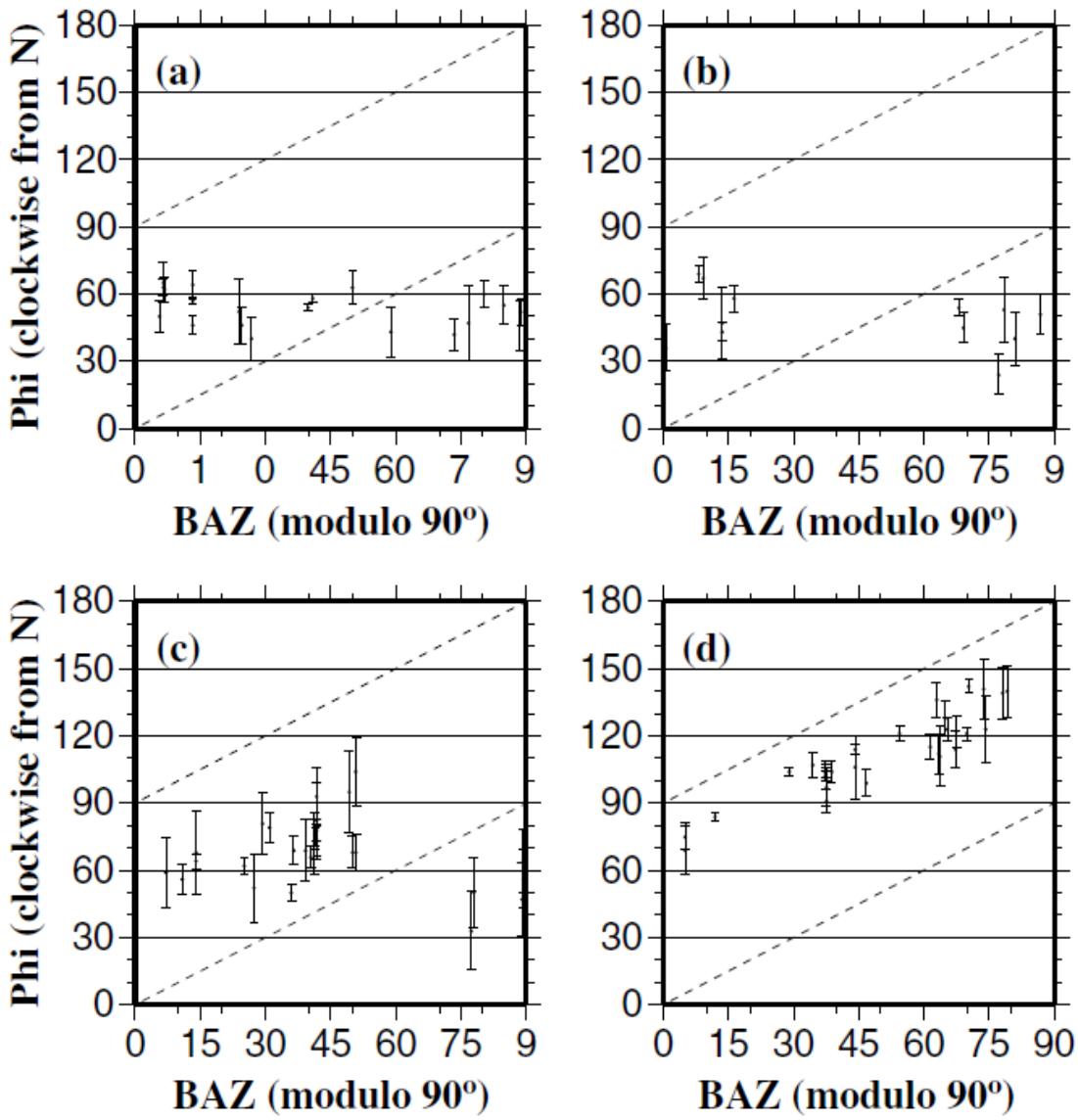

Figure 4.1. Azimuthal variation of observed fast orientations at four stations. (a) A27Axx_TA; (b) E31Axx_TA; (c) B28Axx_TA; and (d) J26Axx_TA.

In order to quantify the complex anisotropy using a two-layer model [Silver and Savage, 1994], we grid search for the two pairs of splitting parameters to fit the observed results in Area C. To obtain stable results, we combine nearby stations with similar patterns of azimuthal variation of the splitting parameters together and divide the area into 11 blocks.

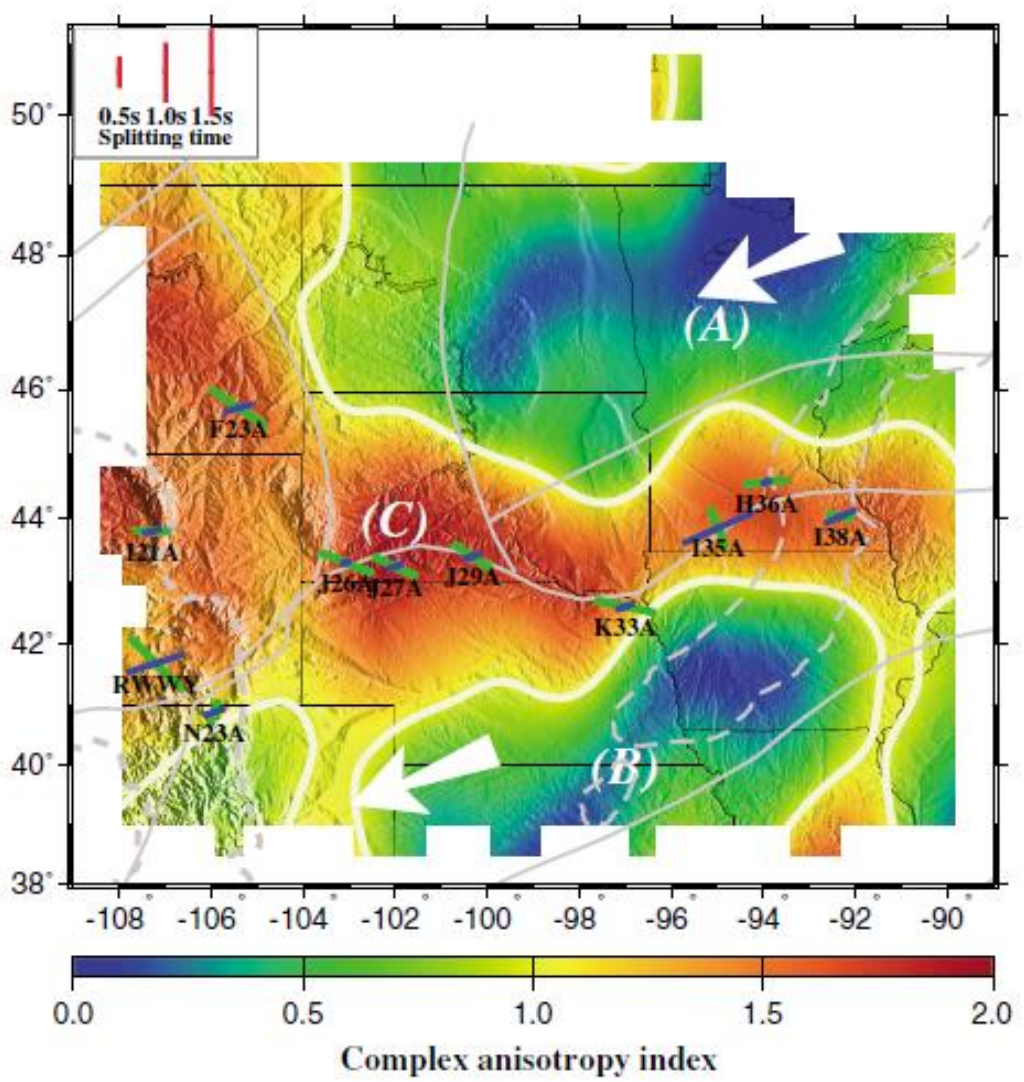

Figure 4.2. Spatial distribution of complex anisotropy index factors and results of grid searching for two-layer anisotropy parameters. The green and blue bars show the splitting parameters of the upper and lower layers, respectively. White arrows show the APM direction, and the white contour lines represent an index value of 1.0.

To reduce well-known ambiguities [Gao and Liu, 2009], we set the ϕ of the lower layer to be parallel to the APM direction and limit the splitting time of the lower layer, $\delta t1$, in the range of 0.2 s to 1.5 s and search for the parameters of the upper layer. We also tested a number of other assumptions (e.g., fixing the ϕ of the upper layer to be parallel to the APM direction) and found that they could not produce a better fit to the observed data than

the above assumption. Figure 4.3. shows the observed splitting parameters and the fitted results for the block in the vicinity of station J27Axx_TA. The resulting optimal splitting parameters for all the 11 blocks are shown in Figure 4.2. The fast orientations of the upper layer are mostly E-W, and for most of the blocks along the northern boundary of the Yavapai province, they are mostly consistent with the strikes of the boundary. The splitting times of the upper layer range from 0.35 s to 1.20 s, corresponding to a thickness of about 40–140 km for a layer with 4% anisotropy. The ϕ of the upper layer observed at the Wyoming Craton and the Rio Grande rift is NW-SE.

4.2 TESTING THE HYPOTHESIS OF THREE-LAYER ANISOTROPY

The three-layer anisotropic structure proposed by Yuan and Romanowicz [2010] from surface-wave inversion in our study area includes two layers in the lithosphere and one layer in the asthenosphere. The fast orientations of the top layer (from the surface to the depth of about 80 km), which has a very weak anisotropy of about 0.6–1.0%, are consistent with the geological trends. The splitting time of this layer can be up to about 0.2 s. The second layer has an approximately N-S fast orientation and a depth range of 80–200 km in the study area. The splitting time from this layer is about 0.6 s with a 2.0% anisotropy. The bottom layer, which resides in the asthenosphere, has an APM-parallel fast orientation and a strong anisotropy of 2.5%. A 1.0 s splitting time would be caused by this layer with a 200 km thickness.

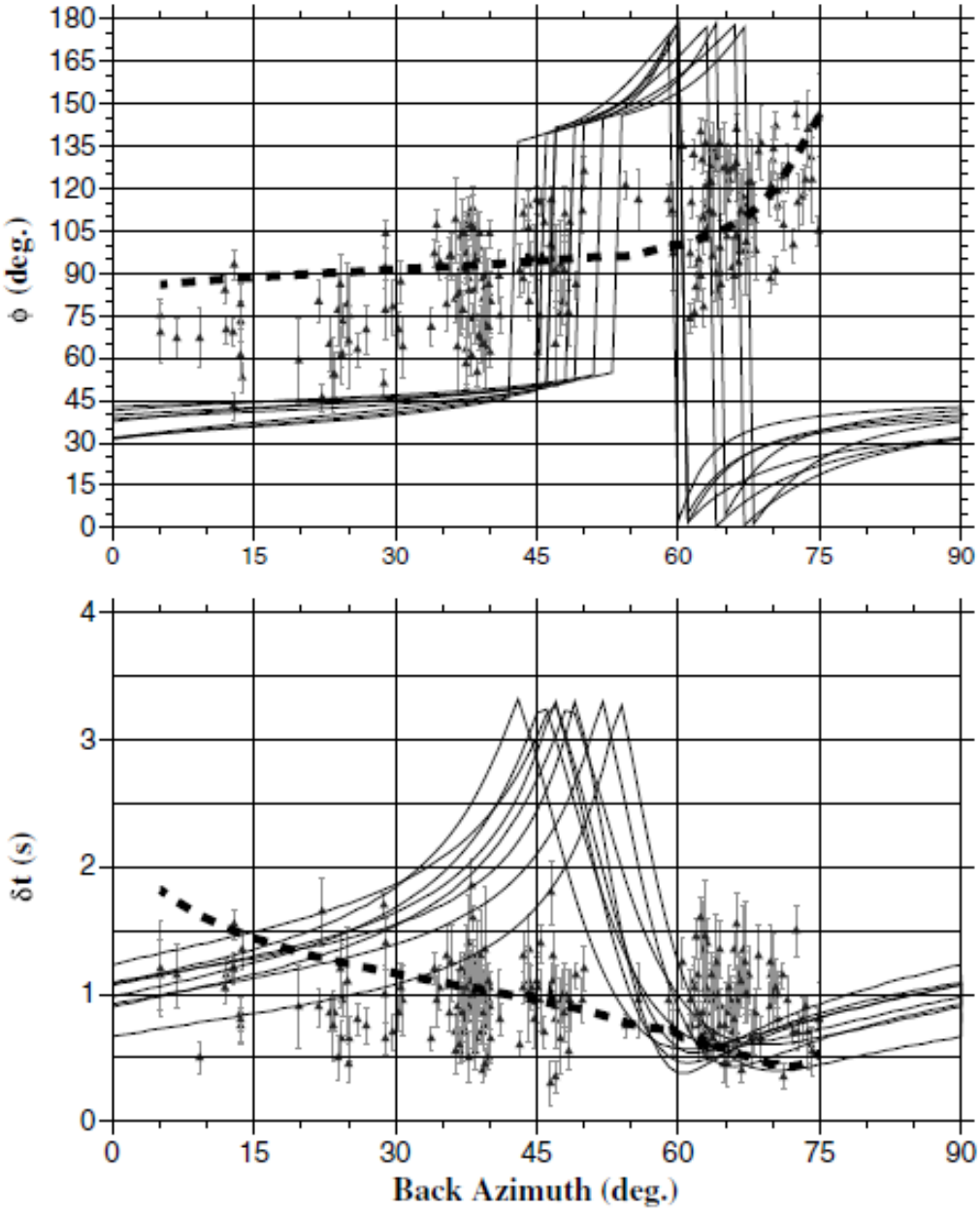

Figure 4.3. Azimuthal variations of observed splitting parameters at stations in the vicinity of J27Axx_TA. Data shown by the thick dashed lines were calculated using optimal parameters grid searched using a two-layer model, in which ϕ1=70.0◦, δt1=0.95 s for the lower layer, and ϕ2=-61.0◦, δt2=0.45 s for the upper layer. The thin solid lines show results calculated based on the three-layer model of Yuan and Romanowicz [2010] described in the text.

To test the three-layer anisotropy model proposed by Yuan and Romanowicz [2010], we calculate theoretical splitting parameters based on the multiple-layer formula

in Silver and Savage [1994]. The model has a lower layer with $\phi 1 = 70^\circ$ and $\delta t1 = 1.0$ s, a middle layer with $\phi 2 = 0^\circ$ and $\delta t2 = 0.7$ s, and an upper layer with $\phi 3 = 60^\circ$ and $\delta t3 = 0.3$ s. The results are plotted in Figures 4.4.d and 4.4.e. A clear pattern of $\pi / 2$ periodicity is observed.

We verify the reliability of the three-layer curves by generating synthetic seismograms from the same three pairs of splitting parameters. The original shear wave before splitting has the form of $R(t) = A0 \sin(2\pi ft)e^{-\alpha t}$ in which the amplitude A0 = 100, frequency f = 0.15 Hz, and the decay factor $\alpha = 0.1$. The original transverse and radial components are calculated from 180 events with back azimuth ranging from 0 to 179° with an interval of 1°. Figure 4.4.a shows the original transverse components. Figures 4.4.d and 4.4.e show the resulting apparent fast orientations and splitting times. The results from the synthetic test match very well with the theoretical curves.

We then compute theoretical apparent splitting parameters for a series of three-layer models with 57.0°–60.0° and 0.2–0.4 s for the top layer, -5.0°–5.0° and 0.6–0.8 s for the middle layer, and 70.0°–75.0° and 0.9–1.1 s for the bottom layer, with an interval of 1° for ϕ and 0.1 s for δt. Figure 4.3. shows some of the representative resulting curves plotted on top of the observed splitting parameters for the block in the vicinity of station J27Axx_TA. A rather poor match is observed, suggesting that the three-layer model suggested by Yuan and Romanowicz [2010] is not consistent with the splitting parameters. The same comparison was made for the rest of the blocks with complex anisotropy, and none of them has a reasonable match between the observed and calculated splitting parameters.

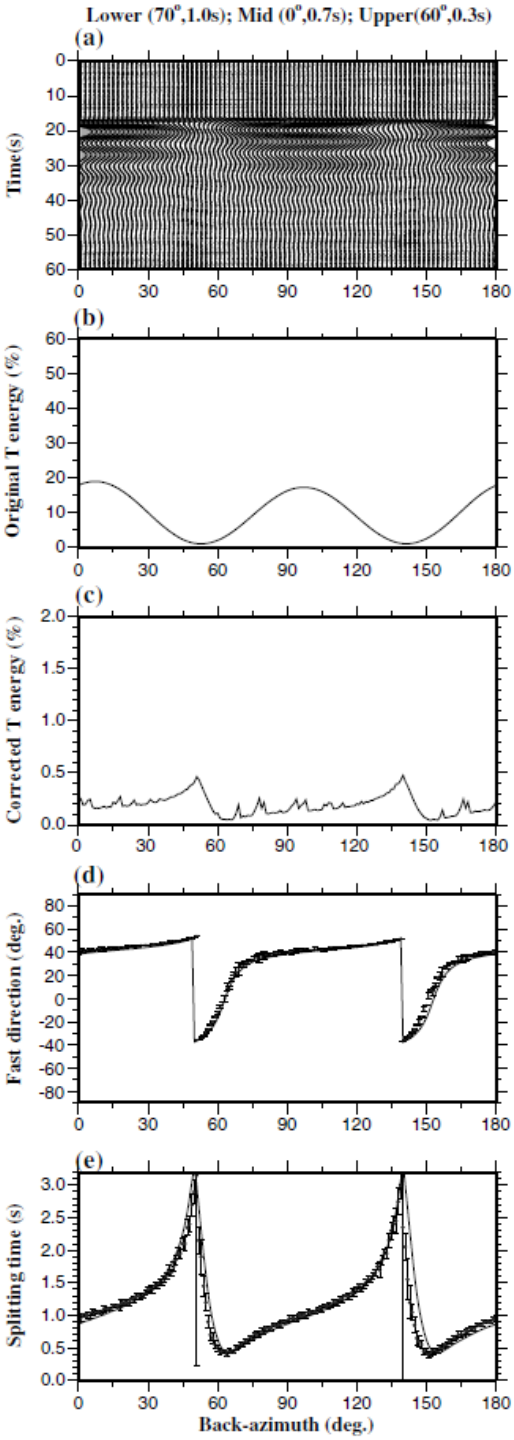

Figure 4.4. Synthetic seismograms and associated splitting parameters of a three-layer model. (a) Original transverse components; (b) energy on the original transverse components displayed as a percentage of that of the presplitting shear wave; (c) same as Figure 4.4.b but for the corrected transverse components; (d) resulting apparent fast orientations; (e) resulting apparent splitting times. The black solid lines in Figures 9d and 9e are theoretical three-layer splitting parameters based on Silver and Savage [1994].

One possible reason for the discrepancy is that our study and the study of Yuan and Romanowicz [2010] used seismic waves in different frequency bands. With much longer period, the surface wave can characterize long-wavelength features, while the heterogeneities (smaller than the wavelength) in the anisotropic materials in the lithosphere cannot be detected. On the other side, XKS waves have shorter wavelengths and are sensitive to small heterogeneities so that the effect of anisotropy observed by XKS waves would be wiped out if the multiple layers and/or dipping axis of symmetry show strong heterogeneities. The above practice indicates that a three-layer model proposed by Yuan and Romanowicz [2010] cannot satisfactorily explain the SWS measurements, and the two-layer model presented in the previous section is adequate to represent the anisotropic structure in areas with complex anisotropy.

4.3 ANISOTROPY DEPTH ANALYSIS

For Areas A and B which have simple anisotropy (Figure 4.2.), we search the optimal depth of the observed anisotropy by computing a spatial variation factor [Gao et al., 2010; Liu and Gao, 2011]. A detailed description of the procedure and an accompanying FORTRAN program can be found in Gao and Liu [2012]. The spatial variation factor, Fv, is computed for each depth from 0 to 400 km with an interval of 5 km [Liu and Gao, 2011]. Figure 4.5. shows the calculated Fv for the Superior Craton (Area A) and the eastern part of the Yavapai province (Area B). Beneath the Superior Craton, the depth estimate shows that the main contribution to the observed anisotropy comes from a depth of about 230–250 km, which is consistent with the depth of the lithosphere suggested by previous seismic tomography studies. van der Lee and Frederiksen [2005] and Bedle and van der Lee [2009] showed that the lithosphere thickness of the Superior Craton was

200–250 km, and Darbyshire et al. [2007] and Darbyshire and Lebedev [2009] inferred from Rayleigh wave phase velocity inversion that in our study area, the Superior province had a lithospheric thickness of approximately 140–200 km. Beneath the eastern Yavapai province, the resulting depth ranges from 200 to 230 km which is also consistent with previous estimates [Yuan and Romanowicz, 2010]. Such agreements suggest that the observed anisotropy mostly originates from the upper asthenosphere, a conclusion that is similar to the southern Great Plains [Refayee et al., 2013].

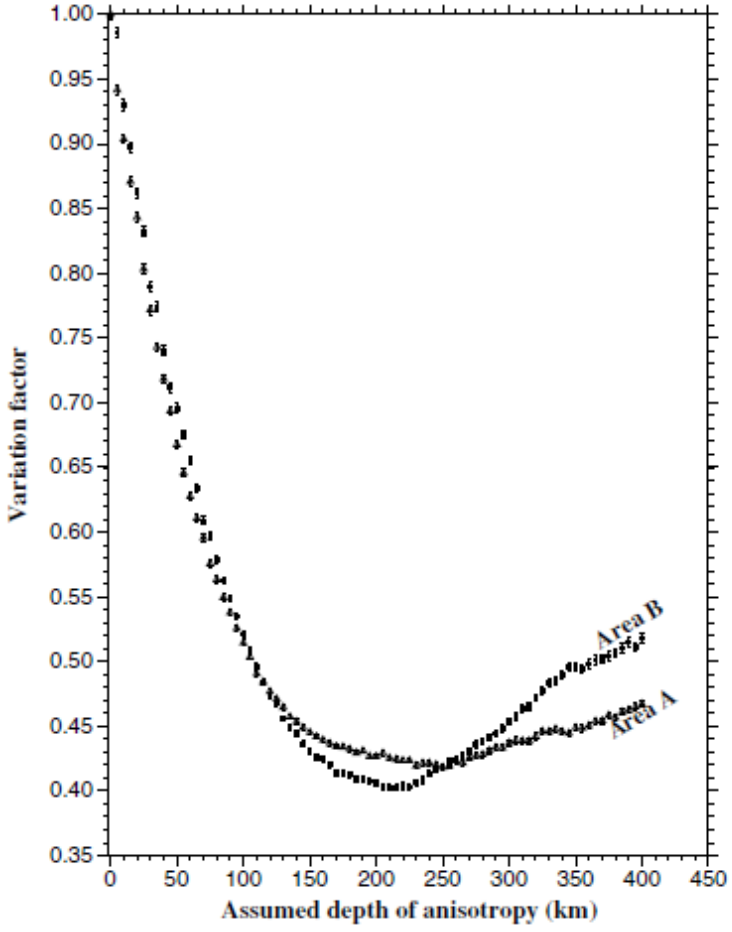

Figure 4.5. Anisotropy depth analysis for Areas A and B (Figure 4.2.), estimated using the approach of Gao and Liu [2012].

4.4 POSSIBLE LITHOSPHERE CONTRIBUTION TO OBSERVED ANISOTROPY

Previous studies argued that much of the detected anisotropy beneath the study area had a lithospheric origin based on a limited number of SWS measurements [e.g., Silver and Kaneshima, 1993; Frederiksen et al., 2013b]. As discussed below, although it is difficult to distinguish the contribution from the lithosphere and asthenosphere in areas where the APM is parallel to the Proterozoic sutures, several pieces of evidence suggest that collisional orogenies associated with the suture zones did not create significant vertically coherent deformation in the lithosphere, perhaps with the exception of the Superior Craton in the study area.

1. Small splitting times are observed along the suture zones. The maximum compressional strain in the study area is expected to be found along the suture zones, and consequently, large splitting times should be observed in the vicinity of the suture zones if the anisotropy is generated by compression. However, such a correlation is not observed at most of the suture zones (Figure 3.2.). On the contrary, small splitting times are observed in the vicinity of the Yavapai-Penokean, the Yavapai-Mazatzal, and the THOPenokean sutures.

2. With the exception of the Superior Craton, large splitting times are not positively correlated with lithospheric thickness revealed by seismic tomography [e.g., Darbyshire et al., 2007; Darbyshire and Lebedev, 2009; Burdick et al., 2014]. The largest splitting times in the study area (up to 1.7 s) are found in the Superior Craton, which has the greatest lithospheric thickness in the study area [van der Lee and Frederiksen, 2005; Bedle and van der Lee, 2009]. The similarity between the direction of the APM and the dominant orientation of lithospheric structures in the Superior Craton makes it impossible to separate

the contributions of fabrics in the lithosphere and the asthenosphere. Thus, the contributions from the lithosphere in this area cannot be quantified using SWS alone. Surface wave anisotropy studies [e.g., Yuan and Romanowicz, 2010] revealed an equivalent splitting time of about 1.0 s in the lithosphere, suggesting significant lithospheric contributions to the observed large splitting times in the Superior Craton.

3. The observed fast orientations are not parallel to some of the terrane boundaries. For instance, the majority of the fast orientations observed in the THO and the MCR are not consistent with their strikes. A pure-shear rifting mechanism, where both sides of the rift are pulled apart evenly [Wilson et al., 2005], would cause a series of parallel fast orientations parallel to the dikes if the anisotropy is lithospheric [Gao et al., 1997; 2010]. This parallelism is not observed.

4. Results of anisotropy depth analysis do not support a lithospheric origin. Results of the depth estimates using spatial coherency of SWS parameters (Figure 4.5.) suggest that the depth of the anisotropy source is in the range of 220–250 km. These values are consistent with the thickness of the lithosphere beneath the area from various seismic tomography studies [van der Lee and Nolet, 1997; Darbyshire and Lebedev, 2009; Bedle and van der Lee, 2009 Yuan and Romanowicz, 2010; Burdick et al., 2012, 2014]. Such agreements suggest that the observed anisotropy mostly originates from the base of the lithosphere and/or the top of the asthenosphere, where the maximum shear strain is expected.

4.5 AN ASTHENOSPHERIC ORIGIN MODEL

For the majority of the study area, the lack of significant lithospheric contribution and the results of depth estimates (Figure 4.5.) discussed above indicate that most of the

observed anisotropy has an asthenospheric origin. A certain degree of coupling caused by the difference in viscosity between the lithosphere and the asthenosphere would generate an APM-parallel anisotropy in the upper asthenosphere [Marone and Romanowicz, 2007; Refayee et al., 2013]. A smaller viscosity difference would lead to a larger degree of coupling [Doglioni et al., 2011], causing a larger splitting time.

Studies on geodynamic modeling and seismic tomography [Becker et al., 2006; Forte et al., 2007] indicated a dominantly northeastward directed asthenospheric flow (relative to the lithosphere) beneath most part of the study area. A mantle flow system proposed by Refayee et al. [2013] provides a viable explanation for the measurements observed on the southwestern edge of the North American continent. Here, we combine our results with those by Refayee et al. [2013] and propose a mantle flow model (Figure 4.6.) that can explain most of our observations.

In the model, the central United States is divided into five zones with different dominant anisotropy-forming mechanisms. This model suggests that partial coupling between the lithosphere and the underlying asthenosphere is responsible for the APM-parallel simple anisotropy observed in Zones I and V (Figure 4.6.). The larger-than-normal splitting times beneath the Superior Craton (Zone II) probably imply a greater degree of coupling between the lithosphere and the asthenosphere, as the result of a reduced viscosity contrast between the thick lithosphere and the asthenosphere. Alternatively, they may reflect significant lithospheric contributions.

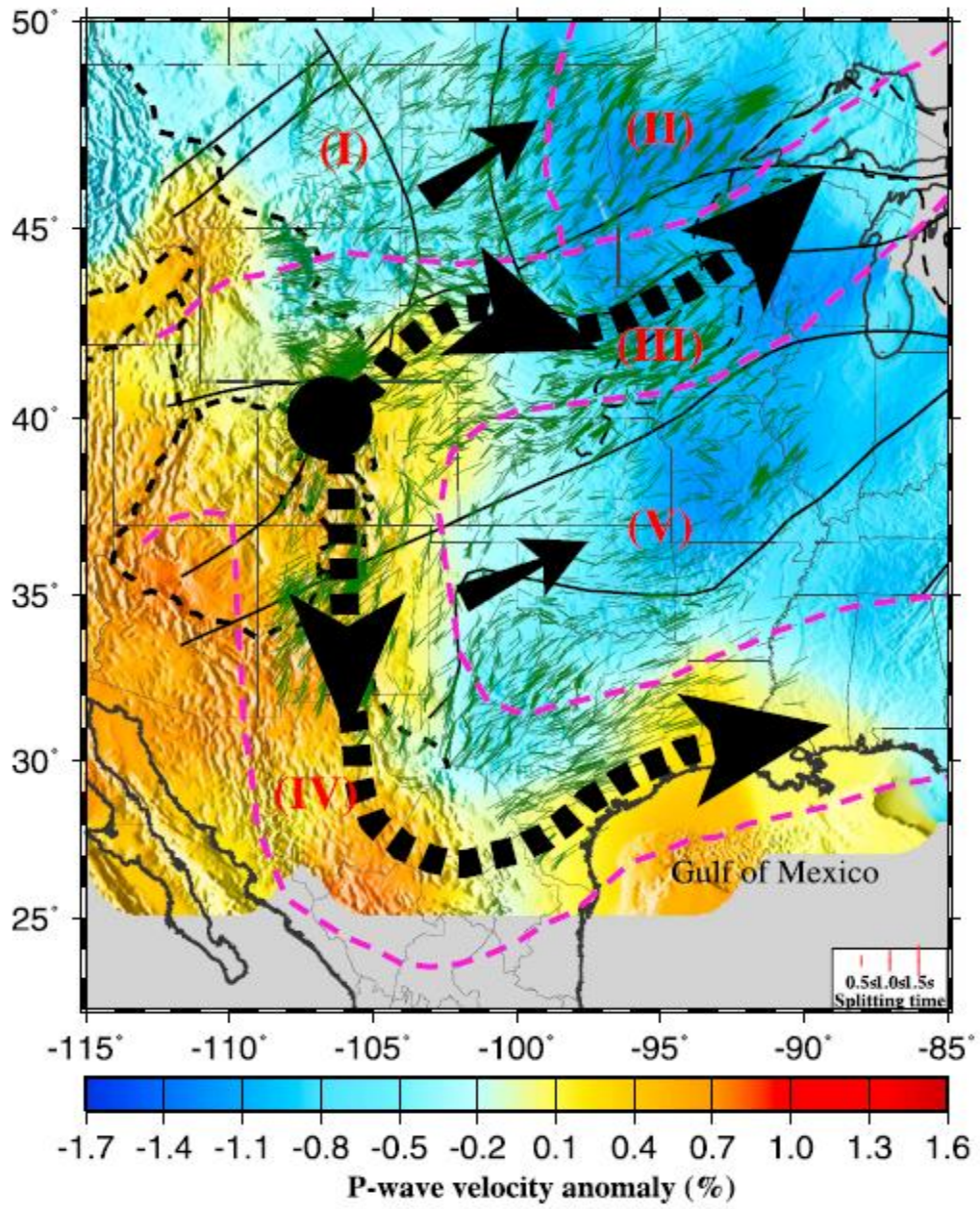

Figure 4.6. Schematic diagram showing direction of flow lines in the asthenosphere relative to the lithosphere with a background of P wave velocity anomalies at the depth of 200 km [Burdick et al., 2012]. The short solid arrows indicate shear strain in the asthenosphere beneath the continent associated with APM, and the thick dashed arrows represent flow deflected by the bottom of the North American lithosphere and flow in the lithospheric channel. The thin bars represent individual shear wave splitting measurements, and the black dot is the joint point of the flow systems. The purple dash lines isolate five zones with different dominant anisotropy-forming mechanisms.

The continental root moving southwestward (relative to the asthenosphere) deflects the asthenospheric flow along its western edge (Figure 4.6., the N-S section of Zone IV), leading to N-S fast orientations. The flow system changes its direction and turns eastward around the southwest corner of the North American continent. The southwestward movement of the North American continent also induces a flow system along a lithospheric channel (Zone III in Figure 4.6.), which is a zone of thinned lithosphere, approximately beneath the northern boundary of the Yavapai province. The existence of the channel is suggested by surface wave tomography using USArray data [Frederiksen et al., 2013a]. We propose that simple shear between the flow system in the channel and the lithosphere is responsible for the anisotropy of the top layer observed in Zone III, and partial coupling between the flow in the channel and the underlying asthenosphere leads to the APM-parallel anisotropy in the bottom layer.

A joint point of the channeled and deflected flow systems may exist beneath the northern Rio Grande rift (Figure 4.6.), approximately at (106.5°W, 40.0°N). The mantle flow separates from this point, with one branch traveling southward and another moving northeastward along the lithospheric channel. The existence of the joint point is supported by the spatially rapid-varying splitting parameters near the proposed location.

5. CONCLUSION

Over 4000 pairs of shear wave splitting parameters with unprecedented spatial resolution are observed on the northern Great Plains of North America. Although lithospheric contributions to the observed anisotropy cannot be completely ruled out especially beneath the Superior province, depth estimates using spatial coherency of the splitting parameters and the dominantly APM-parallel fast orientations imply that coupling between the lithosphere and the asthenosphere is the most likely cause of the observed anisotropy. Along the northern boundary of the Yavapai province, beneath which a zone of thinned lithosphere is revealed by seismic tomography, a double-layer anisotropy model can satisfactorily explain the azimuthal dependence of the splitting parameters. The top layer is most likely associated with simple shear between the base of the lithosphere and mantle flow in the lithospheric channel, and anisotropy in the lower layer could originate from the differential movement between the channel flow and the underlying APM-parallel flow, which is also responsible for the APM-parallel anisotropy observed in areas with simple anisotropy. We propose that the edge-parallel flow system is driven by the southwestward movement of the bottom of the continental lithosphere, which gradually deepens toward the interior of the North American continent, as revealed by seismic tomography studies [van der Lee and Frederiksen, 2005; Darbyshire et al., 2007; Bedle and van der Lee, 2009; Darbyshire and Lebedev, 2009; Burdick et al., 2014]. Such movement deflects mantle flow and leads to N-S and E-W oriented fast orientations observed along the western and southern edges of the North American continent, respectively. Results from this study, when combined with those from previous shear wave splitting and other

geophysical modeling and observational investigations, support the notion that shear strain associated with partial coupling between the lithosphere and the asthenosphere contributes to the bulk of the observed anisotropy on plates with a significant differential movement relative to the underlying asthenosphere.

II. A UNIFORM DATABASE OF TELESEISMIC SHEAR WAVE SPLITTING MEASUREMENTS FOR THE WESTERN AND CENTRAL UNITED STATES: DECEMBER 2014 UPDATE

ABSTRACT

We present a new version of a shear wave splitting database for the western and central United States (WCUS) using broadband seismic data recorded up to the end of 2014 to update a previous version that used data recorded prior to the end of 2012, when the USArray Transportable Array stations were still recording in the east-most region of WCUS. A total of 7452 pairs of additional measurements recorded by 1202 digital broadband seismic stations are obtained, and all the measurements in the previous database are re-checked. The resulting uniform SWS database contains a total of 23448 pairs of well-defined SKS, SKKS, and PKS splitting parameters. Relative to the previous version of the database, the additional measurements notably improved the spatial and azimuthal coverages of the measurements, providing an improved dataset for constraining geodynamic models related to lithospheric deformation and asthenospheric flow, as well as for complex anisotropy recognition and characterization.

1. INTRODUCTION

Shear wave splitting (SWS) parameters, including the polarization orientation of the fast wave and the splitting time between the fast and slow waves traveling in an anisotropic medium, are one of the most fundamental observables in structural seismology (Silver and Chan, 1991). Numerous SWS studies over the past several decades demonstrated that SWS measurements, especially those obtained using the XKS phases which are P-to-S conversions at the core-mantle boundary on the receiver side such as SKS, SKKS, and PKS, can provide important direct information regarding the direction and magnitude of finite strain associated with lithospheric deformation and asthenospheric flow (Silver, 1996). They are also widely used as invaluable constraints for numerical modeling of mantle dynamics (Becker et al., 2006; Bird et al., 2008; Kreemer, 2009), as well as for investigating structure and dynamics in the core-mantle boundary region 21 (Lay et al., 1998).

As recently suggested by Liu and Gao (2013) and others (e.g., Wustefeld et al., 2009), however, significant discrepancies exist in reported splitting parameters obtained at the same stations due to the different measuring techniques and data processing and ranking procedures used by different groups, resulting in compilations of heterogeneous data sets (e.g., http://splitting.gm.univ-montp2.fr/DB/index.html). Additionally, the vast majority of the splitting parameters are reported in the form of station-averaged parameters, which are in principle only valid for areas with simple anisotropy (i.e., a single layer of anisotropy with a horizontal axis of symmetry) and cannot accurately reflect the true anisotropic structure for areas dominated by complex anisotropy. A recent synthetic study (Kong et al., 2015a) suggested that station-averaged splitting times obtained using the multiple-event

stacking procedure (Wolfe and Silver, 1998) are systematically underestimated for areas with complex anisotropy, and that the resulting fast orientation obtained by stacking all the events at a station seating on a two-layer anisotropic structure, which is the most common form of complex anisotropy, is dominated by the fast orientation of the top layer.

Using pre-USArray data and a set of splitting parameter measuring and ranking procedures (Liu and Gao, 2013), Liu (2009) produced the first comprehensive (in the sense that all the available data were used) uniform SWS database of 6224 pairs of individual (rather than station-averaged) splitting parameters for North America. The Western and Central United States (WCUS which herein refers to as the area of the contiguous U.S. west of 90°W) portion of the database was updated later (Liu et al., 2014) in response to the dramatically increased spatial coverage as a result of the deployment of the USArray Transportable Array (TA) stations. The database, which can be found as a Data Product at the Data Management Center (DMC) of the Incorporated Research Institutions for Seismology (IRIS, see http://ds.iris.edu/ds/products/sws-db-mst), includes 16105 pairs of splitting parameters obtained using data recorded prior to the end of 2012 or even earlier, during which some of the USArray TA stations in the eastern portion of the region were still recording.

All the TA stations completed their 2-year recording period and were moved out of the WCUS prior to the end of 2014. Furthermore, outstanding XKS waveforms that were not used by the previous version of the SWS database have been recorded by numerous permanent and non-TA portable broadband stations in the study area over the past several years. To improve both the spatial and azimuthal coverages of the SWS measurements and produce an SWS database utilizing all the TA data in the WCUS, we conducted SWS

analysis using data recorded prior to the end of 2014 that were not used in Liu et al. (2014). We also re-checked all the measurements in the previous version and made necessary modifications to about 0.7% of the 16105 pairs of SWS measurements. The updated database contains a total of 23448 pairs of manually checked splitting parameters and can be found as an electronic supplement.

2. DATA AND METHODS

The broadband seismic data used in the study were obtained from the IRIS DMC (see DATA AND RESOURCES), for the area of 125◦W to 90◦W, and 24◦N to 52◦N which is the same as the study area of the previous version of the database (Liu et al., 2014). The useful epicentral distance range for SKS, PKS and SKKS is 84-180◦, 120-180◦, and 90-180◦, respectively, and the generic cutoff magnitude is 5.6, which is reduced to 5.5 for earthquakes with focal depths greater than 100 km to take advantage of the sharper waveform. The seismic stations belong to one (or more than one for some stations shared by different networks) of the following networks: the U.S. National Seismic Network (network code US), GEOSCOPE (G), USArray Transportable Array (TA), IRIS/USGS Global Seismographic Network (IU), and various campaign-style seismic arrays. Seismograms that were recorded prior to 12/31/2014 and were not included in the previous version of the database were requested from the DMC and processed and manually checked using the same data selection and processing standards and procedure used by Liu et al. (2014) to ensure homogeneity of the resulting database. Similar to the events used for the previous version, the vast majority of the events used to produce the new measurements have a back azimuth in the 90◦ range of 225-315◦ (Figure 2.1.) as the result of the uneven distribution of the world's seismicity at the present time.

A band-pass filter with corner frequencies of 0.04 and 0.5 Hz is applied to the requested traces. The SWS measurements are made using the minimization of transverse energy technique of Silver and Chan (1991), which is considered to be the most reliable technique by some previous studies using synthetic and recorded data (Vecsey et al., 2008;

Kong et al., 2015b). The results are ranked as A(outstanding), B(good), C(poor), and N(null) based on the combination of the S/N ratios on the original and corrected radial and transverse components (Liu et al., 2008), and only Quality A and B measurements are included in the database. Detailed description of the splitting parameter measuring and ranking procedures can be found in Liu and Gao (2013).

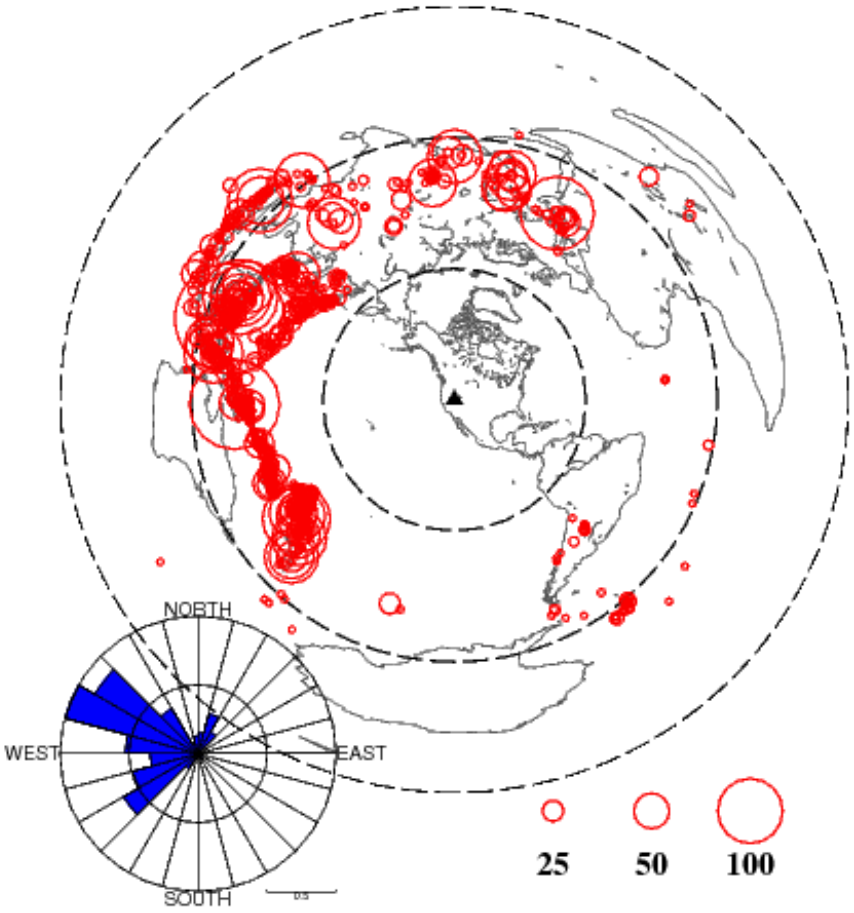

Figure 2.1. Distribution of earthquakes used in the study. The inset rose-diagram shows the distribution of the back azimuth of the events.

3. THE UPDATED RESULTS

A total of 7452 well-defined (Quality A or B) new measurements recorded by 1202 stations have been added to the updated database, including 536 PKS, 1070 SKKS, and 5846 SKS measurements (Figure 3.1.). Most of the new measurements are in southern and northern California due to the numerous permanent stations, the Pacific Northwest due to both permanent and portable stations, southwestern United States and the upper Midwest due to USArray Flexible Array experiments, as well as the eastern margin of WCUS due to new data from the TA stations. We also visually verified all the measurements in the previous version and made adjustments to the 86 measuring parameters (e.g., XKS window selection and ranking) of about 110 (or about 0.7%) of the 16105 measurements. The final product is a uniform database of 23448 pairs of well-defined splitting parameters (Figure 3.2.), among which 11646 (or 49.7%) are from the USArray TA stations. The number of stations with one or more measurements is 2400, including 1144 (or 47.7%) TA stations. The updated database represents a 45.6% increase in the number of measurements over the previous version.

There are 17 columns for the updated database, including the column for station name, phase name (including PKS, SKK for SKKS, and SKS), event name, station latitude, station longitude, fast orientation, standard deviation of fast orientation, splitting time, standard deviation of splitting time, back-azimuth (BAZ), modulo-90 ◦ of the BAZ, epicentral latitude, epicentral longitude, focal depth, rank of the measurements, and latitude and longitude of the ray-piercing points at the depth of 200 km.

The station-averaged measurements are shown in Figure 3.3. and are provided in Table S1 (see SUPPLEMENTARY MATERIALS), in which the columns are station name, station latitude, station longitude, fast orientation and its standard deviation, splitting time and its standard deviation, and the number of observed measurements of each station. In this study the averaged fast orientations are calculated as the circular mean of the individual fast orientations (Mardia and Jupp, 2000), while the averaged splitting times are reported as arithmetic means.

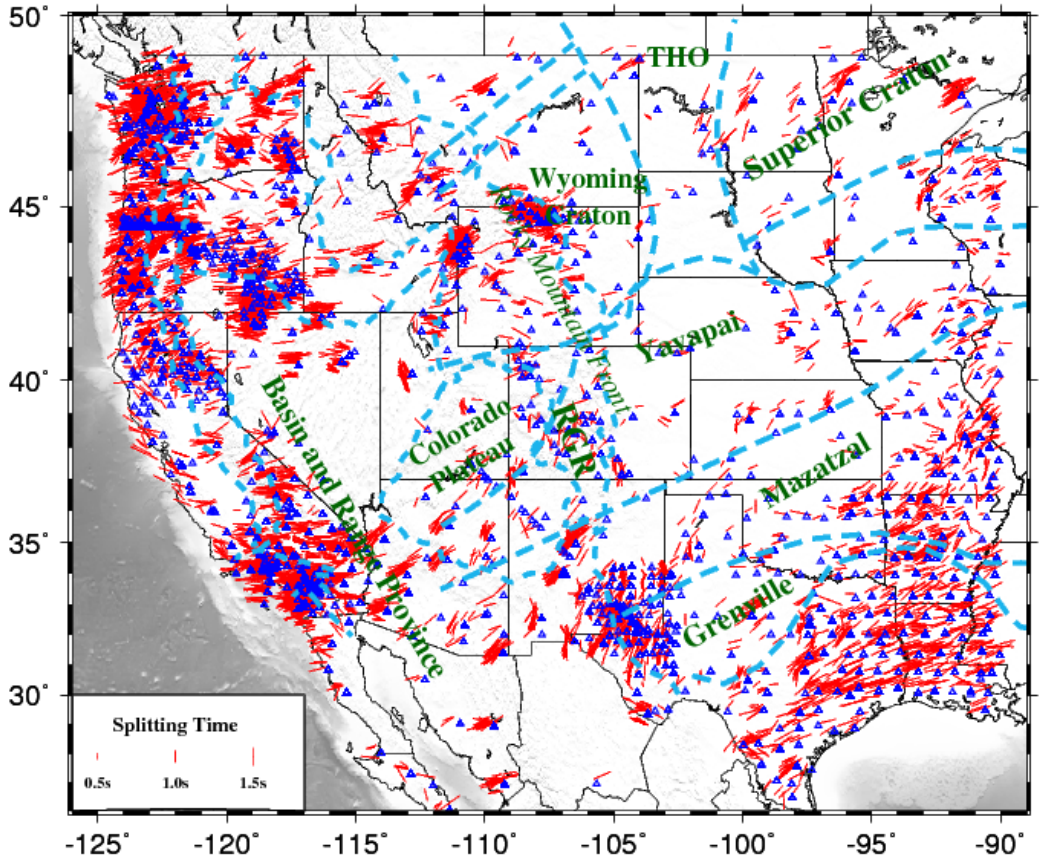

Figure 3.1. New XKS splitting measurements recorded by 1202 stations for western 199 and central United States. The results are plotted above the XKS ray-piercing points at 200 km depth. The orientation of the bars represents the fast orientation and the length is proportional to the splitting time. Major tectonic and basement provinces are marked by the dash lines. Stations are shown as triangles. THO: Trans-Hudson Orogeny; RGR: Rio Grande Rift.

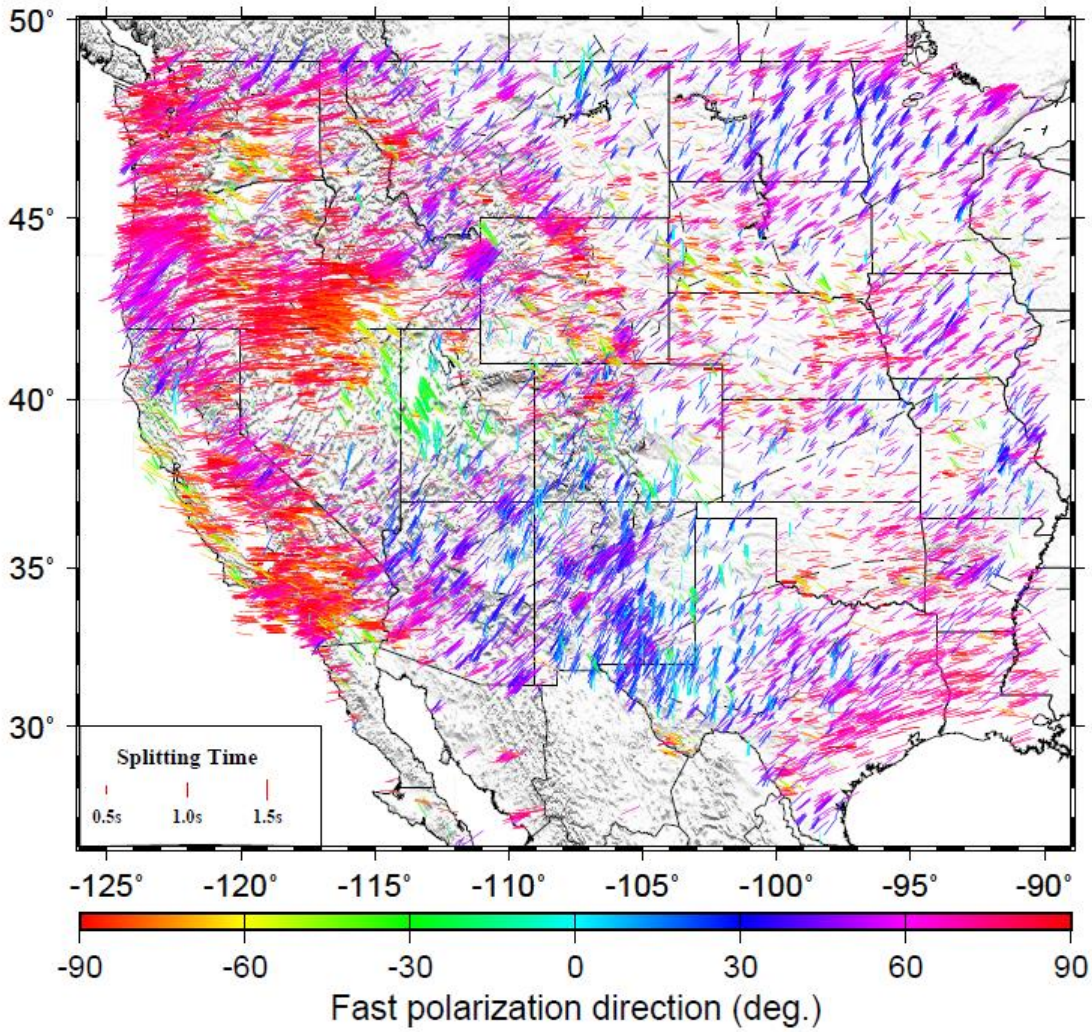

Figure 3.2. Map showing 23448 pairs of XKS shear wave splitting measurements in the database plotted at the surface projection of 200 km ray-piercing points. The colors of the bars represent the fast orientations.

To create an evenly spaced data set of spatially averaged splitting parameters, we first determine the coordinates of the piercing point of the individual measurements at the depth of 200 km, and then compute the averaged splitting parameters in radius=1◦ circles. The distance between the neighboring circles is 1 geographic degree.

Figure 3.4 shows the resulting splitting parameters, which can also be found in Table S2 (see SUPPLEMENTARY MATERIALS). The columns in the table are the latitude and longitude of the center of the circles, fast orientation and its standard deviation,

splitting time and its standard deviation, and the number of individual measurements in the circle.

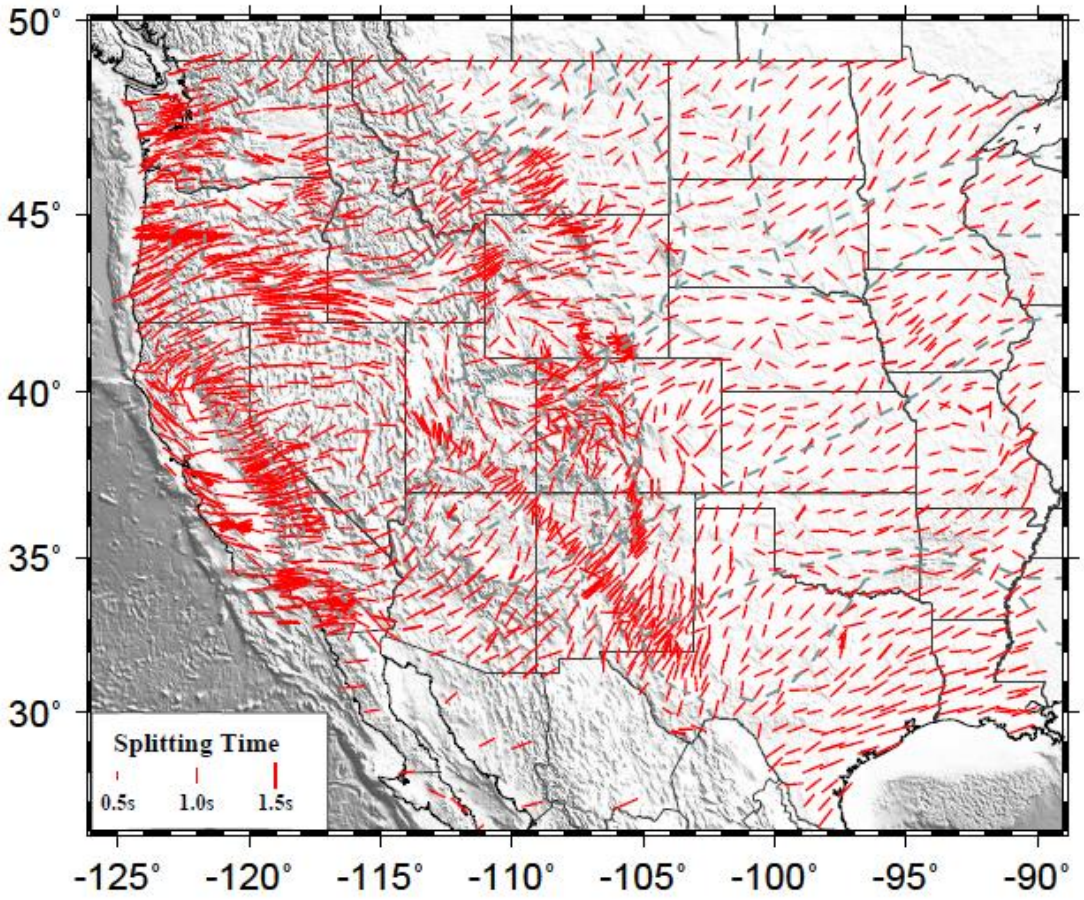

Figure 3.3. Map showing station average of SWS parameters. The results were plotted at the location of each stations.

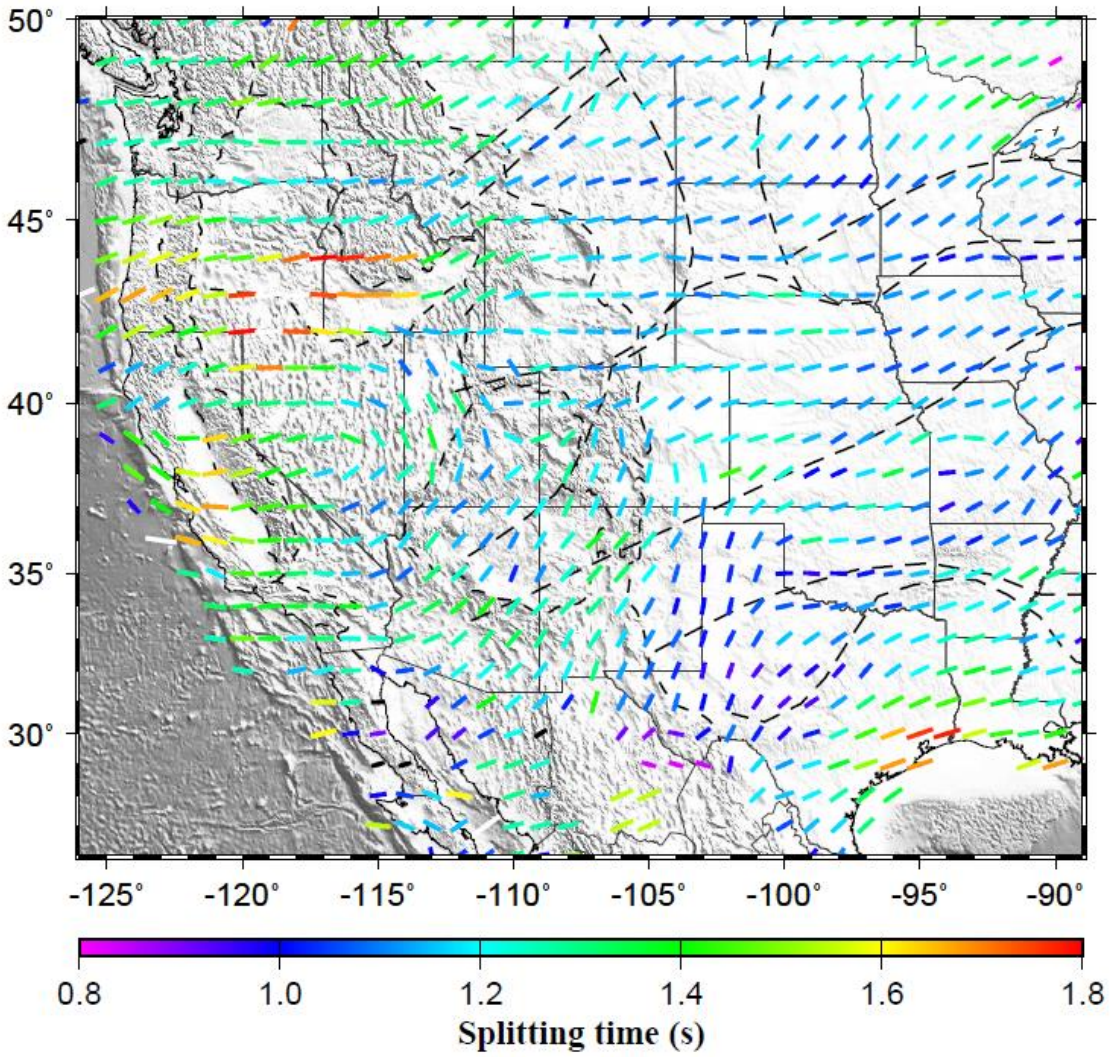

Figure 3.4. Map showing the spatial averaged (in circles with radius of 1 degree) SWS parameters. Splitting time is characterized by the color of the bar.

Figure 3.5. shows averaged splitting parameters in 1 by 1 geographic deg.^{2} blocks with a moving interval of 0.1°. Virtually all of the features summarized in Liu et al. (2014) for the previous version of the database can still be observed. The same is true for the distribution of splitting times in the entire WCUS (Figure 3.6.a), western U.S. (Figure 3.6.b), and central U.S. (Figure 3.6.c). The slight increase (1.02 versus 0.98 s) in the mean splitting time in the central U.S. is mostly caused by the addition of TA stations in the SE

corner of the study area (Figure 3.1.), in which the splitting times are larger than most other areas in the central U.S. (Figure 3.5.b).

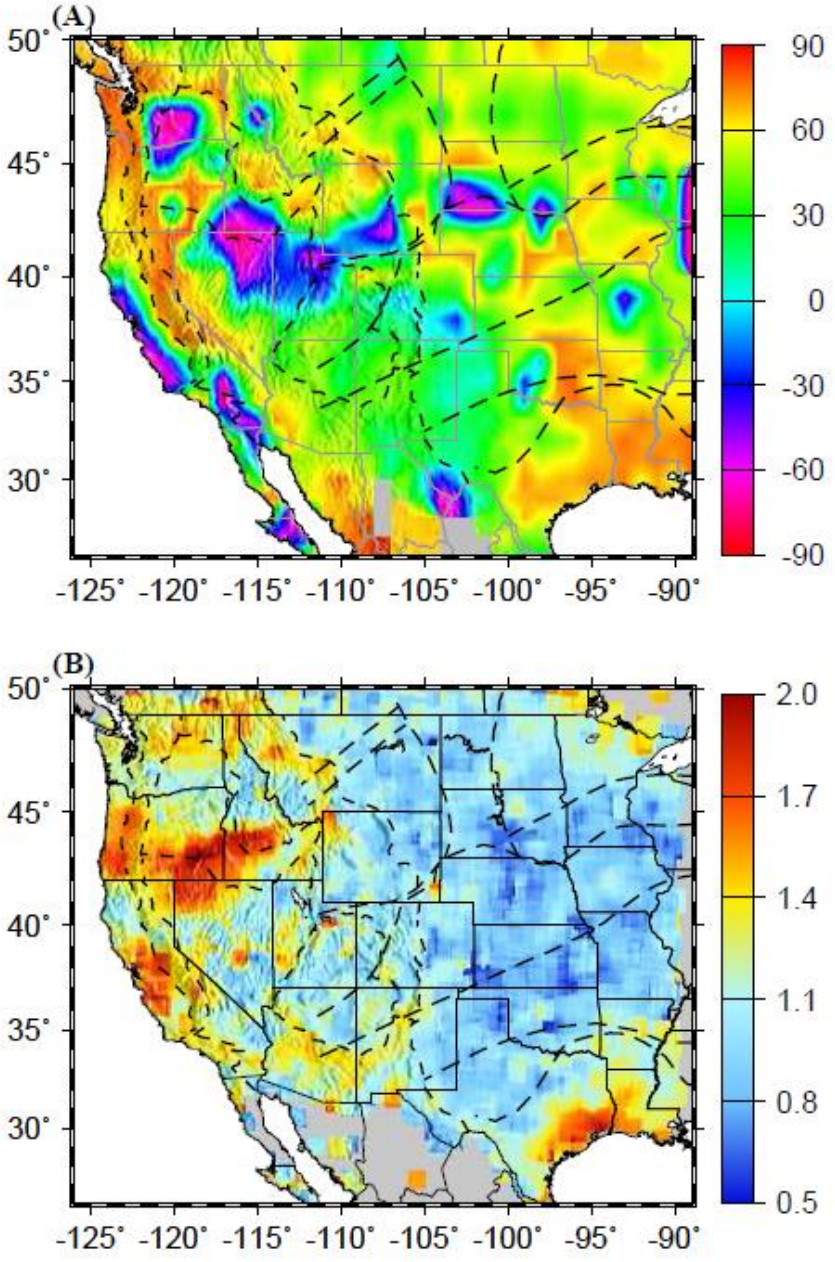

Figure 3.5. Spatially averaged (in overlapping 1 by 1 deg.^{2} blocks with a moving step of 0.1°) for (A) fast orientations and (B) splitting times.

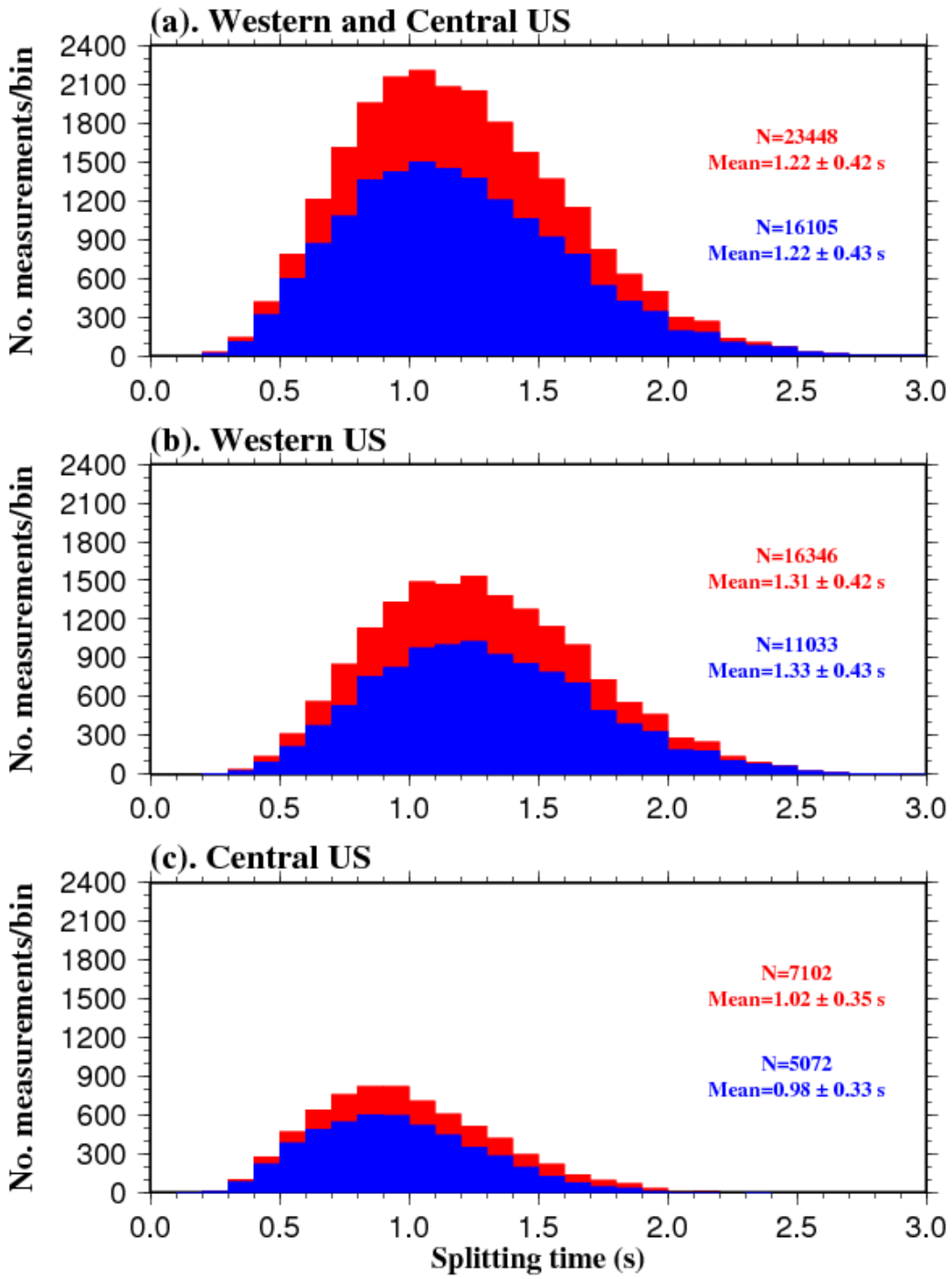

Figure 3.6. Histograms showing the distribution of the XKS splitting times for (A) the entire area, (B) western U.S., and (C) central U.S. for the previous (blue) and updated (red) databases.

In spite of the nearly 50% increase in the number of SWS measurements in the updated database, the two databases are highly similar. To quantify the similarities, we compute the cross-correlation coefficient (XCC) between the spatially averaged splitting parameters in radius=1˚circles produced using the previous and updated (Figure 3.4.) databases. The resulting XCC is 0.954 for the fast orientations, and 0.832 for the splitting times. The high similarity is also demonstrated in the cross-sections of splitting times over longitudinal bands of 1˚ wide across the study area (Figure 3.7).

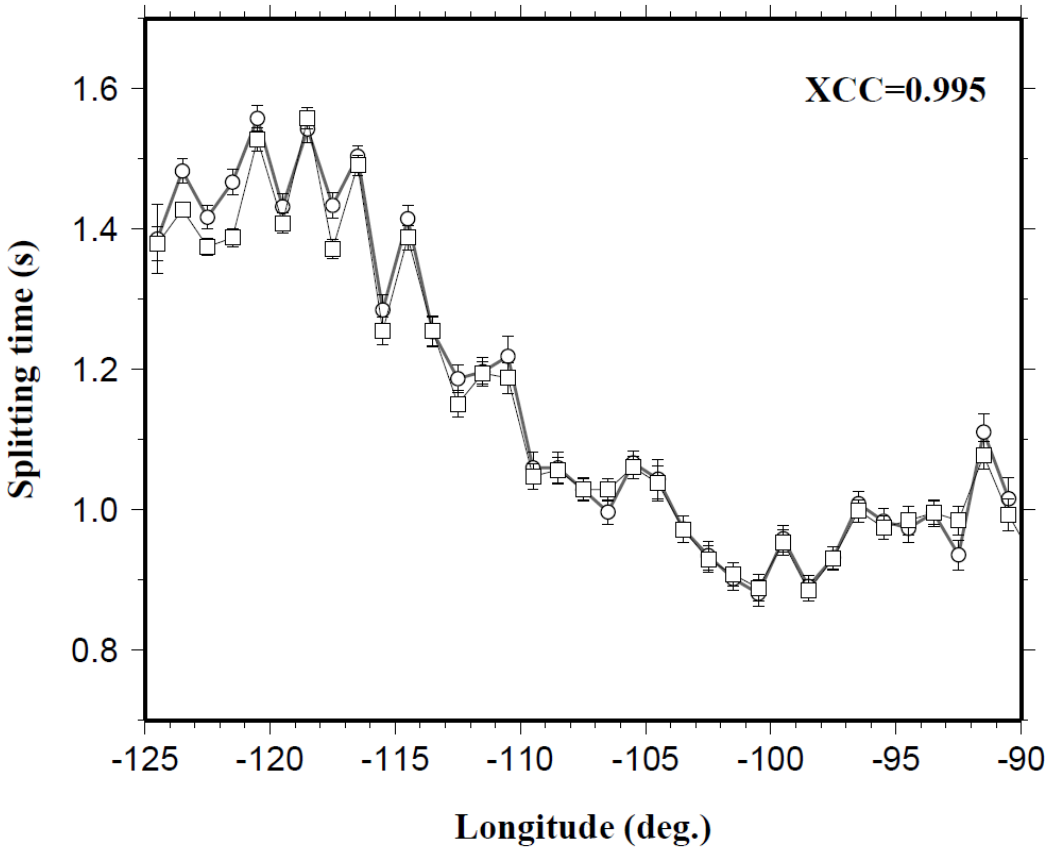

Figure 3.7. Splitting times averaged over longitudinal bands of 1˚ wide. Circles linked by the thick line represent results computed from the previous (Liu et al., 2014) and squares linked by the thin lines are those from the updated databases. The XCC value shows the high similarity between the two curves.

As the result of the increased number of events especially those at the permanent stations, the azimuthal coverage by the events shows a notable increase over the previous version. To specify the increase, we follow the procedure of Liu et al. (2014) to divide the study area into overlapping circles of 0.5° in radius, and compute the number of 30° wide BAZ bins per circle. Relative to the previous version, the number of circles with 6 or more BAZ bands, which can be used for complex anisotropy studies, are more than doubled (Figure 3.8.). Such an increase improves the capability of the database in future research efforts for the recognition and characterization of complex anisotropy (e.g., Liu et al., 2014; Yang et al., 2014), which is identifiable by systematic variations of the splitting parameters with regard to the BAZ of the XKS events.

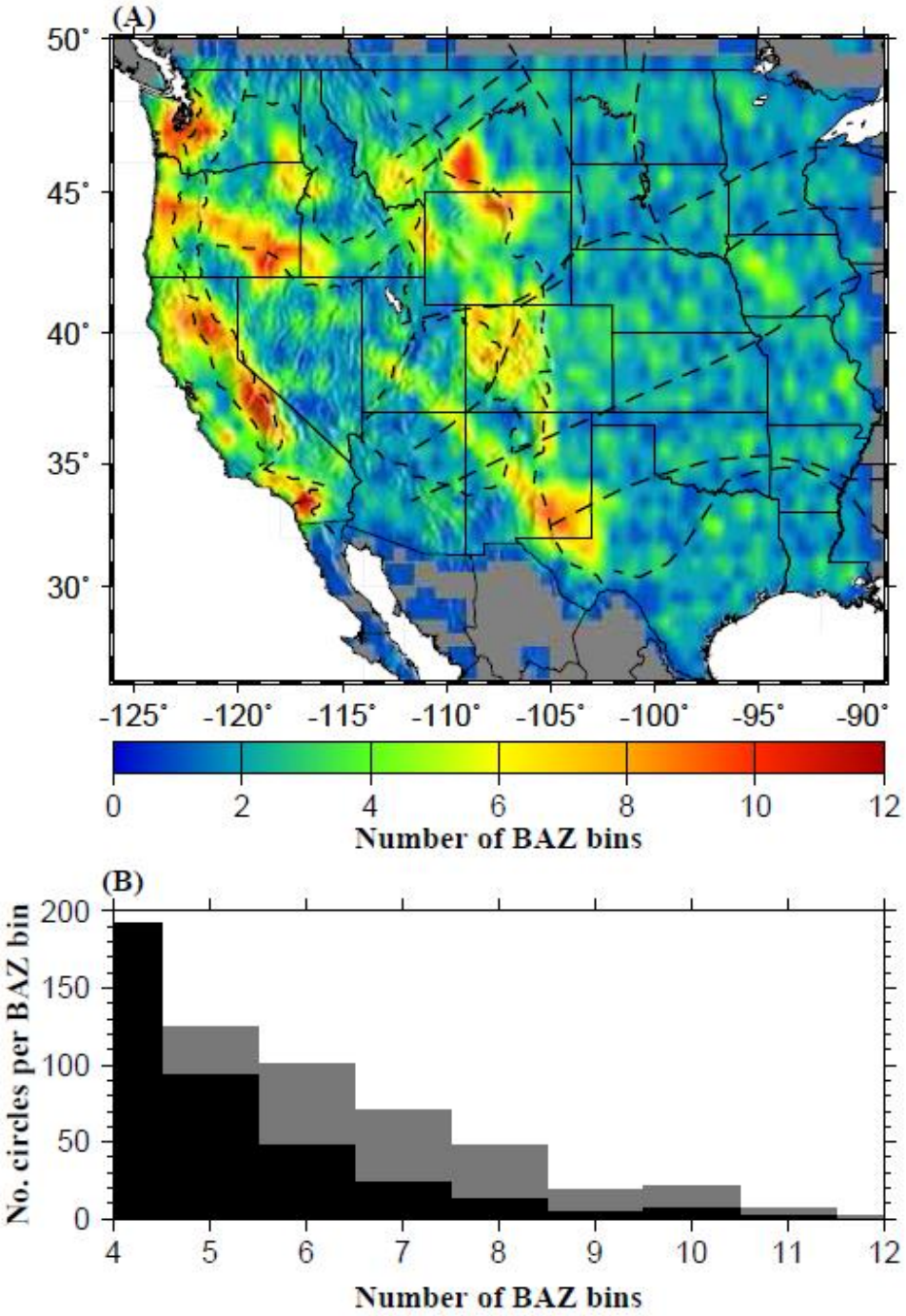

Figure 3.8. Spatial distribution of the number of 30° wide back azimuthal bins using the updated database, and (B) histogram showing the number of radius=1° circles per BAZ bin produced using the previous (black) and updated (gray) databases.

4. CONCLUSION

We have produced a new version of a uniformly created shear wave splitting (SWS) database for the western and central United States using broadband seismic data recorded before the end of 2014, for the purpose of updating a previous version that used data recorded prior to the end of 2012, when the USArray Transportable Array stations were still recording in the east-most region of WCUS. A total of 7452 pairs of new measurements recorded by 1202 digital broadband seismic stations are obtained, and all the measurements in the previous database are re-verified. The resulting uniform SWS database contains a total of 23448 pairs of well-defined and manually-checked XKS splitting parameters. Relative to the previous version of the database, the additional measurements significantly improved the spatial and azimuthal coverages of the measurements, providing an excellent dataset for constraining geodynamic models related to lithospheric deformation and asthenospheric flow, as well as for complex anisotropy recognition and characterization.

5. DATA AND RESOURCES

All the data used in the study are openly accessible from the IRIS DMC (http://ds.iris.edu/ds/nodes/dmc/data/, last accessed March 1, 2015).

6. SUPPLEMENTARY MATERIALS

Table S1. Station-Averaged Splitting Parameters.

St-name	St-lat	St-lon	PHI	PHI-STD	DT	DT-STD	N-meas
002xxx_XN	34.06	-118.58	76	7.5	1.5	0.4	1
005xxx_XN	34.08	-118.6	-14	3	1.2	0.12	1
012xxx_XN	34.14	-118.56	81	4	1.4	0.15	1
028xxx_XN	34.28	-118.54	82	3	1.55	0.13	1
033xxx_XN	34.33	-118.54	-63	9	1.35	0.32	1
034Axx_TA	27.06	-98.68	40.286	11.478	0.914	0.057	7
035Axx_TA	26.94	-98.1	41.58	11.776	1.044	0.106	8
035Zxx_TA	26.46	-98.07	36.781	22.963	1.388	0.118	4
040xxx_XN	34.39	-118.53	-86	3.5	2.4	0.25	1
042xxx_XN	34.41	-118.52	67	7.5	1.85	0.45	1
043xxx_XN	34.42	-118.53	-75	4	1.55	0.2	1
046xxx_XN	34.45	-118.53	78	3	1.25	0.15	1
054xxx_XN	34.52	-118.53	-80	10.5	1	0.25	1
055xxx_XN	34.53	-118.53	-79	8.5	1.1	0.22	1
061xxx_XN	34.58	-118.46	-89	4.5	1.25	0.15	1
065xxx_XN	34.61	-118.43	-70	7	1	0.15	1
066xxx_XN	34.62	-118.44	73	10	1.65	0.33	1
084xxx_XN	34.87	-118.45	-71	14	1	0.3	1
109Cxx_TA	32.89	-117.11	77.563	11.361	1.217	0.045	43
112Axx_TA	32.54	-114.58	-55.584	17.769	1.133	0.254	6
113Axx_AE	32.77	-113.77	78.567	13.892	1.171	0.069	19
113Axx_AR	32.77	-113.77	80.421	12.378	1.146	0.084	14
113Axx_TA	32.77	-113.77	78.516	14.79	1.112	0.055	24
114Axx_TA	32.75	-112.88	64.367	18.403	0.98	0.06	5
115Axx_TA	32.7	-112.23	62.217	12.897	1.064	0.164	7
116Axx_TA	32.56	-111.7	51.346	5.365	1.396	0.091	13
117Axx_TA	32.57	-110.74	42.921	15.324	1.038	0.096	8
118Axx_TA	32.64	-109.97	51.589	9.949	1.33	0.121	5
119Axx_TA	32.77	-109.3	56.502	10.962	1.4	0.12	6
120Axx_TA	32.55	-108.63	46.027	10.472	1.317	0.07	6
121Axx_TA	32.53	-107.79	17.524	11.048	1.113	0.045	68
122Axx_TA	32.7	-107	42.802	17.373	0.95	0.275	3
123Axx_TA	32.63	-106.26	24.958	7.617	1.32	0.118	10
124Axx_TA	32.7	-105.45	24.004	12.435	1.304	0.096	23
125Axx_TA	32.66	-104.66	16.751	15.917	1.004	0.077	23

126Axx_TA	32.65	-104.02	38.5	34.473	1.65	0.35	2
127Axx_TA	32.68	-103.36	-12.443	28.211	0.417	0.017	3
128Axx_TA	32.62	-102.49	1.434	9.813	0.917	0.145	3
129Axx_TA	32.63	-101.87	22.642	18.962	0.637	0.067	8
130Axx_TA	32.6	-100.97	19.232	13.48	0.918	0.089	14
131Axx_TA	32.67	-100.39	14.152	16.401	0.714	0.051	14
133Axx_TA	32.61	-98.92	55.06	8.507	1.077	0.04	26
134Axx_TA	32.57	-98.08	53.468	14.554	0.809	0.06	22
135Axx_TA	32.56	-97.41	37.108	14.213	0.847	0.064	16
136Axx_TA	32.47	-96.53	48.172	27.376	0.571	0.065	7
137Axx_TA	32.6	-95.76	63.328	23.385	1.039	0.135	9
138Axx_TA	32.66	-95.09	67.998	4.617	0.991	0.075	11
139Axx_TA	32.68	-94.39	73.533	12.359	1.188	0.074	13
140Axx_TA	32.64	-93.57	60.281	10.535	1.369	0.139	8
141Axx_TA	32.6	-92.9	62.247	13.579	1.229	0.103	7
142Axx_TA	32.55	-91.95	-82.63	22.917	1.179	0.181	7
143Axx_TA	32.7	-91.4	71.665	13.457	1.046	0.059	12
143Bxx_N4	32.7	-91.4	73.664	15.862	1.075	0.08	6
144Axx_TA	32.63	-90.42	71.019	12.322	1.264	0.092	7
214Axx_TA	31.96	-112.81	72.047	16.235	0.975	0.076	14
216Axx_TA	32	-111.46	47.185	10.157	1.071	0.085	14
217Axx_TA	31.77	-110.82	64.309	7.983	1.194	0.148	8
218Axx_TA	31.97	-110.05	55.837	8.103	1.206	0.131	8
219Axx_TA	32	-109.26	50.098	8.751	1.517	0.125	9
220Axx_TA	31.9	-108.53	71.164	37.722	1.53	0.271	5
221Axx_TA	32.01	-107.78	22.603	10.77	1.117	0.075	9
222Axx_TA	32.1	-107.1	23.929	17.554	1.175	0.088	10
223Axx_TA	32.01	-106.43	20.651	9.285	1.345	0.087	10
224Axx_TA	32.08	-105.52	19.371	14.955	0.91	0.069	10
225Axx_TA	32.11	-104.82	23.617	9.087	0.984	0.036	29
226Axx_TA	32.06	-104.1	18.813	8.419	1.13	0.171	5
226Bxx_TA	32.08	-104.17	13.892	15.853	0.95	0.162	4
227Axx_TA	32.01	-103.29	21.211	5.768	1.025	0.176	4
228Axx_TA	32.12	-102.59	26.934	10.411	0.877	0.059	11
229Axx_TA	31.97	-101.81	12.743	8.429	1.025	0.042	18
230Axx_TA	31.89	-101.11	28.848	10.217	0.985	0.061	23
231Axx_TA	31.94	-100.32	47.546	9.382	0.917	0.135	6
232Axx_TA	31.89	-99.65	52.162	13.09	1.062	0.077	13
233Axx_TA	32.02	-98.9	38.871	12.109	0.8	0.053	19
234Axx_TA	32	-98.14	42.345	19.44	0.764	0.065	18
236Axx_TA	32	-96.53	59.008	14.784	0.767	0.065	9

237Axx_TA	32	-95.81	41.911	11.436	1.296	0.08	14
237Bxx_N4	32	-95.81	37.729	10.362	1.1	0.166	7
238Axx_TA	32	-95.12	46.381	16.029	1.006	0.048	9
239Axx_TA	32.02	-94.47	67.817	13.221	1.38	0.128	10
240Axx_TA	32.04	-93.76	67.191	10.642	1.206	0.056	17
241Axx_TA	32.02	-92.92	85.254	8.407	1.303	0.071	15
242Axx_TA	32.06	-92.15	70.2	1.166	1.22	0.181	5
243Axx_TA	31.88	-91.48	61.502	15.168	1.429	0.218	7
244Axx_TA	32.04	-90.69	73.461	10.657	1.108	0.168	6
318Axx_TA	31.44	-109.99	52.484	4.897	1.533	0.14	6
319Axx_AE	31.38	-109.28	46.281	8.353	1.196	0.058	34
319Axx_AR	31.38	-109.28	49.186	8.525	1.121	0.045	31
319Axx_TA	31.38	-109.28	45.919	6.851	1.14	0.078	29
320Axx_TA	31.34	-108.53	57.571	13.029	0.95	0.102	4
324Axx_TA	31.44	-105.48	30.086	15.125	0.983	0.06	12
325Axx_TA	31.37	-104.97	22.62	11.552	1.138	0.093	17
326Axx_TA	31.32	-103.98	21.622	7.721	1.417	0.051	12
327Axx_TA	31.37	-103.49	8.8	13.002	0.956	0.147	8
328Axx_TA	31.38	-102.81	4.63	9.178	0.822	0.115	9
329Axx_TA	31.49	-101.98	9.638	15.831	0.873	0.067	15
330Axx_TA	31.41	-101.18	46.289	16.579	0.775	0.082	6
331Axx_TA	31.31	-100.43	67.748	8.566	1.138	0.127	8
332Axx_TA	31.38	-99.74	56.211	7.565	0.913	0.045	16
333Axx_TA	31.32	-98.98	61.268	9.909	0.932	0.098	11
334Axx_TA	31.33	-98.24	58.439	11.522	0.997	0.061	16
335Axx_TA	31.28	-97.43	48.918	7.339	1.2	0.076	9
336Axx_TA	31.39	-96.84	48.653	8.988	1.142	0.063	12
337Axx_TA	31.32	-95.89	51.576	7.607	1.261	0.144	9
338Axx_TA	31.36	-95.31	63.989	5.667	1.26	0.102	5
339Axx_TA	31.33	-94.56	73.429	16.663	0.911	0.061	9
340Axx_TA	31.42	-93.89	67.043	6.731	1.186	0.101	11
341Axx_TA	31.33	-93.17	75.078	9.915	1.533	0.071	20
342Axx_TA	31.37	-92.32	72.148	6.784	1.514	0.074	7
342Bxx_N4	31.37	-92.32	77.089	7.497	1.473	0.105	15
343Axx_TA	31.28	-91.62	69.098	13.408	1.338	0.137	4
344Axx_TA	31.45	-90.73	72.965	12.427	1.144	0.126	8
344Bxx_N4	31.45	-90.73	69.16	6.758	1.192	0.129	6
345Axx_TA	31.31	-90.03	79.727	11.89	1.209	0.072	11
425Axx_TA	30.79	-104.99	36.708	10.391	0.889	0.049	9
426Axx_TA	30.67	-104.03	17.226	13.696	1.061	0.086	14
427Axx_TA	30.85	-103.4	1.886	9.683	1.05	0.075	6

428Axx_TA	30.73	-102.68	30.998	24.106	1.111	0.111	9
429Axx_TA	30.62	-101.89	17.296	8.742	1.089	0.042	18
430Axx_TA	30.79	-101.24	6.066	19.059	0.943	0.054	15
431Axx_TA	30.68	-100.61	34.907	14.764	1.019	0.095	13
432Axx_TA	30.88	-99.79	21.023	19.867	0.842	0.07	13
433Axx_TA	30.75	-99.09	88.417	22.818	1.1	0.108	6
434Axx_TA	30.81	-98.27	69.907	7.838	1.096	0.075	13
435Bxx_TA	30.78	-97.58	46.603	19.385	1.261	0.063	47
436Axx_TA	30.77	-96.8	73.995	13.015	1.275	0.078	10
437Axx_TA	30.83	-96.14	57.545	8.36	1.636	0.109	7
438Axx_TA	30.75	-95.47	62.526	9.364	1.491	0.112	11
439Axx_TA	30.79	-94.77	70.734	5.578	1.264	0.055	7
440Axx_TA	30.75	-93.96	69.332	3.163	1.644	0.063	9
441Axx_TA	30.75	-93.19	73.058	7.913	1.556	0.056	9
441Bxx_N4	30.75	-93.19	69.881	5.155	1.567	0.081	9
442Axx_TA	30.71	-92.43	70.314	11.022	1.167	0.104	6
443Axx_TA	30.76	-91.78	66.661	15.089	1.487	0.088	4
444Axx_TA	30.72	-90.75	79.359	9.004	1.188	0.103	8
445Axx_TA	30.73	-90.34	67.034	6.913	1.356	0.096	8
5110xx_XK	50.02	-90.59	51.153	13.726	1.39	0.107	5
5130xx_XK	50.36	-90.67	71.75	0.829	1.25	0.098	4
5150xx_XK	50.69	-90.56	59.269	9.601	1.117	0.083	3
5170xx_XK	51.03	-90.35	71.686	5.571	1.233	0.067	3
5190xx_XK	51.35	-90.22	87	4	1.3	0.15	1
526Axx_TA	30.06	-104.09	-55.979	27.559	0.65	0.154	5
527Axx_TA	30.15	-103.61	16.76	16.494	1.019	0.103	8
528Axx_TA	30.16	-102.79	14	13	0.9	0.25	1
529Axx_TA	30.12	-102.22	12.004	3.746	1.133	0.033	3
530Axx_TA	30.15	-101.34	41.583	7.145	1.105	0.111	11
531Axx_TA	30.16	-100.55	49.398	12.067	1.195	0.074	11
532Axx_TA	30.13	-99.9	48.608	16.91	1.158	0.196	6
533Axx_TA	30.07	-99.04	73.499	11.686	0.854	0.071	13
534Axx_TA	30.03	-98.48	76.607	6.565	0.913	0.081	8
535Axx_TA	30.03	-97.57	56.1	13.513	1.037	0.075	15
536Axx_TA	30.08	-97.07	65.908	7.362	1.319	0.051	16
537Axx_TA	30.08	-96.32	69.733	8.383	1.666	0.072	22
538Axx_TA	30.22	-95.49	68.303	3.927	1.71	0.072	10
539Axx_TA	30.11	-94.72	74.683	4.737	1.86	0.085	10
540Axx_TA	30.21	-93.98	69.856	2.643	1.914	0.07	7
541Axx_TA	30.06	-93.19	76.251	3.033	1.638	0.16	4
542Axx_TA	30.12	-92.55	76.321	4.272	1.583	0.144	6

543Axx_TA	30.09	-91.86	69	3.003	1.4	0	2
544Axx_TA	30.11	-91.16	-81.031	14.125	1.24	0.125	5
545Axx_TA	30.04	-90.49	-69	8.5	0.8	0.15	1
545Bxx_N4	30.04	-90.49	70	5.5	1.65	0.25	1
627Axx_TA	29.45	-103.39	90	11.14	0.85	0.35	2
628Axx_TA	29.49	-102.89	-67.468	19.308	1	0.135	4
631Axx_TA	29.41	-100.58	10.225	13.116	0.9	0.08	6
632Axx_TA	29.51	-99.79	65.47	30.095	1.05	0.17	4
633Axx_TA	29.46	-99.18	68.76	12.192	1.15	0.138	10
634Axx_TA	29.38	-98.35	-78.259	21.692	1.021	0.127	7
635Axx_TA	29.39	-97.77	71.335	10.831	1.488	0.09	16
636Axx_TA	29.48	-97.06	70.103	7.632	1.389	0.05	23
637Axx_TA	29.44	-96.33	70.949	6.787	1.756	0.068	8
638Axx_TA	29.42	-95.45	74.5	2.502	2.125	0.225	2
645Axx_TA	29.46	-90.6	70.25	2.279	1.562	0.143	4
732Axx_TA	28.73	-99.97	55.337	4.115	1.383	0.164	3
733Axx_TA	28.72	-99.29	69.856	22.884	0.98	0.076	10
734Axx_TA	28.85	-98.56	53.736	16.022	1.175	0.128	6
735Axx_TA	28.86	-97.81	74.727	7.837	1.35	0.107	9
735Bxx_N4	28.86	-97.81	71.547	15.156	1.663	0.224	4
736Axx_TA	28.95	-97.07	74.444	6.498	1.55	0.057	11
737Axx_TA	28.76	-96.44	69.566	8.048	1.362	0.103	4
738Axx_TA	28.84	-95.65	63.772	6.783	1.562	0.105	4
832Axx_TA	28.28	-99.97	44.111	15.541	1.177	0.128	11
833Axx_TA	28.32	-99.39	81.067	25.076	1.158	0.036	40
834Axx_TA	28.13	-98.55	67.074	11.161	1.306	0.124	9
835Axx_TA	28.29	-97.83	67.333	2.055	1.533	0.192	3
933Axx_TA	27.61	-99.27	84.819	13.237	1.115	0.073	10
934Axx_TA	27.6	-98.52	51.96	7.966	1.157	0.065	7
936Axx_TA	27.42	-97.31	44.261	16.396	1.183	0.337	3
A01xxx_XZ	44.43	-124.05	76	4.5	1.3	0.15	1
A02xxx_XZ	44.42	-124	76	5	1.3	0.15	1
A03xxx_XZ	44.42	-123.95	71.5	7.544	1.175	0.125	2
A04Axx_TA	48.72	-122.71	73.03	9.343	1.215	0.06	13
A04Dxx_TA	48.72	-122.71	76.896	9.299	1.198	0.044	23
A04xxx_XZ	44.43	-123.89	85.476	13.088	1.4	0.126	3
A05Axx_TA	49	-122.09	64.63	11.675	1.465	0.075	10
A05xxx_XZ	44.43	-123.85	-89.606	10.872	1.462	0.149	4
A06Axx_TA	49.1	-121.48	72.711	8.093	1.507	0.093	7
A06xxx_XZ	44.43	-123.81	-84	7.5	1.45	0.4	1
A07Axx_TA	49.05	-120.38	65.143	17.015	1.418	0.069	11

A07xxx_XZ	44.42	-123.75	73	5.013	1.4	0.15	2
A07xxx_YX	40.56	-115.53	-71.505	13.971	0.956	0.104	16
A08Axx_TA	48.95	-119.27	48.996	12.345	1.293	0.088	14
A08xxx_XZ	44.42	-123.7	76.466	7.589	1.275	0.052	4
A09Axx_TA	48.98	-118.59	42.152	8.462	1.2	0.08	7
A09xxx_XZ	44.43	-123.66	83	2.001	1.375	0.075	2
A10Axx_TA	48.98	-117.56	34.151	6.563	1.656	0.175	9
A10xxx_XZ	44.41	-123.59	80.5	0.5	1.2	0.3	2
A11Axx_TA	48.96	-116.36	64.622	10.037	1.377	0.047	24
A11xxx_XZ	44.42	-123.54	73.39	7.348	1.333	0.109	3
A12Axx_TA	48.93	-115.65	47.915	9.787	1.536	0.048	35
A12xxx_XZ	44.42	-123.5	69	3.269	1.617	0.192	3
A13Axx_TA	48.93	-114.41	50.534	11.647	1.33	0.057	35
A13xxx_XZ	44.43	-123.45	74	8.207	1.7	0.076	3
A14Axx_TA	48.97	-113.42	51.443	25.597	1.121	0.107	7
A14xxx_XZ	44.43	-123.4	73.988	6.182	2.05	0.15	3
A15Axx_TA	48.98	-112.73	73.592	8.852	1.192	0.119	6
A15xxx_XZ	44.43	-123.34	72.483	4.504	1.413	0.151	4
A16Axx_TA	48.95	-111.6	19.8	20.042	0.863	0.106	15
A16xxx_XZ	44.43	-123.29	68	7	1	0.2	1
A17Axx_TA	48.94	-110.7	33.366	15.124	0.883	0.08	9
A17xxx_XZ	44.43	-123.24	82.665	3.303	1.4	0.351	3
A18Axx_TA	48.92	-109.85	32.344	20.268	1.205	0.117	10
A18xxx_XZ	44.43	-123.18	73.669	4.504	1.533	0.117	3
A19Axx_TA	48.93	-108.74	50.786	17.437	0.85	0.104	3
A19xxx_XZ	44.43	-123.14	61	4.908	1.367	0.164	3
A20Axx_TA	48.88	-107.93	29.702	20.784	0.833	0.044	3
A20xxx_XZ	44.42	-123.09	59.5	3.044	1.562	0.128	4
A21Axx_TA	48.99	-106.93	-4.072	15.492	1.18	0.055	10
A21xxx_XZ	44.42	-123.04	67	5	1.3	0.15	1
A22Axx_TA	48.99	-105.92	21.487	16.59	0.896	0.067	14
A22xxx_XZ	44.43	-122.98	57.342	6.571	1.367	0.13	3
A23Axx_TA	48.96	-104.88	33.589	13.386	1.129	0.145	7
A23xxx_XZ	44.43	-122.94	68.568	5.962	1.5	0.101	5
A24Axx_TA	48.92	-104	82.5	7.544	0.85	0.05	2
A24xxx_XZ	44.42	-122.9	60.141	12.985	1.69	0.087	5
A25Axx_TA	48.94	-103.11	40.418	21.173	1.078	0.115	9
A25xxx_XZ	44.42	-122.84	62.994	4.769	1.592	0.051	6
A26Axx_TA	48.9	-102.04	57.738	7.297	0.95	0.089	8
A26xxx_XZ	44.42	-122.8	63.718	5.18	1.593	0.083	7
A27Axx_TA	48.95	-101.24	52.665	8.104	1.014	0.059	21

A27xxx_XZ	44.43	-122.73	67.501	3.575	1.737	0.083	4
A28Axx_TA	48.91	-100.27	53.964	16.335	1.09	0.155	5
A28xxx_XZ	44.43	-122.64	67.663	9.161	1.78	0.025	5
A29Axx_TA	48.92	-99.23	55.208	9.728	1.137	0.046	27
A29xxx_XZ	44.43	-122.55	61.151	14.314	1.337	0.139	4
A30Axx_TA	48.94	-98.3	61.373	13.128	1.034	0.042	28
A30xxx_XZ	44.42	-122.43	65.988	7.178	1.658	0.06	6
A31Axx_TA	48.93	-97.19	72.83	15.094	1.173	0.084	13
A31xxx_XZ	44.43	-122.34	69.85	4.744	1.675	0.119	6
A32Axx_TA	48.92	-96.49	66.992	10.732	1.259	0.059	16
A32xxx_XZ	44.43	-122.24	70.624	4.363	1.7	0.076	5
A33Axx_TA	48.94	-95.39	65.562	7.981	1.454	0.066	23
A33xxx_XZ	44.42	-122.14	72	1	1.95	0.05	2
A34xxx_XZ	44.42	-122.05	68.599	5.212	1.71	0.156	5
A35xxx_XZ	44.43	-121.96	72.994	2.916	2.15	0.046	4
A36xxx_XZ	44.42	-121.85	76	1	2.025	0.125	2
A37xxx_XZ	44.43	-121.74	63	9	1.15	0.25	1
A38xxx_XZ	44.42	-121.62	82.327	4.196	1.967	0.164	3
A39xxx_XZ	44.42	-121.54	78.357	8.425	1.48	0.112	5
A40xxx_XZ	44.41	-121.44	77.663	4.999	1.558	0.146	6
A41xxx_XZ	44.42	-121.34	80.199	2.788	1.68	0.285	5
A42xxx_XZ	44.41	-121.23	84.331	12.907	1.525	0.183	6
A43xxx_XZ	44.41	-121.13	75.232	5.861	1.363	0.114	4
A44xxx_XZ	44.41	-121.03	77	10	1.4	0.35	1
ABTXxx_TA	32.62	-99.64	55.682	11.155	1.177	0.073	30
ADOxxx_CI	34.55	-117.43	-78.663	13.047	1.246	0.047	24
AGAxxx_CI	33.64	-116.4	-82	6.022	1	0.05	2
AGMNxx_US	48.3	-95.86	40.73	13.895	1.141	0.027	104
AHABxx_XN	35.98	-120.54	-69.217	11.456	1.75	0.321	3
AHIDxx_US	42.77	-111.1	67.136	7.474	1.058	0.064	19
ALEXxx_XN	35.98	-120.46	-79.332	28.195	1.3	0.231	3
AMTXxx_US	34.88	-101.68	3.047	14.278	0.996	0.1	12
ANMOxx_IU	34.95	-106.46	40.064	20.404	1.31	0.046	82
ARC2xx_XJ	36.01	-118.33	88	9	1.25	0.23	1
ARVxxx_CI	35.13	-118.83	-77.794	14.86	1.719	0.065	24
ASBSxx_AZ	33.62	-116.47	89.387	11.078	1.82	0.138	10
ASBUxx_CC	43.82	-121.37	69.41	10.477	1.2	0.116	12
AZ45xx_XM	36.46	-109.08	26	3.5	0.8	0.08	1
AZ46xx_XM	36.55	-109.23	33.735	12.825	1.08	0.201	5
AZ47xx_XM	36.64	-109.33	45.087	14.225	0.979	0.092	12
AZ48xx_XM	36.76	-109.54	35.014	9.328	0.978	0.062	16

AZ49xx_XM	36.89	-109.69	33.87	11.759	1.297	0.082	18
AZ50xx_XM	36.98	-109.86	40.922	15.044	1.292	0.081	13
B04Axx_TA	48.06	-123.5	78.189	6.005	1.461	0.085	9
B05Axx_TA	48.26	-122.1	85.884	8.886	1.219	0.076	13
B05Dxx_TA	48.26	-122.1	86.126	16.94	1.215	0.034	47
B06Axx_TA	48.52	-121.48	81.215	6.119	1.07	0.041	5
B07Axx_TA	48.46	-120.12	67.201	9.093	1.019	0.06	8
B082Ax_PB	33.6	-116.6	-78.457	20.55	1.142	0.1	6
B086Ax_PB	33.56	-116.53	-74.259	9.203	1.237	0.136	8
B088Ax_PB	33.37	-116.62	85.787	22.109	0.96	0.084	5
B08Axx_TA	48.36	-119.33	61.12	10.368	1.546	0.081	25
B09Axx_TA	48.42	-118.15	55.344	5.581	1.353	0.054	19
B10Axx_TA	48.3	-117.23	68.598	9.473	1.207	0.043	7
B11Axx_TA	48.44	-116.37	72.84	8.687	1.54	0.088	21
B12Axx_TA	48.47	-115.59	60.746	7.383	1.529	0.065	26
B13Axx_TA	48.37	-114.47	62.675	12.13	1.32	0.076	22
B14Axx_TA	48.36	-113.27	52.776	9.012	1.144	0.143	9
B15Axx_TA	48.31	-112.56	62.72	7.498	1.081	0.044	13
B16Axx_TA	48.41	-111.71	32.962	18.756	0.72	0.098	10
B17Axx_TA	48.29	-110.8	52.998	4.589	1.319	0.13	8
B18Axx_TA	48.39	-109.78	52.081	7.994	1.231	0.114	13
B19Axx_TA	48.46	-108.94	57.537	6.59	1.15	0.065	4
B20Axx_TA	48.44	-108.02	-22.5	3.504	1.175	0.175	2
B21Axx_TA	48.43	-107.02	3.721	21.206	1.181	0.05	34
B22Axx_TA	48.3	-106	29.865	12.548	0.856	0.128	9
B23Axx_TA	48.46	-104.99	34.256	10.425	1.067	0.342	3
B25Axx_TA	48.27	-103.16	56.405	13.904	1.078	0.083	9
B26Axx_TA	48.38	-102.23	36.205	13.652	0.886	0.135	7
B27Axx_TA	48.4	-101.26	53.582	19.571	0.862	0.094	8
B28Axx_TA	48.45	-100.36	68.068	15.076	0.839	0.049	28
B29Axx_TA	48.46	-99.35	41.631	12.276	1.079	0.058	21
B30Axx_TA	48.45	-98.33	54.893	9.182	1.247	0.052	18
B31Axx_TA	48.42	-97.65	52.694	8.162	1.162	0.038	17
B32Axx_TA	48.4	-96.54	39.838	10.954	1.074	0.055	21
B33Axx_TA	48.27	-95.59	43.22	11.903	0.931	0.051	13
B34Axx_TA	48.49	-94.65	62.083	13.759	1.136	0.069	14
B35Axx_TA	48.36	-93.73	60.283	9.834	1.42	0.066	15
B35Bxx_N4	48.36	-93.73	67.164	4.144	1.3	0.168	6
BABRxx_UW	44.62	-123.79	71.169	7.568	1.254	0.068	12
BAKxxx_CI	35.34	-119.1	-85.39	14.441	1.023	0.1	11
BARxxx_CI	32.68	-116.67	71.145	15.623	1.202	0.043	80

BARxxx_TS	32.68	-116.67	73.931	8.879	0.968	0.057	11
BB1xxx_XV	44.54	-107.63	80	0	0.9	0	2
BB2xxx_XV	44.55	-107.78	84.086	22.482	0.983	0.165	6
BB3xxx_XV	44.52	-107.9	-87.288	18.252	1.031	0.108	13
BBRxxx_CI	34.26	-116.92	-80.357	7.642	1.33	0.078	27
BBSxxx_CI	33.92	-116.98	84.29	12.513	1.337	0.065	8
BC3xxx_CI	33.66	-115.45	-81.583	21.952	1.253	0.045	36
BCCxxx_CI	33.58	-117.26	-89.448	12.325	1.571	0.118	7
BD11xx_XU	47.31	-121.97	76.398	5.691	1.43	0.101	10
BECHxx_XN	35.95	-120.55	-71.988	6.182	1.7	0.539	3
BEKxxx_NN	39.87	-120.36	86.455	9.47	1.178	0.069	9
BELxxx_CI	34	-116	-87.297	16.065	1.387	0.059	57
BFSxxx_CI	34.24	-117.66	86.68	8.309	1.428	0.044	39
BGNExx_TA	41.41	-98.15	85.611	15.325	0.704	0.035	42
BGRxxx_XJ	36.63	-119.02	80.21	9.27	1.25	0.159	4
BH1Axx_XV	44.98	-108.58	46.078	13.963	0.908	0.156	6
BH1Bxx_XV	44.82	-108.23	58.889	6.84	1.053	0.074	17
BH1Cxx_XV	44.93	-107.77	65	2.001	1.7	0.25	2
BH1Dxx_XV	44.83	-107.31	77.414	17.396	0.96	0.073	10
BH1Exx_XV	44.2	-106.96	77.561	14.55	0.95	0.057	12
BH1Fxx_XV	45.28	-106.65	17	8.5	1.1	0.2	1
BH1Gxx_XV	45.49	-105.86	-71.929	26.551	0.756	0.077	9
BH1Hxx_XV	44.95	-105.07	21.674	22.099	0.967	0.317	3
BH2Axx_XV	44.69	-108.61	80.923	15.449	0.782	0.086	11
BH2Bxx_XV	45.2	-108.26	-88.984	28.919	1.263	0.205	4
BH2Cxx_XV	44.14	-107.83	88.343	13.549	1.081	0.111	13
BH2Dxx_XV	44.66	-107.54	82.659	17.332	1.286	0.129	7
BH2Exx_XV	43.89	-106.88	73.647	15.794	0.914	0.05	11
BH2Fxx_XV	45.1	-106.63	50.5	0.5	1.125	0.025	2
BH2Gxx_XV	44.79	-106.02	31.899	21.971	0.562	0.072	4
BH3Axx_XV	44.25	-108.74	-82.268	18.2	1.1	0.257	3
BH3Cxx_XV	44.71	-107.96	-89.14	11.62	0.84	0.064	15
BH3Dxx_XV	44.42	-107.39	-88.372	11.916	0.928	0.082	18
BH3Exx_XV	43.59	-106.89	-86.138	14.457	0.783	0.069	24
BH3Fxx_XV	44.83	-106.64	77.429	15.58	0.7	0.115	3
BH3Gxx_XV	44.61	-105.98	44.99	4.327	0.883	0.06	3
BH4Axx_XV	43.7	-108.71	72.028	22.191	0.98	0.104	5
BH4Cxx_XV	43.52	-107.71	86.851	10.537	0.873	0.106	11
BH4Dxx_XV	44.06	-107.27	68.772	17.547	0.928	0.067	23
BH4Fxx_XV	44.27	-106.59	88.641	13.143	0.825	0.149	4
BH4Gxx_XV	44.19	-105.78	77	30.888	0.725	0.175	2

BH5Gxx_XV	43.64	-106.03	-79.602	11.868	1.163	0.102	8
BHM1xx_XV	44.66	-106.95	73.43	14.84	1.225	0.095	4
BHM2xx_XV	44.62	-107.12	80.883	9.615	1.138	0.13	8
BHM3xx_XV	44.61	-107.2	71.666	13.911	1.036	0.116	11
BHM4xx_XV	44.57	-107.3	77.711	8.716	1.082	0.126	11
BHM5xx_XV	44.54	-107.54	-84.31	11.599	0.969	0.081	21
BHM6xx_XV	44.55	-107.82	72.686	13.216	1.184	0.093	22
BHM7xx_XV	44.49	-108.31	71.498	12.258	1.132	0.079	14
BHN1xx_XV	44.75	-107.5	87.235	7.404	1.02	0.135	5
BLAxxx_CI	34.07	-116.39	-64.98	19.851	1	0.202	3
BLAxxx_XG	37.54	-105.57	22.281	8.194	0.913	0.043	4
BLOWxx_UW	44.68	-122.19	70.865	6.137	1.702	0.042	53
BLUExx_XT	40.99	-108.54	-15	7	1.25	0.38	1
BMNxxx_LB	40.43	-117.22	85.838	7.498	1.272	0.04	102
BMNxxx_US	40.43	-117.22	85.5	3.504	0.8	0.05	2
BMOxxx_US	44.85	-117.31	-81.044	14.676	1.246	0.087	23
BNLOxx_TA	37.13	-122.17	-64.007	15.163	1.225	0.303	4
BORxxx_CI	33.27	-116.42	-68	5.5	1.8	0.45	1
BOZxxx_US	45.6	-111.63	66.182	21.508	1.074	0.062	27
BOZxxx_US	45.65	-111.63	66.182	21.508	1.074	0.062	27
BPH01x_PY	33.61	-116.46	-85	5.013	1.45	0.45	2
BPH02x_PY	33.61	-116.46	-85.5	5.517	1.425	0.425	2
BPH04x_PY	33.61	-116.46	-84	5.013	1.35	0.35	2
BPH05x_PY	33.61	-116.46	-85.5	6.528	1.35	0.35	2
BPH06x_PY	33.61	-116.45	-84.5	7.544	1.025	0.025	2
BPH07x_PY	33.61	-116.46	-82.314	5.571	1.383	0.289	3
BPH09x_PY	33.61	-116.46	85	5.013	1.625	0.675	2
BPH12x_PY	33.61	-116.46	-83	2.001	1.45	0.45	2
BRANxx_UW	45.97	-117.23	78.524	10.272	1.172	0.084	23
BRKxxx_XJ	42.55	-114.96	-77	6.022	1.525	0.275	2
BRRxxx_XJ	36.91	-119.04	78.5	0.5	1.025	0.125	2
BRSDxx_TA	44.44	-98.96	45.857	9.583	1.058	0.143	6
BS11xx_XU	47.96	-122.93	73.006	14.071	1.177	0.111	13
BTCxxx_CI	33.01	-115.22	-42	3	1.6	0.2	1
BTOxxx_XG	40.39	-105.2	74.383	15.81	0.8	0.161	3
BUCKxx_UO	44.2	-122.99	58.816	6.879	1.81	0.07	5
BURxxx_XG	39.39	-102.35	52	3.5	1.3	0.13	1
BUZZxx_XN	36.02	-120.6	-47.721	7.753	0.917	0.073	3
BVDA2x_AZ	33.33	-116.37	-89.736	15.431	1.056	0.113	8
BVDA2x_SB	33.33	-116.37	84.916	11.999	0.85	0.059	6
BW06xx_US	42.77	-109.56	60.199	26.293	1.159	0.139	11

BWO0xx_XA	44.61	-123.57	78	2.001	1.625	0.325	2
BZNxxx_AZ	33.49	-116.67	-84.757	11.205	1.243	0.053	56
C03Axx_TA	47.95	-124.57	78	6.022	0.7	0.05	2
C04Axx_TA	47.72	-122.97	82.107	5.035	1.45	0.104	10
C04Axx_XU	47.72	-122.97	82.916	8.933	1.608	0.046	24
C05Axx_TA	47.69	-121.69	70.8	6.681	1.345	0.065	20
C06Axx_TA	47.92	-120.89	67.431	7.219	1.483	0.118	12
C06Dxx_TA	47.92	-120.89	70.071	10.823	1.54	0.059	47
C07Axx_TA	47.69	-120.06	81.931	5.655	1.479	0.106	12
C08Axx_TA	47.78	-119.05	86.49	10.365	1.382	0.077	17
C09Axx_TA	47.8	-118.27	83.338	14.175	1.386	0.063	21
C10Axx_TA	47.82	-117.31	78.706	11.714	1.461	0.07	14
C11Axx_TA	47.84	-116.26	75.69	8.905	1.535	0.061	26
C12Bxx_TA	47.71	-115.47	-84.801	12.75	1.141	0.073	17
C13Axx_TA	47.68	-114.57	79.996	20.837	1.477	0.11	11
C14Axx_TA	47.77	-113.75	65.335	15.558	1.428	0.135	9
C15Axx_TA	47.78	-112.61	57.584	7.154	1.364	0.039	14
C16Axx_TA	47.8	-111.75	43.726	21.942	0.869	0.081	8
C17Axx_TA	47.63	-110.76	70.248	7.366	0.942	0.098	13
C19Axx_TA	47.73	-109.05	42.052	12.204	1.15	0.136	5
C20Axx_TA	47.71	-108	6.43	28.589	0.979	0.088	7
C21Axx_TA	47.83	-107.1	31.357	16.934	1.041	0.086	22
C22Axx_TA	47.75	-105.88	22	9.076	1.025	0.075	2
C23Axx_TA	47.8	-105.18	30.739	24.913	0.917	0.166	6
C24Axx_TA	47.53	-104.43	78.5	14.829	0.475	0.025	2
C25Axx_TA	47.71	-103.26	66	17.859	0.969	0.094	8
C26Axx_TA	47.83	-102.1	77.207	27.978	0.906	0.114	8
C27Axx_TA	47.71	-101.5	42.841	28.917	1.008	0.104	12
C28Axx_TA	47.72	-100.39	43.2	30.033	0.895	0.059	20
C30Axx_TA	47.7	-98.48	45.493	6.613	1.015	0.032	17
C31Axx_TA	47.79	-97.73	40.787	14.147	1.1	0.043	17
C32Axx_TA	47.83	-96.53	31.447	14.2	1.141	0.059	22
C33Axx_TA	47.76	-95.77	36.61	16.022	1.16	0.089	15
C34Axx_TA	47.65	-94.91	44.388	11.171	1.085	0.072	13
C35Axx_TA	47.7	-93.98	55.531	15.912	1.219	0.091	13
C36Axx_TA	47.76	-92.84	58.096	12.138	1.157	0.075	14
C37Axx_TA	47.73	-92.19	59.768	7.119	1.345	0.066	11
C38Axx_TA	47.72	-91.27	58.556	14.478	0.975	0.113	10
C39Axx_TA	47.82	-90.13	50.979	13.628	0.971	0.129	7
CALAxx_XT	40.11	-108.54	86.206	13.179	1.025	0.287	4
CALBxx_CI	34.14	-118.63	87.624	10.459	1.421	0.132	7

CALBxx_TS	34.14	-118.63	83.807	9.822	1.439	0.107	9
CALIxx_XT	40.37	-108.57	39	8	1.75	0.43	1
CAPxxx_CI	33.39	-117.19	86.558	17.14	1.337	0.114	12
CBKSxx_US	38.81	-99.74	37.159	37.365	0.924	0.055	23
CCMxxx_IU	38.06	-91.24	30.887	13.805	0.891	0.035	76
CCMxxx_US	38.06	-91.24	30.837	11.303	1.09	0.137	5
CCPE4x_YA	36.07	-117.79	-27	13	0.65	0.2	1
CCPS5x_YA	36.05	-117.83	78	6	1.65	0.25	1
CCRKxx_HW	46.56	-119.85	-58.461	18.048	1.138	0.068	13
CCRKxx_UW	46.56	-119.85	-64.176	7.122	1.24	0.145	5
CESxxx_XG	39.39	-101.07	-71	8.053	0.95	0.1	2
CGASxx_XN	35.97	-120.5	-77.316	12.818	1.7	0.401	3
CHFxxx_CI	34.33	-118.03	87.852	10.857	1.319	0.053	37
CIAxxx_CI	33.4	-118.42	85.005	11.124	1.359	0.037	53
CICxxx_XJ	42.95	-113.21	85.285	5.408	1.062	0.27	4
CIHLxx_CC	43.75	-121.15	82.122	23.836	1.531	0.102	16
CIUxxx_CI	33.45	-118.48	86	9	1.65	0.32	1
CLAxxx_Y5	50.01	-113.52	68	1	0.95	0.05	2
CLCxxx_CI	35.82	-117.6	88.237	9.162	0.95	0.236	3
CLEA1x_X9	32.36	-97.43	-8	24.454	0.875	0.125	2
CLEF1x_X9	32.35	-97.38	13.282	17.425	0.992	0.185	6
CLEF2x_X9	32.32	-97.42	27.424	13.985	0.85	0.185	5
CLELKx_X9	32.3	-97.35	1.122	15.072	0.667	0.088	3
CMBxxx_BK	38.03	-120.39	84.544	9.822	1.784	0.031	125
CMBxxx_US	38.03	-120.39	84.336	7.644	1.855	0.084	19
CORxxx_IU	44.59	-123.3	75.993	8.725	1.546	0.032	128
CORxxx_US	44.59	-123.3	78	4.088	1.567	0.235	3
CPExxx_AZ	32.89	-117.11	75.683	8.328	1.262	0.052	30
CPRxxx_XJ	36.8	-118.58	70.006	3.562	1.933	0.033	3
CRABxx_XN	36.01	-120.55	71	5	2.05	0.3	1
CRAKxx_XN	35.96	-120.52	-74.988	6.182	1.733	0.441	3
CRYxxx_AZ	33.57	-116.74	-82.996	11.024	1.483	0.04	89
CSDxxx_XT	40.44	-108.28	77.716	14.369	1.025	0.131	4
CTCxxx_CI	33.66	-115.99	-62	9.5	0.9	0.17	1
CVCRxx_XN	35.99	-120.53	-64.5	23.851	1.525	0.125	2
CVSxxx_BK	38.35	-122.46	-41.997	3.394	1.275	0.13	4
CWCxxx_CI	36.44	-118.08	89.96	9.657	1.467	0.049	47
CWCxxx_TS	36.44	-118.08	89.793	8.78	1.46	0.108	5
CYFxxx_XH	37.55	-109.87	11.548	13.213	0.85	0.136	5
D03Axx_TA	47.12	-123.77	83	7.035	1.5	0.1	2
D03Dxx_TA	47.53	-123.09	79.417	11.015	1.144	0.043	36

D04Axx_TA	47.11	-122.8	65.5	0.5	1.175	0.125	2
D04Dxx_TA	47.18	-122.77	80.221	17.309	0.863	0.052	4
D04Exx_TA	47.18	-122.77	71	4	1.6	0.2	1
D05Axx_TA	47.19	-121.99	77.811	6.833	1.283	0.091	9
D06Axx_TA	47.19	-120.84	-81.097	13.722	1.18	0.151	10
D07Axx_TA	47.19	-119.97	-82.693	5.232	1.361	0.09	9
D08Axx_TA	47.06	-118.92	-89.101	6.56	1.238	0.115	13
D09Axx_TA	47.06	-118.31	75.896	17.016	1.431	0.1	8
D10Axx_TA	47.05	-117.28	65.148	6.475	1.507	0.138	7
D11Axx_TA	47.05	-116.34	85.081	14.116	1.172	0.076	18
D12Axx_TA	47.05	-115.35	-86.226	14.525	0.892	0.122	6
D13Axx_TA	47.09	-114.46	-83.458	18.268	0.975	0.136	4
D14Axx_TA	47.08	-113.51	69.243	9.579	1.46	0.103	15
D15Axx_TA	47.04	-112.52	57.954	8.947	1.461	0.089	14
D16Axx_TA	47.03	-111.55	48.31	5.593	1.292	0.08	13
D17Axx_TA	47.15	-110.69	38.077	12.778	1.308	0.111	6
D18Axx_TA	47.2	-109.8	63.203	5.826	1.07	0.051	5
D19Axx_TA	47.16	-108.88	40.456	18.388	0.9	0.079	11
D20Axx_TA	47.09	-108.14	55.218	19.623	0.96	0.137	5
D21Axx_TA	47.07	-106.99	-85.584	30.731	1.036	0.137	7
D22Axx_TA	47.15	-106.18	68.618	22.715	1.18	0.124	5
D23Axx_TA	47.17	-105.21	62.602	11.192	1.15	0.176	3
D24Axx_TA	47.12	-104.33	39	4.007	1.275	0.175	2
D25Axx_TA	47.15	-103.32	-88.838	15.085	0.95	0.114	5
D26Axx_TA	47.03	-102.44	-84.911	22.789	0.9	0.144	3
D27Axx_TA	47.11	-101.53	19.232	8.95	0.8	0.079	9
D28Axx_TA	47.19	-100.57	34.915	11.21	1.13	0.056	20
D29Axx_TA	47.06	-99.6	21.756	12.203	0.996	0.102	12
D30Axx_TA	47.11	-98.76	48.715	11.987	1.074	0.049	23
D31Axx_TA	47.05	-97.72	40.726	15.064	0.952	0.056	22
D32Axx_TA	47.14	-97.02	38.706	10.575	0.985	0.063	13
D32Bxx_N4	47.14	-97.02	49.018	11.428	0.788	0.101	4
D33Axx_TA	47.14	-95.84	32.847	8.649	1.156	0.089	17
D34Axx_TA	47.09	-95.2	43.74	9.697	1.232	0.07	17
D35Axx_TA	47.08	-94.05	28.963	19.07	1.174	0.079	19
D36Axx_TA	47.18	-93.16	39.46	11.49	1.062	0.056	21
D37Axx_TA	47.16	-92.43	31.617	12.315	1.067	0.057	21
DACxxx_LB	36.28	-117.59	-86.361	15.635	1.337	0.157	16
DANxxx_CI	34.64	-115.38	80.59	13.709	1.011	0.043	56
DAVNxx_UW	47.8	-118.27	83.035	18.076	1.458	0.036	96
DBLTxx_XN	35.96	-120.58	-74.5	1.5	1.825	0.275	2

DBOxxx_UO	43.12	-123.24	57.834	8.028	1.604	0.032	58
DBQxxx_XG	39.25	-108.18	57	8	1.05	0.25	1
DBT2Ax_YE	33.96	-106.85	47.97	11.178	1.39	0.128	5
DBT2xx_YE	33.96	-106.85	46.094	11.43	1.358	0.105	6
DBTTPx_YE	33.96	-106.85	50	2.001	1.3	0.1	2
DCID1x_IW	43.59	-111.18	71.307	8.123	1.15	0.089	6
DDRFxx_HW	46.49	-119.06	-67.934	17.003	1.171	0.055	31
DDRFxx_UW	46.49	-119.06	-78.215	12.092	1.258	0.124	12
DECxxx_CI	34.25	-118.33	81.78	11.641	1.334	0.044	28
DEVxxx_CI	33.94	-116.58	78.6	15.606	1.15	0.087	7
DGMTxx_US	48.47	-104.2	60.251	14.992	1.066	0.071	25
DGRxxx_CI	33.65	-117.01	-89.113	11.58	1.261	0.04	70
DGRxxx_TS	33.65	-117.01	-86.565	9.528	1.236	0.056	33
DJJxxx_CI	34.11	-118.46	78.541	9.701	1.433	0.043	42
DLMTxx_IW	45.36	-112.6	52.073	22.42	0.841	0.042	55
DOSExx_UW	47.72	-122.97	80.216	11.038	1.454	0.039	41
DOSExx_XC	47.71	-122.93	90	7.5	1.05	0.17	1
DOUGxx_XT	40.57	-108.69	-63	6.5	1.55	0.45	1
DP00xx_XJ	36.26	-117.66	-79	12	1.1	0.3	1
DPPxxx_CI	33	-116.94	56.758	6.937	1.175	0.131	4
DRYxxx_XT	40.7	-108.54	-14	2.001	0.975	0.025	2
DUGxxx_US	40.19	-112.81	-28.93	12.221	1.238	0.044	86
DVTxxx_CI	32.66	-116.1	22	10	1.1	0.3	1
E010xx_XU	48.1	-121.8	78.501	2.292	1.212	0.063	4
E020xx_XU	47.85	-121.63	63.525	11.243	1.075	0.172	6
E030xx_XU	47.45	-121.78	68.245	10.814	1.143	0.064	15
E03Axx_TA	46.55	-123.56	69.159	5.811	1.283	0.085	12
E04Axx_TA	46.59	-122.72	71.506	16.818	1.43	0.13	5
E04Dxx_TA	46.56	-122.57	73.246	11.35	1.148	0.078	21
E050xx_XU	46.77	-122.09	79.812	5.652	1.17	0.16	5
E05Axx_TA	46.56	-121.76	83.955	8.664	1.21	0.124	10
E060xx_XU	46.63	-121.26	-89.795	9.121	1.329	0.197	7
E06Axx_TA	46.54	-120.98	-83.652	28.64	1.5	0.218	3
E070xx_XU	46.51	-122.45	77.335	15.724	0.883	0.12	6
E07Axx_TA	46.56	-119.85	-65.311	7.486	1.229	0.081	7
E08Axx_TA	46.49	-119.06	-70.765	6.143	1.364	0.107	11
E09Axx_TA	46.51	-118.15	-79.437	24.1	1.16	0.171	10
E10Axx_TA	46.49	-117.11	-76.928	16.111	1.164	0.103	14
E11Axx_TA	46.36	-116.21	73.827	23.714	1.358	0.148	6
E12Axx_TA	46.42	-115.57	72.527	28.464	1.086	0.196	7
E13Axx_TA	46.44	-114.19	-89.686	9.003	1.16	0.108	10

E14Axx_TA	46.42	-113.49	76.418	7.201	1.243	0.063	20
E15Axx_TA	46.42	-112.64	56.45	20.313	1.136	0.088	14
E16Axx_TA	46.53	-111.68	60.944	10.955	1.733	0.096	6
E17Axx_TA	46.46	-110.86	58.145	16.707	1.454	0.132	13
E18Axx_TA	46.57	-109.91	44.982	20.002	1.23	0.115	5
E19Axx_TA	46.46	-108.79	53.018	21.839	1.181	0.125	8
E20Axx_TA	46.5	-108.13	61	5.013	1.225	0.125	2
E21Axx_TA	46.54	-107.08	85.345	25.364	0.66	0.058	5
E22Axx_TA	46.44	-105.95	41.593	24.704	0.795	0.091	11
E23Axx_TA	46.5	-105.31	-21.845	69.88	0.756	0.05	9
E24Axx_TA	46.56	-104.31	49.96	16.15	1.117	0.06	3
E25Axx_TA	46.5	-103.4	20.264	12.62	0.7	0.084	7
E26Axx_TA	46.47	-102.46	68.697	16.428	0.775	0.107	6
E27Axx_TA	46.43	-101.56	46.03	14.311	1.094	0.183	8
E28Axx_TA	46.57	-100.69	44.385	7.115	1.175	0.062	20
E28Bxx_N4	46.57	-100.69	42.845	7.317	1.189	0.11	9
E29Axx_TA	46.57	-99.64	22.04	11.912	1.26	0.09	10
E30Axx_TA	46.5	-98.91	34.141	9.232	0.9	0.073	9
E31Axx_TA	46.56	-97.89	50.765	14.542	0.8	0.039	14
E32Axx_TA	46.59	-97.07	16.361	6.783	0.96	0.207	5
E33Axx_TA	46.5	-96.01	22.964	14.818	1.011	0.085	9
E34Axx_TA	46.51	-95.17	42.392	9.051	0.925	0.072	16
E35Axx_TA	46.56	-94.4	53.428	10.134	1.094	0.074	9
E36Axx_TA	46.52	-93.26	47.492	8.709	1.286	0.049	21
E37Axx_TA	46.57	-92.4	61.492	12.777	1.095	0.073	10
E38Axx_N4	46.61	-91.55	49.541	8.228	1.375	0.092	4
E38Axx_TA	46.61	-91.55	55.516	17.288	0.89	0.128	10
E39Axx_TA	46.38	-90.56	62.163	8.736	0.85	0.071	4
ECSDxx_US	43.73	-96.61	6.419	61.025	0.923	0.076	13
EDW2xx_CI	34.88	-117.99	87.444	11.958	1.304	0.024	111
EDWxxx_CI	34.88	-117.99	79.586	9.093	1.3	0.117	5
EGMTxx_US	48.02	-109.75	62.822	8.741	1.067	0.057	45
EHMTxx_Z2	45.07	-111.19	71.314	5.571	1.533	0.188	3
ELFSxx_TA	40.62	-120.73	67.054	5.381	1.405	0.059	11
ELKSxx_AZ	33.58	-116.45	-76.5	0.5	1.15	0.15	2
ELKxxx_US	40.74	-115.24	-78.352	11.941	1.121	0.037	67
EMLxxx_CI	32.89	-116.85	62	1	0.8	0.15	2
EUOxxx_UO	44.03	-123.07	58.767	10.796	1.635	0.057	20
EYMNxx_US	47.95	-91.5	59.537	10.248	1.416	0.026	157
F03Axx_TA	45.93	-123.56	63.347	12.658	1.11	0.178	5
F04Axx_TA	45.93	-122.42	78.337	3.592	1.1	0.093	6

F04Dxx_TA	46.08	-123.01	77.527	8.797	1.306	0.052	31
F05Axx_TA	45.88	-121.46	84.909	6.112	1.269	0.055	8
F05Dxx_TA	45.89	-121.46	-88.29	9.404	1.3	0.117	15
F06Axx_TA	45.77	-120.78	-80.594	8.488	1.007	0.034	7
F07Axx_TA	45.9	-119.93	-67.779	23.188	1.16	0.106	10
F08Axx_TA	45.8	-118.78	-89.608	7.517	1.171	0.082	7
F09Axx_TA	45.71	-117.91	75.211	17.158	1.05	0.131	6
F10Axx_TA	45.97	-117.23	77.433	9.317	1.114	0.195	7
F11Axx_TA	45.89	-116.15	-77	8.053	1.15	0	2
F12Axx_TA	45.76	-115.25	29.441	27.778	0.914	0.09	14
F13Axx_TA	45.79	-114.33	74.848	5.778	1.3	0.104	7
F14Axx_TA	45.81	-113.37	69.681	9.192	1.358	0.178	6
F15Axx_TA	45.84	-112.49	39.32	7.056	1.033	0.13	6
F16Axx_TA	45.78	-111.63	40.898	30.825	1.33	0.335	5
F17Axx_TA	45.91	-110.66	64.784	5.573	1.48	0.187	5
F18Axx_TA	45.9	-109.72	63.639	12.434	1.06	0.081	5
F19Axx_TA	45.85	-108.94	50.868	13.474	1.1	0.122	10
F20Axx_TA	45.8	-108.15	53.243	28.146	1.081	0.089	8
F21Axx_TA	45.82	-107.12	-87.5	13.763	1.125	0.325	2
F22Axx_TA	45.78	-106.26	82.729	43.407	1.025	0.198	4
F23Axx_TA	45.72	-105.41	-89.784	17.969	0.88	0.054	20
F24Axx_TA	45.85	-104.44	89.647	15.073	0.918	0.077	11
F25Axx_TA	45.93	-103.46	33.194	12.988	1.122	0.125	9
F26Axx_TA	45.85	-102.67	53.757	11.231	0.85	0.118	9
F27Axx_TA	45.87	-102.02	71.557	11.932	1.033	0.053	21
F28Axx_TA	45.85	-100.8	42.93	10.257	1.118	0.082	14
F29Axx_TA	45.83	-99.83	53.585	6.174	0.91	0.044	21
F30Axx_TA	45.84	-99.03	64.942	16.305	0.806	0.07	8
F31Axx_TA	45.86	-98.25	49.122	11.427	0.925	0.147	8
F32Axx_TA	45.87	-97.13	37.689	13.512	0.994	0.053	17
F33Axx_TA	45.84	-96.29	33.778	8.647	0.958	0.056	18
F33Bxx_N4	45.84	-96.29	23.647	10.441	0.74	0.066	5
F34Axx_TA	45.8	-95.26	42.241	16.131	1.032	0.069	14
F35Axx_TA	45.86	-94.57	75.454	24.801	0.877	0.062	11
F36Axx_TA	45.86	-93.52	68.608	11.072	0.73	0.159	5
F36Bxx_N4	45.86	-93.52	58.217	6.026	0.75	0.108	4
F37Axx_TA	45.72	-92.63	57.625	6.586	0.9	0.056	12
F38Axx_TA	45.96	-91.88	56.045	8.336	0.906	0.089	9
F39Axx_TA	45.92	-90.92	60.375	11.581	1.211	0.05	14
F40Axx_TA	45.92	-90.12	58.535	11.925	1.148	0.068	20
FA09xx_XR	39.49	-91.79	3.5	41.041	1	0.05	2

FA10xx_XR	40.1	-92.67	69	13	0.6	0.17	1
FA11xx_XR	40.82	-93.29	63	5.013	0.625	0.175	2
FA12xx_XR	41.14	-93.71	46	3.5	1.15	0.2	1
FA13xx_XR	41.31	-94.01	43	1	0.65	0.2	2
FA14xx_XR	41.54	-94.26	51.5	2.502	1	0.2	2
FA15xx_XR	41.77	-94.47	48	9.5	0.55	0.12	1
FA16xx_XR	41.89	-94.6	43.967	7.516	1.217	0.12	3
FA17xx_XR	42.03	-94.84	49.682	11.972	0.683	0.06	3
FA18xx_XR	42.3	-95.05	58.32	5.808	0.967	0.148	3
FA19xx_XR	42.51	-95.35	58	16.5	0.7	0.3	1
FA20xx_XR	42.97	-95.98	70.582	9.757	0.856	0.075	9
FA22xx_XR	44.36	-98.22	58.094	8.9	0.9	0.154	4
FA23xx_XR	45.55	-99.98	60.827	4.224	0.883	0.036	6
FA24xx_XR	46.53	-101.24	23	1.633	0.75	0.218	3
FA25xx_XR	47.58	-103.3	86.248	31.407	0.721	0.083	7
FA26xx_XR	48.79	-105.43	41.152	10.376	1.185	0.12	10
FA28xx_XR	50.76	-111.52	44	14	1.1	0.43	1
FAC1xx_YW	45.04	-123.64	-86.354	5.196	1.1	0.275	3
FAC3xx_YW	44.41	-122.46	68.991	4.542	1.557	0.136	7
FACAxx_YW	47.86	-122.06	77.078	6.501	1.171	0.077	14
FACBxx_YW	47.89	-122.65	80.963	6.919	1.183	0.109	9
FACCxx_YW	47.4	-122.58	-81.5	0.5	1.45	0.4	2
FACDxx_YW	46.66	-122.85	71.612	5.774	1.031	0.065	8
FACFxx_YW	46.33	-122.78	75.324	8.541	1.008	0.084	6
FACGxx_YW	46.08	-123.18	82.429	9.668	1.064	0.103	7
FACHxx_YW	45.88	-123.22	-89.45	14.138	0.979	0.089	7
FACIxx_YW	45.72	-122.46	87.562	7.169	1.144	0.072	16
FACJxx_YW	45.3	-123.29	86.432	7.584	1.375	0.123	6
FACKxx_YW	44.84	-123.07	76.663	3.093	1.517	0.159	3
FACLxx_YW	44.14	-123.02	70.897	6.848	1.483	0.094	9
FACMxx_YW	43.78	-122.45	53.99	5.418	1.67	0.157	5
FACNxx_YW	43.7	-123.35	62.986	5.109	1.633	0.073	3
FACOxx_YW	43.54	-123.81	72.209	4.961	1.44	0.104	5
FACPxx_YW	43.21	-124.09	52.826	14.621	1.417	0.101	3
FACQxx_YW	42.91	-124.06	56.396	4.594	1.66	0.071	5
FACRxx_YW	43.43	-123.12	67.774	4.762	1.611	0.102	9
FACSxx_YW	42.79	-123.37	54.125	6.948	1.723	0.088	15
FACTxx_YW	42.56	-124.07	66.838	6.64	1.417	0.153	6
FACUxx_YW	42.26	-122.83	64.78	9.44	1.521	0.052	28
FACVxx_YW	42.16	-123.6	64.101	17.335	1.267	0.103	6
FARBxx_BK	37.7	-123	-42	2.001	0.975	0.075	2

FERNxx_CT	37.15	-121.81	-61.869	9.13	1.463	0.229	4
FISHxx_UW	45.93	-123.56	61.637	5.922	1.2	0.153	3
FLIPxx_XN	35.97	-120.53	-69	5.013	1.55	0.6	2
FLLxxx_XJ	37.28	-118.97	79.669	4.504	0.983	0.117	3
FLWYxx_IW	44.08	-110.7	70.838	11.4	1.278	0.069	27
FMPxxx_CI	33.71	-118.29	-78.261	12.301	1.475	0.073	16
FORKxx_UW	47.95	-124.57	-74.001	2.161	1	0.132	3
FRDxxx_AZ	33.49	-116.6	-82.185	10.862	1.332	0.053	64
FURxxx_CI	36.47	-116.86	-79.991	7.248	1.35	0.17	8
FVMxxx_NM	37.98	-90.43	62.927	23.346	0.95	0.084	11
FWGPxx_XT	40.96	-108.77	19	12.5	0.65	0.15	1
FXWYxx_IW	43.64	-111.03	47.287	12.573	1.391	0.078	28
G03Axx_TA	45.32	-123.28	77.749	8.303	1.3	0.144	3
G03Dxx_TA	45.21	-123.26	81.428	8.774	1.4	0.071	29
G04Axx_TA	45.21	-122.48	76.039	6.707	1.318	0.079	11
G05Axx_TA	45.24	-121.32	79.793	19.445	1.375	0.109	8
G05Dxx_TA	45.24	-121.32	79.15	12.582	1.248	0.069	26
G06Axx_TA	45.24	-120.64	-58.597	11.501	1.196	0.096	12
G07Axx_TA	45.27	-119.67	-58.816	14.855	1.433	0.167	6
G08Axx_TA	45.29	-118.96	66.852	31.505	1.42	0.207	5
G09Axx_TA	45.28	-117.78	85.837	16.124	1.059	0.096	11
G10Axx_TA	45.29	-117.12	-62.624	24.935	0.95	0.15	7
G11Axx_TA	45.4	-116.27	86.816	8.538	0.962	0.085	13
G12Axx_TA	45.13	-115.33	55.441	14.298	0.858	0.123	6
G13Axx_TA	45.09	-114.23	59.041	8.49	1.073	0.07	11
G14Axx_TA	45.24	-113.46	65.845	6.935	1.142	0.117	6
G15Axx_TA	45.17	-112.49	51.977	11.135	1.194	0.084	16
G16Axx_TA	45.23	-111.8	49.421	11.286	1	0.106	8
G17Axx_TA	45.32	-110.74	-85.726	5.9	1.412	0.047	4
G18Axx_TA	45.32	-109.56	85.437	18.82	1.038	0.074	8
G20Axx_TA	45.22	-108.21	41.061	15.46	1.211	0.105	14
G21Axx_TA	45.22	-107.21	36.991	13.483	0.967	0.093	3
G22Axx_TA	45.22	-106.29	62.363	43.442	0.775	0.078	4
G23Axx_TA	45.2	-105.39	-78.613	28.111	0.783	0.159	3
G24Axx_TA	45.33	-104.42	69.993	6.745	0.81	0.048	5
G25Axx_TA	45.19	-103.42	64.145	11.564	1.107	0.12	7
G26Axx_TA	45.29	-102.6	80.893	9.239	0.918	0.073	11
G27Axx_TA	45.38	-101.93	70.085	12.412	1.075	0.092	12
G28Axx_TA	45.07	-100.92	71.727	9.25	0.921	0.074	14
G29Axx_TA	45.19	-99.92	59.286	5.571	1.123	0.046	20
G30Axx_TA	45.13	-99.14	59.58	6.25	1.262	0.041	17

G31Axx_TA	45.23	-98.21	59.86	13.192	0.819	0.056	13
G32Axx_TA	45.26	-97.5	54.767	8.844	0.931	0.073	8
G33Axx_TA	45.19	-96.44	49.131	8.434	0.937	0.042	15
G34Axx_TA	45.24	-95.64	34.153	7.261	0.865	0.079	10
G35Axx_TA	45.22	-94.49	75.448	21.052	1.013	0.094	4
G36Axx_TA	45.23	-93.75	66.329	13.139	0.667	0.017	3
G38Axx_TA	45.17	-91.85	65.967	11.72	0.95	0.097	6
G39Axx_TA	45.29	-91.17	80.996	26.169	0.615	0.046	10
G40Axx_N4	45.27	-90.2	55.958	8.33	0.95	0.029	3
G40Axx_TA	45.27	-90.2	64.631	9.14	0.991	0.068	16
GASBxx_BK	39.65	-122.72	-83	5	0.95	0.25	1
GLACxx_AZ	33.6	-116.48	-88.629	14.497	1.167	0.28	3
GLAxxx_AZ	33.05	-114.83	-33	3.5	1.3	0.2	1
GLAxxx_CI	33.05	-114.83	-72.235	19.266	1.201	0.051	57
GLAxxx_TS	33.05	-114.83	-77.833	12.144	1.511	0.153	14
GLENxx_XN	35.93	-120.56	-66.219	13.365	1.44	0.271	5
GMRxxx_CI	34.78	-115.66	-86.872	13.06	1.125	0.063	48
GNWxxx_UW	47.56	-122.82	73.949	15.633	1.339	0.064	31
GNWxxx_UW	47.56	-122.83	73.949	15.633	1.339	0.064	31
GOBIxx_XN	35.94	-120.54	-73.659	3.775	1.933	0.361	3
GOLxxx_US	39.7	-105.37	31	10	0.55	0.12	1
GORxxx_CI	33.15	-117.23	83.699	8.115	1.25	0.139	8
GPOxxx_CI	35.65	-117.66	-88.669	2.626	1.083	0.136	3
GPOxxx_TS	35.65	-117.66	-89	5	1.25	0.15	1
GPSS1x_YS	42.5	-123.37	67	5	1.95	0.35	1
GRANxx_XT	41.11	-108.64	-19	4.5	1.95	0.38	1
GRAxxx_CI	37	-117.37	85.106	10.117	1.351	0.037	66
GSCxxx_CI	35.3	-116.81	-83.655	12.026	1.134	0.028	88
GSCxxx_TS	35.3	-116.81	-81.076	12.469	1.048	0.032	32
GULYxx_XN	35.95	-120.51	-75.29	7.969	1.733	0.488	3
GUNxxx_XG	38.47	-107.06	16	10.5	1.15	0.5	1
H02Axx_TA	44.68	-124	68	8	1.15	0.3	1
H03Axx_TA	44.68	-123.29	74.952	10.125	1.461	0.125	9
H04Axx_TA	44.68	-122.19	70.246	5.236	1.792	0.079	19
H04Dxx_TA	44.52	-122.74	62.029	7.984	1.694	0.045	32
H05Axx_TA	44.65	-121.23	81.401	5.703	1.446	0.106	13
H06Axx_TA	44.73	-120.33	-57.16	25.046	1.181	0.13	8
H07Axx_TA	44.59	-119.56	-87.313	21.218	1.294	0.118	9
H08Axx_TA	44.52	-118.67	65.468	9.169	1.05	0.052	10
H09Axx_TA	44.67	-117.66	78.899	7.719	1.25	0.057	7
H10Axx_TA	44.59	-116.75	84.375	6.797	1.37	0.204	5

H11Axx_TA	44.7	-116.01	81.767	10.645	1.204	0.064	13
H12Axx_TA	44.55	-114.86	71.739	9.049	1.177	0.067	26
H13Axx_TA	44.56	-114.25	70.791	12.36	1.079	0.062	17
H14Axx_TA	44.62	-113.37	67.977	19.929	1.32	0.187	5
H15Axx_TA	44.62	-112.64	42.682	9.748	1.337	0.063	8
H16Axx_TA	44.7	-111.25	49.213	15.897	1.244	0.103	9
H18Axx_TA	44.68	-109.66	55.5	25.064	0.85	0.1	2
H19Axx_TA	44.67	-108.99	-79	1	1.3	0.35	2
H20Axx_TA	44.49	-108	74.301	13.062	1.002	0.055	29
H21Axx_TA	44.63	-107.04	74.113	18.362	0.85	0.107	12
H22Axx_TA	44.59	-106.35	66.31	28.899	1.2	0.312	3
H23Axx_TA	44.56	-105.4	30	0	0.975	0.125	2
H24Axx_TA	44.75	-104.55	57.687	16.74	1.023	0.069	15
H25Axx_TA	44.62	-103.6	74.057	11.966	0.744	0.138	8
H26Axx_TA	44.62	-102.77	73.44	22.222	1.008	0.097	13
H27Axx_TA	44.63	-102.08	82.459	25.199	0.818	0.061	11
H28Axx_TA	44.68	-101.02	70.875	27.025	0.796	0.059	23
H29Axx_TA	44.63	-100.21	46.979	22.994	0.971	0.063	17
H31Axx_TA	44.48	-98.48	48.293	19.335	0.943	0.15	7
H32Axx_TA	44.5	-97.44	56.652	13.727	0.888	0.056	13
H33Axx_TA	44.68	-96.74	65.965	8.019	1.09	0.056	5
H34Axx_TA	44.67	-95.78	67.823	21.859	0.521	0.029	7
H35Axx_TA	44.7	-94.83	-82.308	26.675	0.844	0.09	9
H36Axx_TA	44.58	-93.93	-56.801	19.315	1.038	0.142	4
H37Axx_TA	44.58	-92.92	59.512	15.076	0.808	0.115	6
H38Axx_TA	44.68	-92.28	83.754	20.778	0.796	0.062	12
H39Axx_TA	44.68	-91.28	32.925	59.366	0.83	0.087	5
H40Axx_TA	44.62	-90.39	48.013	28.507	0.9	0.104	10
HASTxx_TA	36.39	-121.55	-78.25	1.479	1.9	0.124	4
HATCxx_TA	40.82	-121.46	51.627	7.767	1.219	0.098	8
HAWAxx_US	46.39	-119.53	-76.865	14.924	1.077	0.048	50
HEBOxx_UW	45.21	-123.76	81.987	12.708	1.288	0.061	21
HECxxx_CI	34.83	-116.33	-84.54	9.241	1.05	0.045	35
HELLxx_TA	36.68	-119.02	83.603	11.069	1.219	0.069	8
HGTCOx_GS	37.11	-104.67	1.977	22.467	1.267	0.174	3
HIAWxx_XT	41.01	-108.73	61.5	49.485	0.825	0.425	2
HIDExx_XN	35.97	-120.55	-78.5	2.502	1.9	0.3	2
HKTxxx_IU	29.96	-95.84	69.067	9.806	1.558	0.054	24
HLDxxx_XG	39.23	-109.14	61	19	0.85	0.38	1
HLIDxx_US	43.56	-114.41	81.347	13.084	1.805	0.026	198
HOODxx_UW	45.32	-121.65	75.053	7.869	1.469	0.035	52

HOPSxx_BK	38.99	-123.07	-39.5	18.112	1.2	0.195	4
HPIGxx_MX	26.94	-105.66	66	12	1.55	0.38	1
HSIGxx_MX	29.02	-110.95	62	7.035	1.05	0.2	2
HSLxxx_XG	39.03	-105.75	-6	4	1.8	0.37	1
HUMOxx_BK	42.61	-122.96	60.07	6.939	1.934	0.035	81
HVYxxx_XJ	36.7	-119.32	78.676	9.457	1.167	0.26	3
HWBxxx_AZ	33.03	-116.96	74.321	9.315	1.153	0.037	46
HWUTxx_US	41.61	-111.57	-84.865	15.096	1.19	0.078	29
I02Axx_TA	44	-123.83	66	12.183	1.45	0.3	2
I02Dxx_TA	44.11	-123.85	69.82	14.634	1.35	0.09	11
I03Axx_TA	43.97	-123.28	52.763	3.963	1.775	0.111	4
I03Dxx_TA	43.7	-123.35	60.763	5.232	1.651	0.05	36
I04Axx_TA	43.79	-122.41	58.998	7.318	1.571	0.036	49
I05Axx_TA	44.16	-121.27	74.597	8.445	1.756	0.099	8
I05Dxx_TA	44.34	-121.34	82.306	18.261	1.361	0.058	32
I06Axx_TA	43.94	-120.21	78.933	7.262	1.573	0.061	13
I07Axx_TA	44.08	-119.5	85.14	6.887	1.391	0.104	11
I08Axx_TA	43.91	-118.57	76.427	12.476	1.453	0.041	19
I09Axx_TA	43.97	-117.74	68.344	15.875	1.205	0.059	11
I10Axx_TA	44.09	-116.8	79.286	11.933	1.592	0.201	6
I11Axx_TA	43.91	-115.96	-81.915	7.365	1.607	0.086	15
I12Axx_TA	43.79	-115.13	83.259	7.984	1.83	0.084	22
I13Axx_TA	43.91	-114.12	68.373	6.325	1.605	0.054	33
I14Axx_TA	43.93	-113.45	51.28	11.243	1.528	0.136	9
I15Axx_TA	44	-112.49	44.01	19.278	1.195	0.095	10
I16Axx_TA	43.88	-111.49	82.073	6.193	1.355	0.088	11
I17Axx_TA	43.92	-110.58	69.168	11.922	1.5	0.075	6
I18Axx_TA	43.7	-109.82	85.335	4.114	1.225	0.115	6
I19Axx_TA	44.04	-108.99	-65.5	2.502	1.025	0.375	2
I20Axx_TA	43.95	-108.13	87.725	11.719	1.1	0.061	4
I21Axx_TA	43.81	-107.29	83.589	14.74	0.903	0.059	29
I22Axx_TA	43.89	-106.48	-82.349	12.942	1.25	0.114	4
I23Axx_TA	43.96	-105.46	84.557	19.814	0.783	0.217	3
I24Axx_TA	43.86	-104.63	33.5	3.504	1.025	0.075	2
I25Axx_TA	44.02	-103.73	-88.054	44.539	0.725	0.105	12
I26Axx_TA	44.03	-102.86	-59.796	19.325	1.01	0.049	24
I27Axx_TA	44.07	-102.05	-89.315	20.745	0.871	0.041	28
I28Axx_TA	44	-101.17	79.756	22.859	0.719	0.055	24
I29Axx_TA	44.02	-100.3	74.022	42.049	0.643	0.034	15
I30Axx_TA	43.91	-99.43	78.56	26.198	0.58	0.067	15
I31Axx_TA	44.03	-98.54	43.731	28.662	0.538	0.143	4

I32Axx_TA	44.03	-97.46	32.667	1.247	0.517	0.117	3
I33Axx_TA	44.05	-96.8	-66.5	12.707	1.05	0.15	2
I34Axx_TA	44.04	-95.86	86.829	30.364	0.78	0.124	5
I35Axx_TA	43.86	-94.98	67.126	34.587	0.789	0.071	9
I36Axx_TA	44.02	-94.01	72.601	19.759	0.761	0.077	9
I37Axx_TA	44.01	-93.4	65.968	37.362	1.014	0.162	7
I37Bxx_N4	44.01	-93.4	49	16.5	0.4	0.17	1
I38Axx_TA	44.04	-92.33	-58.093	27.379	0.661	0.035	9
I39Axx_TA	43.85	-91.52	68.229	9.05	0.65	0.076	3
I40Axx_TA	43.89	-90.62	-73.202	32.352	0.795	0.057	10
I40Bxx_N4	43.89	-90.62	-72.087	22.509	0.69	0.12	5
ICANxx_CT	37.5	-121.33	-73.396	20.915	1.36	0.201	5
ID001x_XC	43.29	-116.98	77.011	6.313	1.968	0.074	25
ID002x_XC	43.19	-116.51	87.979	7.174	1.675	0.178	8
ID004x_XC	42.92	-116.63	-86.988	4.767	1.644	0.104	8
ID005x_XC	42.83	-116.13	-81.032	7.32	1.731	0.06	29
ID007x_XC	42.66	-116.36	-81.344	5.303	1.79	0.04	42
ID008x_XC	42.55	-115.98	-75.373	5.757	1.626	0.061	34
ID009x_XC	42.6	-116.98	-80.022	13.313	1.653	0.08	36
ID010x_XC	42.54	-116.78	-81.722	10.395	1.629	0.048	56
ID014x_XC	42.34	-116.29	-81.458	7.154	1.592	0.05	45
ID015x_XC	42.31	-116.17	-78.636	8.133	1.656	0.069	40
ID016x_XC	42.29	-116.69	-84.119	9.01	1.685	0.066	36
ID017x_XC	42.28	-115.99	-80.041	9.471	1.428	0.054	41
IDAxxx_YC	45.42	-116.18	83	10	1	0.4	1
IMWxxx_IW	43.9	-110.94	62.874	10.371	1.283	0.048	55
IRMxxx_CI	34.16	-115.15	73.016	12.523	1.188	0.062	24
IRONxx_UW	43.36	-118.47	79.135	9.239	1.935	0.06	40
ISAxxx_CI	35.66	-118.47	86.842	20.474	1.228	0.116	9
ISAxxx_TS	35.66	-118.47	-89.67	17.533	0.917	0.224	3
ISCOxx_US	39.8	-105.61	40.309	25.736	1.032	0.049	31
ISKKxx_XN	36	-120.5	-37	10	0.8	0.17	1
IZEExx_UW	44.08	-119.5	82.638	13.69	1.354	0.091	14
J01Dxx_TA	43.16	-123.93	61.081	7.771	2.005	0.151	10
J01Exx_TA	43.16	-123.93	61.044	7.287	1.717	0.217	3
J02Axx_TA	43.37	-123.57	66.295	9.483	1.688	0.031	4
J03Axx_TA	43.37	-122.96	57.695	7.878	2.069	0.078	8
J04Axx_TA	43.24	-122.11	66.143	10.009	1.567	0.044	3
J04Dxx_TA	43.24	-122.11	67.183	13.771	1.531	0.059	21
J05Axx_TA	43.28	-121.24	76.715	4.237	1.743	0.124	7
J05Dxx_TA	43.28	-121.23	79.787	12.715	1.509	0.067	41

J06Axx_TA	43.25	-120.15	-88.98	9.113	1.703	0.104	17
J07Axx_TA	43.37	-119.31	88.753	10.241	1.674	0.079	17
J08Axx_TA	43.36	-118.47	79.248	6.441	1.962	0.081	29
J09Axx_TA	43.35	-117.75	75.342	7.353	2.07	0.061	27
J10Axx_TA	43.43	-116.77	81.222	5.921	2.071	0.074	24
J11Axx_TA	43.42	-115.83	89.907	5.729	1.948	0.052	48
J12Axx_TA	43.25	-115.1	85.055	4.958	1.602	0.06	24
J13Axx_TA	43.4	-114.17	82.732	15.347	1.505	0.065	37
J14Axx_TA	43.32	-113.52	74.564	10.982	1.38	0.13	5
J15Axx_TA	43.4	-112.43	76.461	17.206	1.121	0.095	7
J16Axx_TA	43.27	-111.61	69.381	9.764	1.312	0.121	8
J17Axx_TA	43.36	-110.71	46.969	13.194	1.337	0.067	8
J18Axx_TA	43.21	-110.02	65.628	18.686	1.171	0.068	7
J19Axx_TA	43.26	-109.05	79.073	13.033	1.179	0.088	26
J20Axx_TA	43.35	-108.08	70.665	2.496	1.4	0.202	3
J21Axx_TA	43.35	-107.45	-85.778	15.725	0.947	0.077	17
J22Axx_TA	43.41	-106.48	-84.654	15.394	0.733	0.064	21
J23Axx_TA	43.4	-105.55	79.827	23.912	0.664	0.083	11
J24Axx_TA	43.33	-104.66	84	6.022	0.975	0.075	2
J25Axx_TA	43.39	-103.8	58.811	15.633	0.94	0.102	10
J26Axx_TA	43.31	-103.08	-67.608	18.5	0.978	0.042	29
J27Axx_TA	43.25	-102.01	-70.312	10.472	1.033	0.066	27
J28Axx_TA	43.42	-101.24	-61.65	18.521	1.016	0.054	29
J29Axx_TA	43.41	-100.33	-76.102	23.486	0.611	0.056	19
J30Axx_TA	43.32	-99.49	-80.113	22.384	0.831	0.054	13
J31Axx_TA	43.29	-98.74	49.454	20.154	0.85	0.131	8
J32Axx_TA	43.37	-97.85	-49.593	18.747	1.073	0.052	15
J33Axx_TA	43.32	-96.97	73.2	36.469	0.759	0.079	11
J34Axx_TA	43.28	-95.96	39.934	24.368	0.727	0.056	11
J35Axx_TA	43.37	-95.21	68.01	8.516	0.845	0.065	10
J36Axx_TA	43.33	-94.34	65.999	15.789	0.842	0.045	18
J37Axx_TA	43.31	-93.55	78.578	27.177	0.86	0.074	15
J38Axx_TA	43.32	-92.48	41.293	11.272	0.77	0.102	5
J39Axx_TA	43.34	-91.71	66.863	35.48	0.7	0.124	7
J41Axx_TA	43.37	-90.01	86.561	7.024	0.7	0.072	5
JCCxxx_BK	40.82	-124.03	73.902	13.251	0.825	0.185	4
JCSxxx_CI	33.09	-116.6	-84.42	9.762	1.487	0.082	8
JCTxxx_US	30.48	-99.8	29.262	16.881	0.816	0.068	28
JEDSxx_UW	43.75	-124.05	63.24	13.958	1.509	0.089	11
JETSxx_XN	35.96	-120.51	-80	1	1.6	0.45	2
JFWSxx_US	42.91	-90.25	22.925	18.798	0.712	0.117	8

JNMTxx_XT	40.46	-108.02	48.668	1.886	1.917	0.033	3
JROxxx_CC	46.28	-122.22	-84.999	2.122	1.25	0.209	4
JRSCxx_BK	37.4	-122.24	-29.5	8.564	1.225	0.075	2
JTMTxx_MB	47.75	-114.28	62.085	22.509	1.261	0.113	9
JUNxxx_XJ	36.58	-118.41	77	5.5	1.5	0.2	1
K01Axx_TA	42.81	-124.47	68	5.013	2.15	0.45	2
K02Axx_TA	42.77	-123.49	58.828	9.067	1.659	0.053	11
K02Dxx_TA	42.7	-123.67	54.664	5.581	1.634	0.03	19
K04Axx_TA	42.61	-121.73	78.202	2.483	1.65	0.1	5
K04Dxx_TA	42.62	-121.75	73.412	10.16	1.46	0.059	36
K05Axx_TA	42.73	-120.89	79.383	6.52	1.771	0.121	19
K06Axx_TA	42.8	-120.25	84.334	6.169	1.905	0.117	19
K07Axx_TA	42.69	-119.25	85.369	6.474	1.938	0.074	30
K08Axx_TA	42.73	-118.49	85.62	5.929	1.941	0.064	23
K09Axx_TA	42.7	-117.73	86.912	8.889	1.954	0.067	24
K10Axx_TA	42.78	-116.87	-80.554	8.217	1.608	0.06	31
K11Axx_TA	42.77	-116.03	-78.906	7.054	1.634	0.053	34
K12Axx_TA	42.64	-114.9	-74.834	7.17	1.417	0.065	18
K13Axx_TA	42.65	-114.08	-65.368	11.797	1.065	0.04	31
K14Axx_TA	42.55	-113.18	86.563	6.804	1.293	0.117	7
K15Axx_TA	42.69	-112.53	68.777	8.212	1.45	0.099	7
K16Axx_TA	42.83	-111.59	86.844	22.117	1.794	0.135	8
K17Axx_TA	42.75	-110.92	54.912	8.572	1.2	0.229	3
K18Axx_TA	42.64	-110.04	58.785	14.676	1.062	0.195	4
K19Axx_TA	42.82	-108.85	-72.063	27.924	0.925	0.057	18
K20Axx_TA	42.66	-108.34	-89.906	13.481	1.422	0.167	9
K21Axx_TA	42.63	-107.25	73.713	10.798	0.988	0.11	8
K22Axx_TA	42.65	-106.52	-87.686	19.351	0.977	0.046	58
K23Axx_TA	42.75	-105.63	81.171	18.345	1.011	0.053	33
K24Axx_TA	42.72	-104.82	71.731	18.932	0.775	0.115	8
K25Axx_TA	42.61	-103.87	54.935	10.966	1.07	0.223	5
K26Axx_TA	42.7	-103.18	-74.882	16.48	0.886	0.046	25
K27Axx_TA	42.7	-102.24	81.229	15.292	1.042	0.076	12
K28Axx_TA	42.71	-101.37	-83.06	13.138	0.936	0.065	21
K29Axx_TA	42.76	-100.32	-74.604	9.623	0.994	0.115	8
K30Axx_TA	42.67	-99.61	73.951	19.174	0.596	0.072	13
K31Axx_TA	42.62	-98.75	81.6	22.79	0.654	0.035	13
K31Bxx_N4	42.62	-98.75	85.711	18.382	0.587	0.037	4
K32Axx_TA	42.66	-97.97	-66.572	13.489	0.825	0.047	18
K33Axx_TA	42.61	-97	-89.574	14.385	0.728	0.035	23
K34Axx_TA	42.69	-96.1	77.42	9.12	1.02	0.072	15

K35Axx_TA	42.72	-95.23	63.525	12.441	0.961	0.078	14
K36Axx_TA	42.64	-94.45	62.579	17.203	0.811	0.096	9
K37Axx_TA	42.77	-93.64	46.065	3.796	0.824	0.047	17
K38Axx_TA	42.65	-92.77	45.273	20.017	0.972	0.101	9
K39Axx_TA	42.71	-91.89	-64.754	26.276	1.1	0.325	3
K40Axx_TA	42.7	-91.14	33.568	11.676	1.217	0.224	3
K41Axx_TA	42.61	-90.3	27	12.183	1.2	0.15	2
KARLxx_XN	36.01	-120.52	-78	38.426	1.375	0.475	2
KCCxxx_BK	37.32	-119.32	85.381	10.26	1.465	0.075	10
KENTxx_UW	45.24	-120.64	-53.004	18.709	1.236	0.189	7
KIDDxx_EP	31.77	-106.51	1.21	19.538	1.615	0.086	20
KINNxx_XT	41.18	-108.59	6.5	8.564	0.725	0.225	2
KNBxxx_US	37.02	-112.82	23.999	1.732	0.925	0.043	4
KNWxxx_AZ	33.71	-116.71	-86.639	11.83	1.363	0.037	75
KRMxxx_XG	40.13	-106.4	50.5	21.492	1.45	0.1	2
KSCOxx_TA	39.01	-102.63	77.307	30.387	0.856	0.06	18
KSU1xx_US	39.1	-96.61	42.567	15.472	0.786	0.069	14
KVTXxx_US	27.55	-97.89	50.837	11.602	1.235	0.055	31
L01xxx_XF	41	-105.53	73	10.104	1.025	0.075	2
L02Axx_TA	42.16	-123.6	49.196	30.253	1.15	0.104	3
L02Dxx_TA	42.16	-123.6	62.536	7.067	1.343	0.058	14
L02Exx_TA	42.16	-123.6	55.06	10.948	1.48	0.122	5
L02xxx_XF	41.02	-105.54	75.5	14.829	1.1	0.1	2
L03xxx_XF	41.04	-105.55	62	4	0.95	0.17	1
L04Axx_TA	42.17	-121.89	67.493	14.118	1.6	0.082	6
L04Dxx_TA	42.22	-122.3	61.1	10.99	1.467	0.07	21
L04xxx_XF	41.06	-105.57	67	7.5	0.75	0.15	1
L05Axx_TA	42.05	-120.83	70.364	4.446	1.6	0.052	8
L05xxx_XF	41.08	-105.59	66	1	0.85	0.1	2
L06xxx_XF	41.1	-105.61	23	60.883	1.125	0.125	2
L07Axx_TA	42.02	-119.34	82.294	7.734	1.776	0.065	21
L07xxx_XF	41.12	-105.62	-44.034	51.749	1.12	0.145	5
L08Axx_TA	42.19	-118.34	88.124	5.682	1.64	0.076	20
L08xxx_XF	41.14	-105.64	-73.385	30.035	1.013	0.194	4
L09Axx_TA	42.02	-117.67	-87.23	7.599	1.723	0.063	20
L09xxx_XF	41.16	-105.66	77.652	31.349	1.138	0.059	4
L10Axx_TA	42.08	-116.47	-86.031	4.177	1.597	0.052	34
L10xxx_XF	41.18	-105.67	-79.772	47.972	0.92	0.133	5
L11Axx_TA	42.17	-115.75	-73.289	11.758	1.341	0.056	23
L11xxx_XF	41.2	-105.69	-73.38	29.656	0.987	0.126	4
L12Axx_TA	42.15	-115.02	-61.915	11.721	1.347	0.056	31

L12xxx_XF	41.22	-105.71	82	13.234	1.675	0.175	2
L13Axx_TA	42.09	-113.94	-63.375	10.381	1.015	0.048	17
L13xxx_XF	41.23	-105.73	-75.457	29.048	0.975	0.078	4
L14Axx_TA	42.03	-113.24	-60.779	8.959	0.98	0.102	5
L14xxx_XF	41.26	-105.74	57	28.217	1.45	0.3	2
L15Axx_TA	42	-112.39	53.872	27.325	1.175	0.116	4
L16Axx_TA	42.01	-111.43	62.966	13.59	1.114	0.097	11
L16xxx_XF	41.29	-105.79	61.759	45.975	1.125	0.127	4
L17Axx_TA	42.1	-110.87	33.891	30.913	0.94	0.255	5
L17xxx_XF	41.32	-105.79	-62.71	44.476	1.112	0.083	4
L18Axx_TA	41.92	-110.04	-25.882	37.549	1.225	0.06	4
L18xxx_XF	41.33	-105.81	-55.513	43.619	1.179	0.071	7
L19Axx_TA	42.1	-109.36	-76.874	15.381	1.1	0.115	6
L19xxx_XF	41.36	-105.83	-68.812	38.024	1.043	0.093	7
L20Axx_TA	42.01	-108.34	-86.708	11.977	0.9	0.161	8
L20xxx_XF	41.38	-105.84	69.426	37.299	0.962	0.043	4
L21Axx_TA	41.96	-107.37	88.244	31.714	1.15	0.102	9
L21xxx_XF	41.4	-105.86	-84.17	50.447	0.958	0.098	6
L22Axx_TA	42.03	-106.43	-80.379	21.764	0.964	0.133	7
L22xxx_XF	41.42	-105.88	-89.5	56.18	1.025	0.215	4
L23Axx_TA	42.11	-105.7	-83.135	24.346	0.763	0.101	8
L23xxx_XF	41.44	-105.89	80.104	31.652	1.075	0.22	4
L24Axx_TA	42.04	-104.93	59.796	12.074	0.97	0.108	5
L24xxx_XF	41.49	-105.89	-33	19.5	0.7	0.4	1
L25Axx_TA	42.15	-103.97	71.523	13.884	0.97	0.075	5
L25xxx_XF	41.48	-105.93	82	25.68	1.375	0.125	2
L26Axx_TA	42.04	-103.08	83.159	19.363	0.823	0.08	15
L26xxx_XF	41.5	-105.95	66.717	28.928	1.217	0.109	3
L27Axx_TA	42.08	-102.32	74.366	26.413	0.967	0.155	6
L27xxx_XF	41.52	-105.96	59	8	1.3	0.25	1
L28Axx_TA	42.01	-101.52	-85.202	11.503	0.928	0.094	9
L28xxx_XF	41.54	-105.98	-45.014	49.749	1.2	0.132	3
L29Axx_TA	42.06	-100.48	68.441	24.382	0.806	0.078	8
L29xxx_XF	41.56	-106	-8	74.212	1.5	0.05	2
L30Axx_TA	41.95	-99.72	-83.854	9.974	0.667	0.148	3
L30xxx_XF	41.59	-106.01	-88.84	30.69	1.263	0.2	4
L31Axx_TA	42.18	-98.84	66.513	9.961	1.031	0.071	8
L31xxx_XF	41.6	-106.03	78.38	31.354	1.217	0.188	3
L32Axx_TA	42	-98.01	-81.996	20.527	0.733	0.106	15
L33Axx_TA	42.17	-97.27	82.517	20.787	0.823	0.069	15
L34Axx_TA	41.97	-96.38	65.851	5.941	0.869	0.046	8

L34Bxx_N4	41.97	-96.38	70.274	7.317	0.69	0.048	5
L35Axx_TA	42.11	-95.54	39.251	18.943	0.943	0.091	14
L36Axx_TA	42.1	-94.67	42.144	15.575	0.745	0.071	11
L37Axx_TA	42.12	-93.75	59.296	4.769	1.142	0.077	13
L38Axx_TA	42.14	-92.96	58.561	11.09	1.038	0.076	12
L39Axx_TA	42.12	-92	52.946	19.003	0.74	0.081	5
L40Axx_N4	42.06	-91.22	78.501	19.221	0.8	0.161	3
L40Axx_TA	42.06	-91.22	83.254	10.955	0.913	0.139	4
L41Axx_TA	42.08	-90.5	65.394	31.73	0.683	0.107	6
LA02xx_GS	30.02	-91.15	-84	7.5	1.55	0.37	1
LAOxxx_US	46.69	-106.22	54.431	20.847	0.837	0.068	16
LAVAxx_TA	38.76	-120.74	77.371	11.785	1.345	0.119	11
LBTE5x_YA	36.06	-117.57	69	6.5	1.2	0.25	1
LBTN5x_YA	36.08	-117.6	63	9	1.6	0.53	1
LCCRxx_UW	45.21	-122.48	77.895	7.577	1.306	0.047	27
LDFxxx_CI	35.13	-115.18	72.933	14.237	1.345	0.117	11
LDSxxx_LB	37.24	-113.35	67	11	1.2	0.3	1
LEBAxx_UW	46.55	-123.56	68.497	8.13	1.288	0.045	26
LEDxxx_XG	39.15	-106.35	-33	13	0.6	0.15	1
LEEPxx_XN	35.99	-120.51	-66	23.253	1.2	0.1	2
LGUxxx_CI	34.11	-119.07	74.695	16.127	1.429	0.055	29
LIZxxx_XG	39.36	-104.55	7	12.5	0.95	0.28	1
LKLxxx_CI	34.62	-117.82	-89	2.001	1.325	0.175	2
LKWYxx_US	44.57	-110.4	-43.72	12.846	1.806	0.126	9
LLLBxx_CN	50.61	-121.88	6.715	6.34	1.033	0.103	6
LMCxxx_XJ	36.36	-119.03	-83	5	1	0.18	1
LMNxxx_XG	39.42	-103.62	18	8.053	0.975	0.225	2
LMPxxx_XH	37.98	-111.2	16.811	8.991	1.087	0.155	4
LOHWxx_IW	43.61	-110.6	54.61	13.083	1.219	0.066	27
LONxxx_UW	46.75	-121.81	-88.461	16.317	1.316	0.095	19
LRIVxx_UW	48.06	-123.5	79.558	7.799	1.335	0.044	34
LRLxxx_CI	35.48	-117.68	83.062	11.288	1.293	0.051	38
LSCxxx_XT	40.53	-108.44	-63	2	2.1	0.27	1
LTHxxx_LI	46.46	-119.42	-60.229	18.776	1.177	0.134	11
LTLxxx_LI	30.54	-90.77	76.752	5.417	1.263	0.136	4
LTXxxx_US	29.33	-103.67	-83.275	9.677	0.91	0.18	5
LTYxxx_UW	47.25	-120.67	-85.838	12.943	1.229	0.067	35
LTYxxx_UW	47.26	-120.67	-85.838	12.943	1.229	0.067	35
LVA2xx_AZ	33.35	-116.56	87.912	15.346	1.098	0.063	33
LYAxxx_Y5	51.16	-113.47	42.706	22.774	1.071	0.043	26
M01Cxx_TA	41.85	-124.12	61	16	0.7	0.38	1

M02Cxx_TA	41.39	-122.85	69.904	9.101	1.167	0.037	53
M03Cxx_TA	41.27	-122.12	70.018	7.714	1.513	0.065	8
M04Cxx_TA	41.78	-121.84	62.558	12.946	1.395	0.052	20
M05Cxx_TA	41.36	-121.15	58.544	14.285	1.375	0.137	8
M06Cxx_TA	41.2	-120.48	71.87	6.295	1.538	0.078	17
M07Axx_TA	41.39	-119.17	80.936	5.268	1.932	0.105	14
M08Axx_TA	41.45	-118.38	-82.477	7.911	1.654	0.089	12
M09Axx_TA	41.42	-117.45	82.94	4.001	1.654	0.075	14
M10Axx_TA	41.52	-116.54	-74.563	15.376	1.297	0.038	29
M11Axx_TA	41.43	-115.79	-84.614	9.27	1.322	0.041	20
M12Axx_TA	41.42	-114.92	-67.592	8.862	1.069	0.09	16
M13Axx_TA	41.36	-114.17	-43.367	7.817	1.203	0.076	15
M14Axx_TA	41.5	-113.35	-29.993	14.521	0.7	0.054	4
M15Axx_TA	41.46	-112.45	4.921	6.651	0.906	0.067	9
M16Axx_TA	41.31	-111.63	-58.873	12.59	1.2	0.122	6
M17Axx_TA	41.47	-110.67	46	7	0.9	0.15	1
M18Axx_TA	41.43	-110.07	-43	8.5	0.75	0.17	1
M19Axx_TA	41.5	-109.16	17.734	12.591	0.8	0.057	7
M20Axx_TA	41.49	-108.19	-61.321	31.52	1.217	0.19	6
M21Axx_TA	41.61	-107.36	-85.237	21.447	0.95	0.099	16
M22Axx_TA	41.4	-106.6	-65.685	13.418	0.95	0.097	8
M23Axx_TA	41.47	-105.72	89.256	24.685	0.863	0.072	8
M24Axx_TA	41.47	-104.82	42	19	0.6	0.28	1
M25Axx_TA	41.43	-104.06	52.109	7.195	1.67	0.166	5
M26Axx_TA	41.47	-103.14	73.101	17.295	1.055	0.161	10
M27Axx_TA	41.53	-102.39	66.013	14.413	0.975	0.135	6
M28Axx_TA	41.4	-101.37	45.38	35.729	0.89	0.181	5
M29Axx_TA	41.44	-100.69	43.243	22.303	0.9	0.089	4
M30Axx_TA	41.54	-99.87	19	12	0.75	0.23	1
M31Axx_TA	41.34	-98.98	69	6.022	0.75	0.2	2
M33Axx_TA	41.57	-97.19	-87.254	13.56	0.813	0.059	23
M34Axx_TA	41.5	-96.58	73.871	5.946	0.943	0.035	21
M35Axx_TA	41.47	-95.69	68.857	7.765	0.977	0.053	22
M36Axx_TA	41.45	-94.8	53.799	9.157	1.006	0.051	17
M37Axx_TA	41.4	-94.06	42.511	8.682	1.035	0.102	13
M38Axx_TA	41.42	-93.2	62.03	8.004	1	0.07	16
M39Axx_TA	41.48	-92.17	56.502	14.905	0.964	0.1	11
M40Axx_TA	41.41	-91.51	62.58	24.749	0.832	0.059	11
M41Axx_TA	41.38	-90.54	63.558	18.595	1.087	0.071	8
MAP0xx_XA	44	-123.83	65	3.003	1.425	0.075	2
MAP0xx_XN	44	-123.83	66.741	3.769	1.375	0.052	4

MB01xx_XM	33.34	-106.03	19.625	23.123	1.15	0.157	6
MB04Bx_XM	34.07	-106.94	53.671	6.146	1.183	0.219	3
MB04xx_XM	34.07	-106.92	53	6.5	1.85	0.38	1
MB05xx_XM	34.66	-108.01	62	16	1.45	0.68	1
MCCMxx_BK	38.14	-122.88	-53.631	16.75	1.581	0.156	13
MDNDxx_TA	47.85	-99.6	40.716	14.248	1.074	0.035	39
MDWxxx_XH	38.89	-112.36	-7.115	3.96	1.356	0.111	9
ME01xx_XQ	41.78	-123.4	46.776	5.268	1.35	0.144	4
ME02xx_XQ	41.69	-122.34	65.128	7.585	1.35	0.074	5
ME03xx_XQ	41.7	-123.88	48	25.68	0.675	0.125	2
ME04xx_XQ	41.35	-123.51	16	18.5	0.8	0.3	1
ME05xx_XQ	41.53	-122.05	65.003	17.661	1.233	0.096	6
ME06xx_XQ	41.34	-121.69	67.778	18.354	1.308	0.069	6
ME08xx_XQ	40.22	-123.31	-39	19.5	1.05	0.5	1
ME09xx_XQ	41.09	-122.73	55.056	21.813	1.1	0.187	8
ME10xx_XQ	40.96	-122.46	47.6	8.221	1.117	0.044	3
ME11xx_XQ	41.06	-121.37	63.013	11.762	1.255	0.124	10
ME12xx_XQ	40.1	-122.5	86.143	10.009	0.867	0.217	3
ME13xx_XQ	40.76	-122.92	43.881	21.727	0.938	0.211	4
ME14xx_XQ	41.01	-121.9	61.994	3.562	1.133	0.083	3
ME15xx_XQ	40.81	-121.68	61.836	13.651	1.34	0.144	5
ME16xx_XQ	40.58	-122.09	68.83	20.862	1.319	0.138	8
ME17xx_XQ	40.54	-121.72	45	6	1.1	0.17	1
ME18xx_XQ	40.73	-121.02	69.877	10.327	1.381	0.085	8
ME20xx_XQ	40.48	-120.98	73.027	11.458	1.209	0.054	11
ME21xx_XQ	40.35	-121.24	73	1	0.775	0.175	2
ME22xx_XQ	40.12	-121.56	77.143	10.009	0.933	0.083	3
ME23xx_XQ	40.4	-121.46	70.343	9.165	1.55	0.186	4
ME24xx_XQ	40.36	-122.05	29.801	9.742	1.35	0.076	3
ME25xx_XQ	40.29	-121.8	68.86	21.609	0.883	0.13	3
ME26xx_XQ	40.16	-122.1	12	9	0.7	0.15	1
ME27xx_XQ	40.45	-123.15	4	9	0.95	0.23	1
ME28xx_XQ	40.33	-122.47	18	14.295	1.2	0.45	2
ME29xx_XQ	41.14	-123.14	67.38	9.529	1.183	0.196	3
ME30xx_XQ	40.84	-123.57	50	9	1.05	0.2	1
ME32xx_XQ	40.59	-123.86	-84	4	1.85	0.33	1
ME37xx_XQ	40.28	-123.65	79	18	0.75	0.25	1
ME38xx_XQ	40.1	-123.5	-64	23.253	1.025	0.075	2
ME39xx_XQ	40.19	-123.59	-57.5	52.144	1.5	0.3	2
ME44xx_XQ	39.49	-123.19	-48	6.022	1.625	0.125	2
ME46xx_XQ	39.2	-122.97	-47	9.5	1.1	0.32	1

ME49xx_XQ	39.86	-123.72	-32	13.5	1.2	0.35	1
ME52xx_XQ	39.32	-123.22	-48	4	1.8	0.32	1
ME53xx_XQ	39.22	-123.59	-36	18	1.05	0.42	1
ME54xx_XQ	39.01	-123.38	-47	9.076	0.975	0.025	2
ME55xx_XQ	38.66	-123.08	-66	6	1.2	0.18	1
ME56xx_XQ	39.89	-122.87	-22	8.5	1.05	0.2	1
ME57xx_XQ	39.91	-122.57	-24	6	1	0.13	1
ME60xx_XQ	39.95	-121.54	53	9	1.1	0.32	1
ME61xx_XQ	39.53	-122.3	-20	11	0.75	0.18	1
ME64xx_XQ	39.28	-122.16	-34	15	0.9	0.3	1
ME80xx_XQ	40.35	-120.6	79.259	14.556	1.388	0.096	8
ME81xx_XQ	40.11	-121.17	86.057	11.069	1.525	0.136	6
ME82xx_XQ	39.72	-121.53	88.265	26.975	1.075	0.116	6
ME83xx_XQ	40.18	-120.4	85.665	3.303	1.683	0.311	3
ME84xx_XQ	40.03	-120.19	79.165	23.839	1.39	0.141	5
ME85xx_XQ	40.01	-120.64	75.447	14.362	0.833	0.073	3
ME86xx_XQ	39.8	-120.71	-73	19.775	1.125	0.175	2
ME87xx_XQ	39.68	-121.09	-83	4.5	1.05	0.12	1
ME88xx_XQ	39.24	-121.35	31.5	81.516	0.6	0.1	2
ME89xx_XQ	39.38	-121.16	-35	19.5	0.55	0.32	1
ME90xx_XQ	39.48	-120.85	-17	7	0.8	0.12	1
ME91xx_XQ	39.65	-120.22	85	17.543	0.9	0.4	2
ME92xx_XQ	39.47	-120.04	-87	2.001	1.125	0.175	2
ME93xx_XQ	39.05	-120.15	69	13.234	1.075	0.075	2
MEGWxx_UW	46.27	-123.88	53.89	9.327	1.362	0.068	20
MFIDxx_IW	43.42	-115.83	88.976	6.436	1.799	0.044	59
MGExxx_CI	33.82	-116.37	78.512	7.963	1.388	0.043	4
MGMOxx_NM	37.15	-92.27	41.946	13.076	1.063	0.114	15
MHBxxx_Y5	50.32	-110.16	53.574	19.913	1.367	0.442	3
MHTCOx_GS	37.13	-104.69	-3	2.001	1.075	0.175	2
MIARxx_US	34.55	-93.58	79.076	22.119	1.053	0.052	38
MKRxxx_XG	40.03	-107.74	62.731	37.908	0.88	0.159	5
MLACxx_CI	37.63	-118.84	54.603	12.028	1.368	0.041	36
MLACxx_TS	37.63	-118.83	56.161	7.883	1.545	0.094	10
MM18xx_XA	38.53	-90.57	64.689	5.449	1.1	0.076	3
MNRCxx_BK	38.88	-122.44	-54.826	14.699	1.45	0.104	4
MNTXxx_US	31.7	-105.38	35	14.871	1.056	0.039	68
MNVxxx_US	38.43	-118.15	81.77	12.779	1.357	0.093	14
MODxxx_BK	41.9	-120.3	74.11	16.628	1.473	0.051	13
MOH9xx_XN	35.97	-120.57	-77	1	1.95	0.25	2
MONP2x_AZ	32.89	-116.42	89.883	11.629	1.282	0.093	14

MONPxx_AZ	32.89	-116.42	89.078	16.962	1.318	0.096	14
MONxxx_XG	38.53	-108	-11.5	0.5	0.7	0.1	2
MOOWxx_IW	43.75	-110.74	59.922	15.759	1.399	0.064	41
MPK01x_GS	37.51	-121.88	-73	6	2.3	0.45	1
MPMxxx_CI	36.06	-117.49	-84.388	15.388	1.514	0.101	14
MPPxxx_CI	34.89	-119.81	-48.604	16.868	1.387	0.092	12
MRBLxx_UW	48.52	-121.48	76.986	8.822	1.203	0.039	35
MREDxx_XN	35.96	-120.48	-76.5	20.343	1.45	0.55	2
MSJxxx_CI	33.81	-116.97	15.5	9.589	1.8	0.3	2
MSOxxx_US	46.83	-113.94	-85.287	15.061	1.307	0.045	106
MSTXxx_TA	33.97	-102.77	-2.416	22.774	0.933	0.034	41
MTPxxx_CI	35.48	-115.55	-78	8.5	0.75	0.1	1
MURxxx_CI	33.6	-117.2	88.135	10.077	1.215	0.031	63
MVCOxx_US	37.21	-108.5	17.21	14.949	1.108	0.077	30
MVUxxx_LB	38.5	-112.21	-44	2.5	1.8	0.35	1
MWCxxx_CI	34.22	-118.06	79.333	10.732	1.234	0.037	47
N00xxx_XK	42.46	-107.7	-76.132	27.82	1.033	0.295	3
N01xxx_XK	42.28	-107.6	89.737	8.027	1.088	0.165	4
N01xxx_XP	40.14	-106.88	71.039	27.682	1.087	0.149	4
N01xxx_XS	46.28	-109.41	58	1	1.125	0.375	2
N020xx_XU	47.12	-123.97	62.369	14.429	1.062	0.075	4
N025xx_XU	47.16	-123.92	-86	14.5	0.95	0.38	1
N02Cxx_TA	40.82	-123.31	46	66.111	1.275	0.025	2
N02Dxx_TA	40.97	-122.71	63.115	30.496	1.093	0.046	28
N02xxx_XK	42.15	-107.5	-76.322	26.649	1.208	0.091	6
N02xxx_XP	40.1	-106.21	84.628	26.126	1.08	0.14	5
N02xxx_XS	46.25	-109.21	38	0	0.725	0.025	2
N030xx_XU	47.19	-123.86	74	4.5	1.25	0.2	1
N03xxx_XP	40.04	-107.89	57.331	10.612	1.167	0.069	6
N040xx_XU	47.19	-123.61	86	8	0.95	0.15	1
N04xxx_XK	41.98	-107.43	74.54	31.784	1.567	0.174	3
N04xxx_XP	39.92	-106.72	84.868	23.814	1.188	0.094	12
N04xxx_XS	46.21	-108.54	68.215	34.589	0.6	0.029	3
N050xx_XU	47.22	-123.4	62	13	1	0.28	1
N05xxx_XK	41.89	-107.39	-65.077	15.399	0.867	0.192	3
N05xxx_XP	39.89	-106.31	87.274	14.733	1.112	0.081	8
N05xxx_XS	46.25	-108.3	66	3	0.75	0.1	1
N060xx_XU	47.15	-123.16	79.607	11.69	1.235	0.093	10
N06Axx_TA	40.75	-119.83	78.744	12.069	1.603	0.081	15
N06xxx_XK	41.8	-107.35	27	16.5	0.7	0.25	1
N06xxx_XP	39.73	-107.06	-89.818	25.432	1.108	0.17	6

N06xxx_XS	46.42	-109.52	59.496	3.779	1.225	0.171	4
N070xx_XU	47.05	-122.72	81.5	4.509	0.95	0.15	2
N07Axx_TA	40.77	-118.97	89	11	1.1	0.25	1
N07Bxx_TA	40.78	-118.97	85.262	5.606	1.682	0.119	14
N07xxx_XK	41.72	-107.32	-40	19	0.6	0.43	1
N07xxx_XS	46.44	-109.24	60.001	2.161	1.133	0.283	3
N080xx_XU	47.16	-122.55	86	3	1.95	0.25	1
N085xx_XU	47.07	-122.38	70.878	12.438	1.214	0.144	7
N08Axx_TA	40.78	-118.13	-87.335	4.012	1.562	0.114	12
N08xxx_XK	41.62	-107.28	72.931	16.849	0.75	0.236	3
N08xxx_XP	39.55	-106.05	-36.37	41.164	1.4	0.208	3
N08xxx_XS	46.5	-108.86	-46.5	23.851	1.675	0.225	2
N090xx_XU	47.19	-122.2	73.021	11.065	1.06	0.199	5
N09Axx_TA	40.85	-117.52	-87.028	7.022	1.547	0.11	15
N09xxx_XK	41.54	-107.24	88.475	29.796	0.9	0.148	8
N09xxx_XP	39.49	-107.11	-80.67	29.442	1.12	0.138	5
N09xxx_XS	46.51	-108.59	65	1	1.4	0.05	2
N100xx_XU	47.29	-121.79	70	9.076	0.975	0.025	2
N10Axx_TA	40.72	-116.51	87.817	9.404	1.272	0.063	16
N10xxx_XK	41.45	-107.21	-86.227	17.324	1.012	0.152	4
N10xxx_XP	39.48	-107.88	-62	25.68	1.1	0	2
N10xxx_XS	46.61	-109.19	50.333	1.247	0.783	0.033	3
N110xx_XU	47.15	-121.64	82.798	6.456	1.294	0.085	8
N11Axx_TA	40.82	-115.74	86.762	9.179	1.212	0.072	13
N11xxx_XP	39.34	-107.21	88.29	20.322	1.333	0.203	3
N11xxx_XS	46.67	-108.89	52.516	11.352	0.975	0.092	4
N120xx_XU	47.22	-121.48	76.507	8.485	1.115	0.092	10
N12Axx_TA	40.85	-115.04	-78.79	13.62	1.05	0.144	9
N12xxx_XK	41.25	-107.25	-28	18	0.85	0.43	1
N12xxx_XP	39.27	-108.21	59	11.5	1.15	0.35	1
N12xxx_XS	46.65	-108.65	59.268	11.766	0.938	0.083	4
N130xx_XU	47.25	-121.05	-79.429	13.24	0.957	0.106	15
N13Axx_TA	40.86	-114.2	-32.846	15.229	0.888	0.055	13
N13xxx_XK	41.16	-107.22	-48.984	25.609	1.083	0.174	3
N13xxx_XP	39.23	-106.3	-44.72	11.173	1.15	0.16	5
N14Axx_TA	40.85	-113.19	-23	0	0.7	0.05	2
N14Axx_XK	41.08	-107.18	-68.5	10.621	1.05	0	2
N14xxx_XK	41.08	-107.18	39.5	6.528	1.2	0.1	2
N14xxx_XP	39.21	-107.95	-28.5	30.206	1.475	0.225	2
N15Axx_TA	40.89	-112.52	-3.853	11.227	1.07	0.07	10
N15Axx_XK	41	-107.03	41	15	0.65	0.27	1

N15xxx_XP	39.19	-105.76	-12.378	40.314	0.9	0.074	4
N16Axx_TA	40.89	-111.44	78.332	3.686	1.067	0.309	3
N16xxx_XK	40.92	-106.99	70	48.264	1.125	0.275	2
N16xxx_XP	39.15	-108.59	-1	15	0.95	0.38	1
N17Axx_TA	40.94	-110.83	-56.65	10.16	0.97	0.06	5
N17xxx_XK	40.81	-106.94	59.5	10.621	1.225	0.225	2
N17xxx_XP	39.07	-106.48	89.293	55.817	1.09	0.083	5
N18xxx_XP	39.02	-107.36	-47	12	1.15	0.32	1
N19Axx_TA	40.89	-109.18	79	18.5	0.85	0.43	1
N19xxx_XP	39	-105.56	63	66.111	0.9	0.15	2
N20Axx_TA	40.83	-108.26	-72	7.035	1.4	0	2
N20xxx_XK	40.57	-106.88	62	13	1.05	0.32	1
N20xxx_XP	38.92	-106.19	0.344	22.093	1.083	0.159	3
N21Axx_TA	40.76	-107.52	25.234	14.153	0.67	0.098	5
N21xxx_XK	40.45	-106.92	56.997	14.056	1.029	0.09	7
N21xxx_XP	38.87	-108.51	-58.276	33.616	0.8	0.161	3
N22Axx_TA	40.8	-106.45	35.924	29.566	1.042	0.1	13
N22xxx_XP	38.81	-107.82	-26	25.68	0.8	0	2
N23Axx_TA	40.89	-105.94	80.871	35.732	1.051	0.041	41
N23xxx_XP	38.76	-105.52	-69	9.076	0.75	0.1	2
N24Axx_TA	40.83	-104.88	86.474	8.123	1.035	0.081	10
N24xxx_XK	40.21	-106.78	80	7.5	1.1	0.2	1
N24xxx_XP	38.69	-106.1	-33.74	21.995	1.1	0.058	3
N25Axx_TA	40.81	-104.09	60.815	23.757	1.108	0.151	6
N25xxx_XK	40.13	-106.7	46	2.001	1.05	0.1	2
N25xxx_XP	38.64	-108.01	8.5	4.509	1.6	0.1	2
N26Axx_TA	40.83	-103.22	66.161	13.195	1.078	0.118	9
N26xxx_XK	40.05	-106.66	67	19.329	0.95	0.115	3
N26xxx_XP	38.51	-106.73	51.913	31.231	1.233	0.393	3
N27Axx_TA	40.81	-102.54	73.316	11.773	0.887	0.109	4
N27xxx_XP	38.49	-107.32	25	5	1.85	0.2	1
N28Axx_TA	40.69	-101.54	74.397	14.454	0.855	0.085	10
N29Axx_TA	40.82	-100.63	31	3.003	0.725	0.125	2
N29xxx_XP	38.4	-106.48	-64.5	5.517	1.25	0.1	2
N30Axx_TA	40.8	-100.1	-64.079	18.729	0.783	0.158	6
N31Axx_TA	40.82	-98.95	62.974	24.073	0.829	0.064	7
N32Axx_TA	40.76	-98.3	82.982	20.747	0.847	0.065	17
N33Axx_TA	40.74	-97.45	56.981	13.071	0.912	0.044	24
N33Bxx_N4	40.74	-97.45	65.973	17.555	1.05	0.117	4
N34Axx_TA	40.84	-96.5	73.045	13.217	1.013	0.078	15
N35Axx_TA	40.86	-95.64	77.453	10.996	0.958	0.047	19

N35Bxx_N4	40.86	-95.64	87.014	9.138	0.883	0.086	6
N36Axx_TA	40.82	-94.96	68.398	8.702	1.063	0.054	24
N37Axx_TA	40.76	-94.21	58.749	12.94	0.819	0.048	13
N38Axx_TA	40.79	-93.24	75.455	19.238	0.828	0.037	9
N39Axx_TA	40.88	-92.5	61.794	4.922	0.945	0.057	10
N40Axx_TA	40.88	-91.58	69.698	24.448	0.793	0.079	15
N41Axx_TA	40.71	-90.86	58.687	17.506	0.735	0.055	10
N42Axx_TA	40.83	-90.03	84.324	4.998	0.983	0.169	3
NATXxx_US	31.76	-94.66	68.005	13.641	1.286	0.057	21
NE70xx_NR	32.42	-115.26	-38	14.951	1.467	0.159	3
NE71xx_NR	31.69	-115.91	83.125	17.225	1.423	0.137	15
NE72xx_NR	30.85	-116.06	83.352	5.26	1.333	0.159	3
NE73xx_NR	30.07	-115.35	81.506	24.143	0.9	0.106	7
NE74xx_NR	28.01	-114.01	81.547	10.621	0.983	0.306	3
NE75xx_NR	27.29	-112.86	-64.602	19.261	1.09	0.119	5
NE76xx_NR	26.89	-112	-47	38.426	1.3	0.3	2
NE77xx_NR	26.02	-111.36	52.793	14.851	1.075	0.364	4
NE78xx_NR	24.4	-111.11	54	11.14	1.125	0.025	2
NE80xx_NR	30.5	-112.32	48.134	13.284	0.936	0.098	7
NE81xx_NR	28.92	-109.64	69.429	16.063	1.295	0.091	20
NE82xx_NR	26.92	-109.23	75.492	8.705	1.262	0.062	25
NE83xx_NR	24.73	-107.74	79.218	11.745	1.3	0.163	6
NE84xx_NR	24.91	-111.55	73	10.5	0.95	0.17	1
NE85xx_NR	24.13	-110.44	88	15	1	0.4	1
NEE2xx_CI	34.77	-114.62	59.285	14.533	0.934	0.033	45
NEExxx_CI	34.82	-114.6	50.302	12.26	0.782	0.035	17
NEExxx_TS	34.82	-114.6	60.84	11.386	0.769	0.022	18
NEWxxx_US	48.26	-117.12	76.151	8.78	1.201	0.022	105
NLKCGx_X9	32.87	-96.97	77.257	18.272	1.33	0.306	5
NLWAxx_US	47.39	-123.87	86.639	12.193	1.174	0.068	23
NM07xx_XM	32.08	-103.84	27	3.269	0.867	0.13	3
NM08xx_XM	32.2	-103.97	1.369	22.842	0.917	0.342	3
NM09xx_XM	32.33	-104.12	30.563	12.486	1.15	0.148	7
NM10xx_XM	32.47	-104.27	38.729	18.578	1.128	0.068	9
NM11xx_XM	32.58	-104.41	41.572	10.755	1.054	0.111	13
NM12xx_XM	32.68	-104.51	26.48	12.336	0.942	0.055	13
NM13xx_XM	32.8	-104.65	10.673	7.859	1.02	0.111	5
NM14xx_XM	32.91	-104.76	37.436	9.614	0.95	0.07	11
NM15xx_XM	33.01	-104.91	42.085	8.766	1.23	0.072	10
NM16xx_XM	33.17	-105.13	41.563	8.034	1.093	0.046	7
NM17xx_XM	33.26	-105.17	32.333	14.72	0.985	0.062	10

NM18xx_XM	33.4	-105.34	27.433	13.626	1.178	0.099	9
NM19xx_XM	33.49	-105.46	30.808	11.847	1.094	0.068	8
NM20xx_XM	33.6	-105.59	32.863	13.147	1.183	0.103	12
NM22xx_XM	33.84	-105.87	33.215	11.606	1.471	0.145	7
NM23xx_XM	33.95	-106.01	37.594	8.981	1.65	0.154	4
NM24xx_XM	34.05	-106.12	42.5	7.544	1.25	0.05	2
NM25xx_XM	34.17	-106.26	48.5	0.5	1.675	0.425	2
NM26xx_XM	34.26	-106.36	39.112	15.372	1.05	0.141	6
NM27xx_XM	34.39	-106.52	50.502	4.16	1.55	0.248	4
NM28xx_XM	34.54	-106.7	66	20.916	1.25	0.2	2
NM29xx_XM	34.65	-106.85	30.5	10.621	1.7	0.2	2
NM30xx_XM	34.74	-106.97	46	17.5	1.05	0.45	1
NM31xx_XM	34.85	-107.1	24.207	19.482	1.12	0.094	10
NM32xx_XM	34.98	-107.26	45.519	18.208	1.215	0.065	13
NM33xx_XM	35.11	-107.42	38.79	11.078	1.184	0.072	19
NM34xx_XM	35.27	-107.64	47.089	10.507	1.25	0.156	5
NM35xx_XM	35.34	-107.71	35.211	22.832	1.25	0.163	8
NM36xx_XM	35.45	-107.82	55.63	22.034	1.125	0.207	6
NM37xx_XM	35.58	-108	44.972	9.481	1.05	0.05	3
NM38xx_XM	35.7	-108.16	-22	2	1.9	0.25	1
NM39xx_XM	35.79	-108.27	42.68	5.808	1.483	0.142	3
NM40xx_XM	35.95	-108.43	41.5	8.564	0.825	0.125	2
NM41xx_XM	36.04	-108.57	23	16.448	0.775	0.125	2
NM42xx_XM	36.15	-108.72	48	17.5	0.8	0.4	1
NM43xx_XM	36.25	-108.89	19.031	6.458	1.163	0.161	4
NM44xx_XM	36.42	-108.96	15.753	4.388	0.637	0.072	4
NORMxx_CC	43.74	-121.25	61.135	11.666	1.428	0.07	16
NOXVxx_XN	35.96	-120.56	-73.025	5.73	1.667	0.433	3
NSTxxx_XJ	42.91	-113.98	-83.137	10.707	1.292	0.17	6
NV001x_XC	41.97	-118.66	88.264	6.821	1.759	0.076	23
NV004x_XC	41.92	-115.96	-80.786	8.845	1.513	0.063	27
NV007x_XC	41.84	-119.3	83.819	16.591	1.833	0.052	9
NV008x_XC	41.83	-118.61	89.595	6.088	1.777	0.062	22
NV009x_XC	41.83	-116.32	-87.3	11.854	1.613	0.099	19
NV011x_XC	41.68	-118.94	84.196	3.991	1.741	0.095	11
NV013x_XC	41.62	-118.58	87.791	12.316	1.871	0.079	19
NV014x_XC	41.58	-118.83	-84.994	20.013	1.95	0.233	6
NV31xx_IM	38.43	-118.15	82.185	18.688	1.405	0.11	19
NV31xx_IM	38.43	-118.16	82.185	18.688	1.405	0.11	19
NV32xx_IM	38.33	-118.3	63.018	7.144	1.55	0.074	12
NV33xx_IM	38.49	-118.42	-79.605	39.382	1.5	0.202	3

O02Cxx_TA	40.18	-122.79	30.258	37.577	1.42	0.097	5
O02Dxx_TA	40.18	-122.79	42.297	41.874	1.19	0.195	5
O03Dxx_TA	40.29	-121.8	76.797	23.7	0.989	0.064	9
O03Exx_TA	40.29	-121.8	89	2.001	0.975	0.075	2
O04Cxx_TA	40.32	-121.09	71.483	8.097	1.238	0.064	17
O05Cxx_TA	39.96	-120.92	-88.056	12.819	1.83	0.165	5
O06Axx_TA	40.17	-119.83	86.091	24.363	1.131	0.074	8
O07Axx_TA	40.16	-118.88	84.045	12.023	0.99	0.051	5
O08Axx_TA	40.29	-118.15	89.413	14.848	1.267	0.19	6
O09Axx_TA	40.17	-117.19	89.825	8.102	1.329	0.065	7
O10Axx_TA	40.29	-116.5	80.658	10.558	1.237	0.091	8
O11Axx_TA	40.13	-115.66	-42.825	14.587	1.14	0.058	10
O12Axx_TA	40.27	-114.75	-43.37	5.853	1.317	0.177	6
O13Axx_TA	40.13	-113.98	-17.885	15.329	1.238	0.072	8
O15Axx_TA	40.28	-112.47	-11.855	19.249	1.175	0.169	4
O16Axx_TA	40.21	-111.5	-77	9	1.05	0.2	1
O18Axx_TA	40.27	-110.01	-73	9	0.85	0.28	1
O19Axx_TA	40.3	-109.12	72.647	27.943	1.383	0.248	6
O20Axx_TA	40.13	-108.24	72.987	8.586	0.831	0.057	16
O21Axx_TA	40.21	-107.47	59.949	31.812	1.085	0.096	10
O22Axx_TA	40.16	-106.55	-84.699	13.204	1.375	0.101	4
O23Axx_TA	40.21	-105.92	73.075	15.072	1.006	0.091	16
O24Axx_TA	40.12	-105.07	75.447	25.094	0.78	0.095	10
O25Axx_TA	40.11	-104.12	60.665	10.001	1.12	0.102	5
O26Axx_TA	40.24	-103.31	80.595	14.173	1.092	0.17	6
O27Axx_TA	40.19	-102.48	22.96	16.15	0.95	0.257	3
O28Axx_TA	40.13	-101.77	69.029	23.509	1.079	0.143	7
O29Axx_TA	40.13	-100.8	-88.785	20.62	0.758	0.083	12
O30Axx_TA	40.18	-100.06	72.075	12.418	0.56	0.08	5
O31Axx_TA	40.15	-99.33	-83.675	24.441	0.956	0.123	9
O32Axx_TA	40.26	-98.28	73.684	13.184	0.76	0.079	15
O33Axx_TA	40.08	-97.58	58.41	12.363	0.85	0.057	18
O34Axx_TA	40.18	-96.69	32.735	18.563	1.157	0.174	7
O35Axx_TA	40.27	-95.91	16.403	6.884	0.69	0.073	5
O36Axx_TA	40.13	-94.96	20.759	17.817	0.744	0.125	9
O37Axx_TA	40.17	-94.15	60.177	9.071	0.757	0.061	7
O38Axx_TA	40.12	-93.47	54.811	10.985	0.7	0.05	5
O39Axx_TA	40.25	-92.54	78.133	14.043	0.728	0.062	9
O40Axx_TA	40.12	-91.87	-89.313	19.184	0.7	0.08	9
O41Axx_TA	40.12	-90.88	47.69	18.762	0.886	0.145	7
O42Axx_TA	40.2	-90.08	62.28	6.315	0.775	0.042	6

OBSRxx_CC	46.9	-121.82	70	24.454	1	0.15	2
OCWAxx_US	47.75	-124.18	84.469	7.484	1.06	0.091	5
OFRxxx_UW	47.93	-124.4	72.001	3.974	1.144	0.083	8
OGNExx_US	40.95	-102.03	89.192	44.787	1.222	0.095	16
OMAKxx_UW	48.36	-119.33	61.96	9.985	1.561	0.056	22
OPCxxx_UW	48.1	-123.41	68.538	5.911	1.1	0.115	7
OR002x_XC	45.02	-117.87	74	4.088	1.167	0.073	3
OR007x_XC	44.37	-121.31	-84	4	1.2	0.13	1
OR009x_XC	44.47	-119.41	73.58	6.815	1.217	0.129	6
OR016x_XC	44.21	-120.6	88	4	1.1	0.12	1
OR021x_XC	44.18	-118.6	79.495	5.739	1.4	0.114	4
OR025x_XC	44.03	-119.86	52	10.5	1.05	0.3	1
OR032x_XC	43.86	-120.89	78.5	8.564	0.975	0.125	2
OR033x_XC	43.77	-119.03	88	4.007	0.85	0.05	2
OR035x_XC	43.89	-120.02	81	5	1.35	0.2	1
OR039x_XC	43.69	-118.99	82.006	4.553	1.117	0.217	3
OR042x_XC	43.68	-120.73	87	3.5	0.85	0.1	1
OR043x_XC	43.68	-119.71	85	6	1	0.18	1
OR044x_XC	43.63	-119.22	86.337	3.093	1.133	0.169	3
OR048x_XC	43.62	-120.44	83.5	1.5	1.1	0.1	2
OR049x_XC	43.59	-118.6	65	8	0.85	0.15	1
OR051x_XC	43.64	-120.01	77.784	9.951	1.1	0.076	3
OR052x_XC	43.52	-119.02	83	7.5	1	0.2	1
OR053x_XC	43.55	-118.41	65	7	1	0.15	1
OR054x_XC	43.52	-118.1	63	7.5	1.4	0.27	1
OR055x_XC	43.55	-119.76	-65.5	34.473	1.025	0.025	2
OR056x_XC	43.58	-120.68	83	6.5	0.85	0.12	1
OR057x_XC	43.5	-120.12	85.939	9.975	1.15	0.076	3
OR058x_XC	43.49	-119.7	-88.243	12.816	1.461	0.064	31
OR059x_XC	43.45	-119.56	81	6.5	1.05	0.18	1
OR061x_XC	43.39	-120.56	88	1	1	0.05	1
OR062x_XC	43.31	-119.78	-83.382	12.9	1.025	0.092	4
OR064x_XC	43.39	-119.35	-84.5	22.661	1.075	0.375	2
OR069x_XC	43.31	-118.23	69.5	4.509	1.775	0.325	2
OR074x_XC	43.16	-119.85	90	4.007	1.375	0.375	2
OR076x_XC	43.16	-117.34	73	4.007	1.875	0.125	2
OR079x_XC	43.13	-118.57	78	3.5	1.95	0.2	1
OR080x_XC	43.06	-117.65	79	0	2.15	0.05	2
OR083x_XC	43.04	-118.91	67	3.5	1.65	0.15	1
OR086x_XC	43.02	-119.71	-89	3.003	1.775	0.425	2
OR087x_XC	42.99	-118.66	77.5	0.5	1.8	0.4	2

OR088x_XC	42.97	-117.3	73	7	1.35	0.2	1
OR091x_XC	42.88	-119.04	81.5	6.528	1.925	0.075	2
OR093x_XC	42.92	-119.18	87	3.5	1.55	0.13	1
OR094x_XC	43.94	-118.33	76	8	1.95	0.35	1
OR096x_XC	42.81	-117.11	90	6.022	1.75	0.1	2
OR098x_XC	42.78	-119.23	88.667	1.247	1.833	0.186	3
OR099x_XC	42.74	-118.69	-87.346	4.504	1.783	0.249	3
OR100x_XC	42.77	-119.01	84.941	8.49	1.812	0.12	4
OR101x_XC	42.77	-117.41	88.238	4.088	1.738	0.155	4
OR103x_XC	42.83	-118.11	82.5	4.509	2.05	0.1	2
OR104x_XC	42.72	-117.19	-84.678	4.112	1.642	0.15	6
OR105x_XC	42.65	-117.07	-87.669	2.626	1.783	0.044	3
OR106x_XC	42.68	-117.88	-89.308	7.788	1.817	0.103	6
OR108x_XC	42.63	-118.98	89.648	5.26	1.95	0.104	3
OR109x_XC	42.55	-117.46	-89.43	2.442	1.771	0.062	7
OR110x_XC	42.56	-119.29	83	4.007	1.975	0.075	2
OR111x_XC	42.51	-118.9	-86.5	1.5	1.425	0.275	2
OR113x_XC	42.42	-118.25	84.333	2.869	1.817	0.101	3
OR120x_XC	42.42	-117.68	-89.247	4.663	1.788	0.087	4
OR123x_XC	42.25	-118.95	-87	5.5	1.85	0.25	1
OR127x_XC	42.11	-119.03	86.5	2.502	1.65	0.1	2
OR128x_XC	42.26	-118.68	86.5	0.5	1.8	0.15	2
OR132x_XC	42.93	-118.83	83	3.538	2.013	0.183	4
OR133x_XC	43.91	-120.43	72.5	0.5	1.075	0.075	2
ORDxxx_XG	38.53	-103.71	-39	8.5	0.95	0.18	1
ORVxxx_BK	39.55	-121.5	64.653	8.221	1.333	0.148	3
OSIxxx_CI	34.61	-118.72	-87.552	9.492	1.415	0.049	43
OT01xx_XQ	45.04	-123.64	87.672	6.97	1.4	0.161	3
OT01xx_XT	45.04	-123.64	66	4.5	1.25	0.28	1
OT03xx_XQ	44.41	-122.47	68.085	8.352	1.618	0.03	19
OT03xx_XT	44.41	-122.47	83	8	1.55	0.28	1
OT04xx_XQ	44.18	-122.07	65.925	9.239	1.775	0.065	10
OT05xx_XQ	43.86	-121.48	73.84	8.224	1.2	0.091	9
OT06xx_XQ	43.45	-120.81	78.014	3.976	1.579	0.062	12
OT07xx_XQ	43.18	-120.19	88.302	4.684	1.979	0.099	7
OT08xx_XQ	42.96	-119.8	85.333	2.055	2.117	0.083	3
OT09xx_XQ	42.68	-119.19	85.5	2.502	1.95	0.05	2
OT10xx_XQ	42.4	-118.76	87	1	1.5	0.45	2
OT11xx_XQ	42.19	-118.34	89	2	1.95	0.15	1
OT12xx_XQ	41.74	-117.69	-87.132	8.249	1.859	0.069	17
OVYxxx_XJ	36.78	-118.33	72.5	3.504	2.1	0.2	2

P01Cxx_TA	39.47	-123.34	-30	8	1.25	0.33	1
P05Cxx_TA	39.3	-120.61	28.362	22.141	1.05	0.118	5
P06Axx_TA	39.68	-119.9	66	8.053	1.1	0.3	2
P07Axx_TA	39.54	-118.89	67.5	2.502	1.25	0.1	2
P08Axx_TA	39.69	-118.08	76	1.414	1.3	0.25	3
P09Axx_TA	39.55	-117.14	-82.596	3.138	1.05	0.111	5
P10Axx_TA	39.62	-116.46	90	6.022	0.925	0.525	2
P11Axx_TA	39.55	-115.75	-46.295	15.782	1.137	0.219	4
P12Axx_TA	39.47	-114.91	-15.369	17.355	0.77	0.078	5
P13Axx_TA	39.46	-114.02	-24.887	5.721	1.081	0.109	8
P14Axx_TA	39.59	-113.07	-28.419	18.223	1.388	0.071	26
P15Axx_TA	39.57	-112.28	-43.093	13.942	1.02	0.056	5
P16Axx_TA	39.61	-111.66	-23.911	18.156	1.2	0.029	3
P17Axx_TA	39.47	-110.74	-23.093	25.212	1.233	0.338	3
P18Axx_TA	39.63	-110.25	-70	3.003	1.775	0.825	2
P19Axx_TA	39.63	-108.98	81.002	26.434	1.112	0.165	4
P20Axx_TA	39.5	-108.39	84.457	32.237	1.375	0.145	4
P21Axx_TA	39.52	-107.45	58.868	25.289	0.988	0.088	4
P22Axx_TA	39.6	-106.76	-85.667	2.869	0.917	0.044	3
P23Axx_TA	39.37	-105.84	-14.176	15.627	1.062	0.114	4
P24Axx_TA	39.51	-104.91	28.168	14.192	1.35	0.079	4
P25Axx_TA	39.51	-104.17	2.999	2.161	0.667	0.088	3
P26Axx_TA	39.56	-103.35	27.966	14.992	1.1	0.035	5
P27Axx_TA	39.56	-102.58	37	3.003	1.075	0.175	2
P28Axx_TA	39.57	-101.75	64.256	13.136	0.733	0.072	12
P29Axx_TA	39.6	-100.93	-77.321	13.611	0.844	0.091	8
P30Axx_TA	39.54	-100.25	62.999	19.426	0.989	0.098	9
P31Axx_TA	39.52	-99.38	88.289	15.69	0.73	0.068	15
P32Axx_TA	39.62	-98.6	73.009	12.964	0.831	0.054	21
P33Axx_TA	39.44	-97.69	46.145	13.103	1.097	0.072	16
P34Axx_TA	39.55	-96.83	55.479	8.161	1.025	0.051	18
P35Axx_TA	39.53	-96.02	-13.472	49	0.75	0.172	4
P36Axx_TA	39.62	-95.21	23.521	13.953	0.542	0.091	6
P37Axx_TA	39.59	-94.35	42.482	13.049	0.953	0.074	16
P38Axx_TA	39.62	-93.53	49.091	28.027	0.736	0.083	7
P38Bxx_N4	39.62	-93.53	-69	10.104	0.7	0.25	2
P39Axx_TA	39.49	-92.75	-51	16	0.9	0.4	1
P39Bxx_TA	39.49	-92.75	-63.596	34.316	0.91	0.132	5
P40Axx_TA	39.53	-92.05	73.591	40.331	0.75	0.058	3
P40Bxx_N4	39.53	-92.05	64	11	0.85	0.28	1
P41Axx_TA	39.67	-91.06	41.951	17.427	1.194	0.183	8

P42Axx_TA	39.59	-90.34	46.048	13.511	1.033	0.08	12
PAKDxx_XN	35.98	-120.56	-44.321	25.151	1.617	0.268	3
PANHxx_CC	46.86	-121.64	82	0.817	1.25	0.218	3
PARxxx_XG	38.35	-108.98	-37	7.5	0.75	0.12	1
PASCxx_CI	34.17	-118.19	77.057	13.567	1.286	0.061	28
PASSxx_UW	49	-122.09	66.991	4.361	1.345	0.035	10
PASxxx_CI	34.15	-118.17	76.435	8.526	1.454	0.063	28
PASxxx_TS	34.15	-118.17	77.366	8.875	1.356	0.048	52
PBMOxx_NM	36.78	-90.43	28.08	21.719	1.029	0.19	7
PD31xx_IM	42.77	-109.56	50.587	4.495	0.835	0.034	10
PDCxxx_XJ	36.03	-118.98	-74	7.5	1.4	0.37	1
PDMxxx_CI	34.3	-114.14	56.623	14.943	0.809	0.068	11
PFOxxx_AZ	33.61	-116.46	-87.236	10.961	1.425	0.038	62
PFOxxx_CI	33.61	-116.46	-77.542	25.305	1.09	0.162	5
PFOxxx_II	33.61	-116.46	-88.89	10.928	1.493	0.039	74
PFOxxx_TS	33.61	-116.46	-88.885	10.16	1.54	0.07	29
PHINxx_HW	45.9	-119.93	-73.66	3.863	1.067	0.213	3
PHLxxx_CI	35.41	-120.55	-69.77	23.05	1.279	0.099	7
PHWYxx_IW	41.3	-105.46	68.486	17.208	1.102	0.042	29
PIGHxx_XN	35.96	-120.57	-76.5	0.5	1.875	0.275	2
PINExx_UO	43.79	-120.94	77	1	1.525	0.125	2
PINExx_XN	35.97	-120.52	-78	1	1.6	0.4	2
PINRxx_XT	40.36	-108.37	89	1	1.1	0.4	2
PINxxx_UO	43.81	-120.87	79.504	8.336	1.446	0.051	26
PKDxxx_BK	35.95	-120.54	-69.181	11.547	1.77	0.362	5
PKSxxx_XG	39.26	-99.54	-84	60.883	0.775	0.275	2
PL11xx_XU	47.45	-123.15	69.631	8.096	1.065	0.061	10
PLIDxx_IW	45.09	-116	75	13.5	0.9	0.23	1
PLMxxx_CI	33.35	-116.86	87.692	8.797	1.231	0.05	37
POLExx_XN	36.01	-120.57	-84	8	2.25	0.5	1
PONDxx_XN	36.01	-120.57	86	9	2.1	0.42	1
POTRxx_BK	38.2	-121.94	74	7.5	1.85	0.4	1
POWRxx_XN	36.01	-120.53	-82	15	1.75	0.48	1
PRISxx_XN	35.98	-120.49	82.569	8.782	2.05	0.236	3
PRLKxx_CC	44.21	-121.96	76.5	0.5	1.7	0.2	2
Q03Cxx_TA	38.63	-122.01	-87	7.5	1.45	0.4	1
Q04Cxx_TA	38.84	-121.38	83.466	18.698	1.75	0.174	6
Q07Axx_TA	38.94	-118.81	54.34	10.65	0.87	0.169	5
Q08Axx_TA	38.86	-117.93	48.7	11.36	1.017	0.234	6
Q09Axx_TA	38.83	-117.18	61	4	1.75	0.4	1
Q10Axx_TA	38.82	-116.4	65	25.68	1.25	0.1	2

Q11Axx_TA	38.85	-115.65	89	8.053	1.35	0.05	2
Q12Axx_TA	39.04	-114.83	-86.127	20.847	1.4	0.153	5
Q13Axx_TA	38.96	-114.02	-28.322	5.917	1.3	0.13	6
Q14Axx_TA	38.99	-113.28	-25.83	5.619	1.242	0.08	6
Q15Axx_TA	39	-112.38	-13.524	7.832	1.197	0.067	15
Q16Axx_TA	38.92	-111.17	-25.926	22.064	1.49	0.229	10
Q18Axx_TA	39.1	-110.13	-67.168	43.062	0.79	0.058	5
Q19Axx_TA	38.96	-109.26	49.058	30.507	1.45	0.31	6
Q20Axx_TA	38.95	-108.3	-50.575	17.149	0.7	0.153	3
Q21Axx_TA	38.83	-107.57	39.136	17.89	1.1	0.129	11
Q22Axx_TA	38.86	-106.91	9.072	10.804	0.883	0.088	3
Q23Axx_TA	38.9	-105.83	-25.246	26.276	0.75	0.104	3
Q24Axx_TA	38.96	-105.15	17	28.217	1.6	0.3	2
Q25Axx_TA	38.91	-104.25	61	24.454	0.625	0.025	2
Q26Axx_TA	38.92	-103.52	47.308	20.687	0.736	0.115	7
Q28Axx_TA	39.06	-101.83	69.931	15.323	0.757	0.073	20
Q29Axx_TA	38.89	-100.98	37.335	3.303	0.9	0.076	3
Q30Axx_TA	38.98	-100.22	59.994	14.719	0.82	0.111	10
Q31Axx_TA	39	-99.39	-88.022	13.412	0.7	0.104	8
Q32Axx_TA	38.99	-98.56	58.269	6.896	0.914	0.084	11
Q33Axx_TA	39	-97.83	60.229	9.05	0.833	0.044	3
Q34Axx_TA	38.92	-96.94	46.135	8.717	0.722	0.073	9
Q35Axx_TA	38.86	-96.04	34.144	6.211	0.61	0.048	5
Q36Axx_TA	38.96	-95.46	53.243	23.16	1.133	0.393	3
Q37Axx_TA	38.88	-94.45	71.839	11.465	0.763	0.055	4
Q38Axx_TA	38.96	-93.62	73.94	11.206	0.89	0.202	5
Q39Axx_TA	39.05	-92.98	-77.157	35.326	0.9	0.095	13
Q40Axx_TA	38.99	-92.07	-10.5	18.095	0.575	0.075	2
Q41Axx_TA	38.95	-91.23	27.191	16.884	0.71	0.056	5
Q42Axx_TA	38.91	-90.53	45.516	9.134	1.123	0.071	11
R04Cxx_TA	38.26	-120.94	84.46	10.428	1.607	0.059	15
R05Cxx_TA	38.7	-120.08	64.57	11.083	1.287	0.037	15
R06Cxx_TA	38.52	-119.45	63.369	17.122	1.425	0.116	12
R07Cxx_TA	38.09	-119.05	50.825	6.998	1.34	0.137	5
R08Axx_TA	38.35	-118.11	83.625	10.956	1.355	0.117	10
R09Axx_TA	38.24	-117.07	67.48	28.498	0.95	0.167	4
R10Axx_TA	38.29	-116.3	85	11	1.25	0.43	1
R11Axx_TA	38.35	-115.59	12.292	2.864	1.736	0.164	7
R12Axx_TA	38.33	-114.61	45.819	16.329	0.65	0.101	5
R13Axx_TA	38.18	-113.97	46.43	3.621	1	0.049	7
R14Axx_TA	38.3	-113.02	-16.307	37.658	1.64	0.216	5

R15Axx_TA	38.21	-112.28	34.789	12.927	1.167	0.28	3
R16Axx_TA	38.28	-111.48	-0.95	12.125	1.072	0.106	9
R17Axx_TA	38.42	-110.71	18.94	11.884	0.9	0.093	6
R18Axx_TA	38.39	-109.89	49.233	10.536	0.987	0.156	4
R19Axx_TA	38.29	-109.26	75.912	8.572	0.783	0.309	3
R20Axx_TA	38.19	-108.38	-11.521	30.859	0.967	0.347	3
R21Axx_TA	38.37	-107.55	33.234	30.589	1.3	0.217	4
R22Axx_TA	38.23	-106.76	8.531	22.391	0.942	0.07	12
R23Axx_TA	38.19	-105.83	-33.318	22.35	0.775	0.072	4
R24Axx_TA	38.23	-105.11	-7.161	47.733	0.95	0.104	4
R25Axx_TA	38.15	-104.28	-21	66.111	0.9	0.2	2
R26Axx_TA	38.3	-103.45	-37.046	11.991	0.9	0.153	3
R27Axx_TA	38.29	-102.8	46.136	44.853	1.167	0.392	3
R28Axx_TA	38.34	-101.81	63	18.5	0.6	0.32	1
R29Axx_TA	38.42	-101.14	58.5	8.564	1.025	0.125	2
R30Axx_TA	38.28	-100.28	39.513	24.976	0.75	0.17	4
R31Axx_TA	38.29	-99.53	55	7.5	0.85	0.23	1
R32Axx_TA	38.42	-98.71	47.275	7.62	0.75	0.054	4
R32Bxx_N4	38.42	-98.71	30	7	1.05	0.25	1
R33Axx_TA	38.31	-97.98	29.749	8.303	0.767	0.088	3
R34Axx_TA	38.3	-97.25	57.5	16.994	1	0.2	2
R35Axx_TA	38.32	-96.2	56.5	81.516	0.575	0.075	2
R36Axx_TA	38.32	-95.5	55.006	6.226	0.962	0.184	4
R37Axx_TA	38.31	-94.83	37.669	2.626	1.067	0.164	3
R38Axx_TA	38.19	-93.91	76.174	10.771	0.733	0.136	3
R39Axx_TA	38.31	-93.04	-73.946	23.146	0.9	0.156	7
R40Axx_TA	38.29	-92.27	-84.742	35.4	1.038	0.277	4
R40Bxx_N4	38.29	-92.27	89	18.5	0.55	0.22	1
R41Axx_TA	38.3	-91.38	16.67	19.42	0.714	0.056	11
R42Axx_TA	38.28	-90.79	54.557	19.582	0.96	0.089	10
RADRxx_UW	46.42	-123.8	69.996	6.56	1.314	0.103	7
RAINxx_XN	35.98	-120.49	69	8.5	2.05	0.37	1
RAIOxx_IU	46.04	-122.89	69.952	6.305	1.017	0.138	6
RATTxx_UW	47.43	-121.8	69.774	5.521	1.392	0.091	13
RCKYxx_XN	35.96	-120.61	-78	6.5	2	0.43	1
RCTxxx_CI	36.31	-119.24	84.349	12.302	0.994	0.119	8
RDG11x_GS	37.43	-121.73	-61.5	10.621	1.375	0.175	2
RDG12x_GS	37.43	-121.74	-61	11.14	1.3	0.1	2
RDG13x_GS	37.43	-121.74	-52	6.5	1.25	0.18	1
RDG14x_GS	37.43	-121.75	-59.5	7.544	1.225	0.025	2
RDG21x_GS	37.41	-121.72	-42	14.295	1.15	0.05	2

RDG22x_GS	37.41	-121.72	-28	11.5	1.05	0.3	1
RDG23x_GS	37.41	-121.73	-42	11.14	1.125	0.175	2
RDG24x_GS	37.41	-121.73	-51	4.5	1.3	0.15	1
RDMxxx_AZ	33.63	-116.85	-84.166	8.841	1.388	0.04	69
REDWxx_IW	43.36	-110.85	55.235	7.251	1.214	0.085	14
RKFxxx_XG	38.07	-103.63	-18.352	5.26	1.067	0.169	3
RLMTxx_US	45.12	-109.27	72.124	10.071	1.05	0.07	7
RPVxxx_CI	33.74	-118.4	-83.325	13.082	1.468	0.061	19
RPVxxx_TS	33.74	-118.4	-83.656	16.26	1.5	0.065	4
RRI2xx_IW	43.35	-111.32	60.11	8.507	1.386	0.094	11
RRWxxx_XT	41.14	-108.86	-8	7	0.85	0.2	1
RRXxxx_CI	34.88	-117	-87.948	10.056	1.152	0.081	22
RSSDxx_IU	44.12	-104.04	36.585	24.153	0.714	0.034	7
RSSDxx_US	44.12	-104.04	-51.95	31.827	1.439	0.125	9
RWWYxx_IW	41.69	-107.21	82.814	27.241	1.075	0.058	22
S01xxx_XK	37.24	-105.46	19	15.366	1.225	0.375	2
S01xxx_XS	45.18	-109.22	71.5	2.502	1.025	0.325	2
S02xxx_XK	37.15	-105.45	25	14	1	0.33	1
S02xxx_XS	45.27	-108.77	57.861	7.15	0.92	0.111	5
S030xx_XU	47.03	-123.3	75	5	0.85	0.1	1
S03Bxx_XK	37.07	-105.45	29.5	1.5	1.225	0.425	2
S03xxx_XK	37.07	-105.45	10	10	0.9	0.22	1
S03xxx_XS	45.38	-109.43	69.702	21.904	0.842	0.082	6
S040xx_XU	47.04	-123.03	55	6.5	0.85	0.15	1
S04Cxx_TA	37.5	-121.33	-76.964	12.605	1.825	0.303	4
S04xxx_XK	36.97	-105.42	4	15	1.05	0.4	1
S04xxx_XS	45.38	-109.18	78.296	12.526	0.975	0.156	4
S050xx_XU	47.01	-122.87	83	7.5	1.05	0.25	1
S05Bxx_XK	36.85	-105.41	1.676	9.457	0.9	0.202	3
S05Cxx_TA	37.35	-120.33	86.582	4.988	1.688	0.097	17
S05xxx_XS	45.41	-108.94	57.997	10.581	0.969	0.145	8
S065xx_XU	46.87	-122.38	73.5	7.544	0.925	0.125	2
S06Cxx_TA	37.88	-119.85	68.194	5.919	1.505	0.102	10
S06xxx_XK	36.81	-105.3	-1.5	26.303	0.925	0.175	2
S06xxx_XS	45.58	-108.61	76.679	12.36	0.763	0.146	4
S070xx_XU	46.98	-122.24	71	8	0.85	0.15	1
S07xxx_XS	45.57	-109.74	78.015	7.002	0.917	0.159	3
S08Cxx_TA	37.5	-118.17	69.726	9.379	1.4	0.1	13
S08xxx_XK	36.61	-105.32	10.922	21.443	0.8	0.144	3
S08xxx_XP	38.03	-107.31	-21	7	1.1	0.18	1
S090xx_XU	46.99	-121.54	84	12	1.3	0.37	1

S09Axx_TA	37.72	-117.22	78.406	11.979	1.179	0.142	7
S09xxx_XK	36.51	-105.3	24.004	3.746	1.4	0.1	3
S09xxx_XS	45.56	-109.2	72.573	4.839	1.086	0.113	7
S100xx_XU	46.98	-121.11	-76.273	4.923	0.788	0.059	4
S101xx_XL	42.45	-108.89	-85	11.14	1.275	0.025	2
S107xx_XL	41.9	-108.84	-61	2.5	1.45	0.2	1
S10Axx_TA	37.92	-116.59	-56	9	0.9	0.25	1
S10xxx_XK	36.44	-105.29	35.5	20.343	1.35	0.15	2
S10xxx_XS	45.62	-108.87	66.298	12.771	1.083	0.124	6
S11Axx_TA	37.64	-115.75	31.83	13.911	0.875	0.056	6
S11xxx_XK	36.34	-105.28	15	6.022	1.175	0.125	2
S11xxx_XS	45.58	-108.61	57.242	3.346	1.025	0.148	4
S129xx_XL	39.91	-108.68	76	11	0.65	0.2	1
S12Axx_TA	37.61	-114.85	57.79	4.346	1.125	0.057	14
S12xxx_XK	36.24	-105.24	33	12.5	1.1	0.28	1
S12xxx_XP	37.79	-107.14	2	11	0.95	0.2	1
S130xx_XL	39.84	-108.77	71	6	1.05	0.27	1
S131xx_XL	39.75	-108.77	71	3	1.25	0.23	1
S13Axx_TA	37.58	-113.86	44.278	9.164	0.85	0.075	6
S13xxx_XK	36.15	-105.26	25.551	10.157	1.22	0.041	5
S13xxx_XS	45.74	-109.43	63.352	6.255	0.85	0.087	3
S143xx_XL	38.69	-108.73	65	1.5	1.9	0.22	1
S14Axx_TA	37.76	-113.17	34.891	13.195	1.017	0.109	3
S14xxx_XK	36.07	-105.23	26.94	7.505	1.212	0.077	4
S14xxx_XS	45.79	-109.18	53.77	9.994	0.981	0.085	8
S15Axx_TA	37.68	-112.36	-75	38.426	1.275	0.125	2
S15xxx_XK	35.97	-105.22	45.548	8.996	1.175	0.214	4
S15xxx_XS	45.83	-108.82	63.66	12.039	1.031	0.159	8
S16Axx_TA	37.72	-111.6	57.369	9.564	0.775	0.131	4
S16xxx_XK	35.87	-105.2	43	11.5	0.95	0.28	1
S16xxx_XP	37.62	-104.85	-31.003	2.83	0.667	0.117	3
S16xxx_XS	45.84	-108.58	55.576	6.615	0.81	0.033	5
S17Axx_TA	37.64	-110.8	48.96	11.097	0.972	0.066	9
S17xxx_XK	35.79	-105.19	34.5	5.329	1.592	0.096	6
S17xxx_XS	45.8	-108.25	49.572	22.162	0.95	0.168	5
S18Axx_TA	37.69	-109.99	-83.191	66.149	0.85	0.143	5
S18xxx_XK	35.7	-105.17	44.791	16.706	1.13	0.124	5
S18xxx_XS	45.95	-109.5	62.603	3.009	1.02	0.121	5
S19Axx_TA	37.75	-109.14	34.485	30.943	0.8	0.085	9
S19xxx_XK	35.6	-105.18	45.793	11.62	1.423	0.108	11
S19xxx_XS	46.08	-109.15	49.762	9.579	0.8	0.117	5

S20Axx_TA	37.83	-108.36	39.5	7.544	1.1	0.25	2
S20xxx_XK	35.51	-105.22	42.844	11.399	1.342	0.08	12
S20xxx_XS	46.06	-108.94	44.453	11.853	0.767	0.044	3
S21Axx_TA	37.66	-107.79	26.612	6.8	1.025	0.157	8
S21xxx_XK	35.42	-105.2	49.103	8.576	1.275	0.27	4
S21xxx_XS	45.95	-108.6	36.5	0.5	0.8	0.05	2
S22Axx_TA	37.75	-106.83	22.27	11.849	1.363	0.045	20
S22xxx_XK	35.32	-105.15	39.203	13.574	1.047	0.103	15
S22xxx_XS	46	-108.29	69.303	13.657	0.762	0.109	4
S230xx_XL	39.69	-108.54	71	1.5	2	0.28	1
S23Axx_TA	37.71	-106	41	15.366	0.85	0.15	2
S23xxx_XK	35.25	-105.12	39.708	11.529	1.16	0.196	5
S241xx_XL	38.84	-107.54	17	9	0.85	0.12	1
S24Axx_TA	37.64	-105.21	23.192	6.445	0.9	0.072	5
S24xxx_XK	35.15	-105.06	44.955	15.419	0.97	0.134	5
S26Axx_TA	37.62	-103.47	2.664	8.814	1.295	0.094	11
S26xxx_XP	37.1	-105.6	69	14.5	0.85	0.3	1
S27Axx_TA	37.68	-102.9	-46.553	27.532	1.058	0.186	6
S28Axx_TA	37.59	-101.9	-47	13.5	0.55	0.17	1
S29Axx_TA	37.62	-101.12	7.982	14.291	0.592	0.098	6
S30Axx_TA	37.64	-100.46	30.247	14.78	0.646	0.066	14
S31Axx_TA	37.62	-99.48	-83	11.5	0.55	0.12	1
S32Axx_TA	37.7	-98.94	58.5	3.504	0.7	0	2
S33Axx_TA	37.59	-98	52.017	7.54	0.8	0.096	4
S34Axx_TA	37.7	-97.11	85.185	4.403	0.74	0.043	5
S35Axx_TA	37.68	-96.32	-85.815	38.016	0.6	0.102	4
S36Axx_TA	37.72	-95.59	65.574	19.005	0.93	0.189	5
S37Axx_TA	37.76	-94.83	85.5	0.5	1.05	0.5	2
S38Axx_TA	37.63	-93.91	68.259	14.505	0.67	0.051	5
S39Axx_TA	37.69	-93.32	-89.133	9.626	0.722	0.044	9
S39Bxx_N4	37.69	-93.32	-84.785	9.994	0.83	0.111	5
S40Axx_TA	37.6	-92.5	71.712	18.213	0.9	0.065	9
S41Axx_TA	37.59	-91.75	55.164	16.629	0.87	0.155	5
S42Axx_TA	37.77	-90.79	47.432	18.43	0.906	0.069	8
S43Axx_TA	37.57	-90.08	11.345	32.617	1.333	0.176	3
SAGExx_XN	35.98	-120.52	-68.5	16.994	1.525	0.275	2
SALxxx_CI	33.28	-115.99	-64	5	1.05	0.13	1
SAOxxx_BK	36.76	-121.45	-55.78	20.507	1.475	0.196	4
SAOxxx_US	36.76	-121.44	-70.602	12.511	1.8	0.375	3
SAVYxx_CT	37.39	-121.5	-74.895	18.026	1.475	0.153	6
SBCxxx_CI	34.44	-119.71	-86.149	8.499	1.278	0.149	9

SBCxxx_TS	34.44	-119.71	-88.5	6.528	0.975	0.025	2
SBPXxx_CI	34.23	-117.23	-64	12	0.65	0.13	1
SC09xx_XR	34.15	-105	32.5	5.135	0.725	0.097	6
SC10xx_XR	34.19	-104.67	14.928	13.151	0.829	0.097	7
SC11xx_XR	34.23	-104.3	21.504	3.732	0.867	0.044	6
SC13xx_XR	34.21	-103.53	-21	8.5	0.65	0.13	1
SC15xx_XR	33.83	-105.03	40	2.001	1.375	0.525	2
SC16xx_XR	33.89	-104.3	10.588	5.62	0.83	0.072	5
SC17xx_XR	33.89	-103.54	-2.398	15.872	0.683	0.142	3
SC18xx_XR	33.88	-102.84	-24	15.366	0.775	0.075	2
SC19xx_XR	33.52	-105.97	33.405	13.881	1	0.12	6
SC20xx_XR	33.6	-105.59	36	8	1.25	0.25	1
SC21xx_XR	33.6	-105.17	27.681	4.793	0.967	0.13	3
SC22xx_XR	33.57	-104.75	12.272	7.62	0.817	0.169	3
SC23xx_XR	33.6	-104.33	11.84	9.647	1.009	0.029	16
SC25xx_XR	33.58	-103.55	26.239	4.149	0.875	0.097	4
SC26xx_XR	33.5	-103.12	7	1	0.65	0.1	2
SC27xx_XR	33.54	-102.82	-19	13	0.55	0.15	1
SC28xx_XR	33.57	-102.49	34	15	0.7	0.33	1
SC29xx_XR	33.31	-105.67	48	3	1.35	0.1	1
SC30xx_XR	33.27	-105.17	39	7	1.2	0.2	1
SC31xx_XR	33.26	-104.34	21.006	4.553	1.1	0.05	3
SC32xx_XR	33.19	-103.6	1	9	1	0.18	1
SC33xx_XR	33.23	-102.83	-19.501	38.753	1.117	0.142	3
SC34xx_XR	32.95	-105.82	84	13.5	0.85	0.3	1
SC35xx_XR	32.94	-105.52	29.037	6.397	1.267	0.136	3
SC36xx_XR	33.01	-105.18	27.5	1.5	0.9	0.05	2
SC37xx_XR	32.94	-104.62	38.667	1.247	1.033	0.145	3
SC38xx_XR	32.93	-104.34	48	5	0.8	0.1	1
SC39xx_XR	33.03	-103.85	21.5	18.095	0.875	0.075	2
SC40xx_XR	32.93	-103.54	31.19	19.153	0.833	0.101	3
SC41xx_XR	32.98	-103.21	27	19.775	0.725	0.125	2
SC44xx_XR	32.76	-105.95	26.343	4.65	1.133	0.164	3
SC45xx_XR	32.63	-105.16	37.977	8.652	1.05	0.284	3
SC46xx_XR	32.65	-104.36	48.612	8.425	1.017	0.142	3
SC47xx_XR	32.63	-103.63	36	6.5	0.75	0.15	1
SC48xx_XR	32.69	-102.9	69	14	0.95	0.28	1
SC50xx_XR	32.39	-105.62	-12.328	3.303	0.85	0.076	3
SC51xx_XR	32.37	-105.17	23.5	6.528	0.95	0.1	2
SC52xx_XR	32.49	-104.83	41.97	13.239	0.75	0.137	4
SC53xx_XR	32.38	-104.32	56.585	14.62	1.125	0.12	4

SC54xx_XR	32.28	-104.04	29	0	1.15	0.4	2
SC55xx_XR	32.17	-103.67	-29.327	4.196	0.917	0.192	3
SC57xx_XR	32.37	-102.85	22	9.076	0.775	0.175	2
SC58xx_XR	32.29	-102.55	23.583	14.765	0.817	0.093	3
SC59xx_XR	31.97	-105.15	38.944	12.815	0.717	0.148	3
SC60xx_XR	32.09	-104.49	24.305	7.947	1.188	0.113	4
SC61xx_XR	31.99	-103.69	-16.345	7.394	0.95	0.104	3
SC62xx_XR	32.01	-102.94	17.5	11.66	1.4	0.1	2
SC63xx_XR	31.8	-104.85	38.286	14.943	1.267	0.139	6
SC64xx_XR	31.7	-104.43	35.335	2.358	1.367	0.232	3
SC65xx_XR	31.73	-104.02	34.919	8.691	1.467	0.13	3
SC68xx_XR	31.8	-102.77	15.894	17.809	0.89	0.089	5
SC69xx_XR	31.69	-102.59	20.557	19.814	0.9	0.076	3
SC70xx_XR	31.37	-103.74	16.4	2.578	1.06	0.089	5
SC71xx_XR	31.65	-103.07	13.622	4.094	0.969	0.119	8
SC73xx_XR	30.96	-102.99	-4.391	3.556	0.96	0.056	5
SC74xx_XR	31	-102.68	23.768	15.537	0.933	0.044	3
SC75xx_XR	31.87	-105.95	4	14.5	0.9	0.3	1
SCI2xx_AZ	32.92	-118.49	89.211	6.008	1.367	0.057	6
SCI2xx_CI	32.98	-118.55	89.473	6.432	1.308	0.15	6
SCIAxx_US	41.91	-93.22	49.881	15.801	1.032	0.053	42
SCZ2xx_CI	34	-119.64	86.378	7.049	1.423	0.056	11
SCZxxx_Gy	36.6	-121.4	-74.268	10.011	1.719	0.08	27
SDCOxx_US	37.75	-105.5	34.102	10.101	1.035	0.077	10
SDDxxx_CI	33.55	-117.66	78.613	10.761	1.21	0.061	25
SDPxxx_CI	34.57	-120.5	90	5.013	1.25	0.3	2
SEALxx_XC	47.71	-122.89	78	15	1.3	0.47	1
SFKxxx_XG	37.69	-106.62	38.5	11.66	1	0.05	2
SFTxxx_XJ	36.23	-118.06	81	9	1.1	0.2	1
SHLxxx_XG	38.6	-102.46	32.5	18.095	1.4	0.35	2
SHOxxx_CI	35.9	-116.28	-89.49	21.849	0.842	0.047	13
SHUKxx_UW	48.85	-121.68	72.89	8.031	1.281	0.068	8
SHUMxx_AZ	33.63	-116.44	86.206	9.92	1.757	0.159	7
SLAxxx_CI	35.89	-117.28	83.476	10.664	1.106	0.068	18
SLCxxx_XJ	36.52	-117.72	-85	5.013	0.975	0.425	2
SLMxxx_NM	38.64	-90.24	44.635	7.397	1.067	0.065	27
SMCOxx_IW	39.18	-106.97	80	11.5	1.95	0.57	1
SMDxxx_XJ	36.97	-118.63	73.5	1.5	1.8	0.3	2
SMER2x_AZ	33.46	-117.17	86	3.5	2	0.2	1
SMERxx_AZ	33.46	-117.17	84.01	7.044	1.337	0.073	23
SMMxxx_CI	35.31	-120	-77.143	12.378	1.062	0.133	4

SMMxxx_XA	35.31	-120	-71	6.5	1.45	0.38	1
SNCCxx_CI	33.25	-119.52	-88.911	6.452	1.56	0.092	10
SNCCxx_TS	33.25	-119.52	-87.5	5.517	1.35	0.1	2
SNDxxx_AZ	33.55	-116.61	-86.684	8.515	1.191	0.035	46
SNOWxx_IW	43.46	-110.76	53.495	10.103	1.213	0.083	19
SNP11x_XE	36.7	-119.31	76.667	0.471	1.167	0.093	3
SNP12x_XE	36.91	-119.04	71	11.5	1.05	0.23	1
SNP14x_XE	37.14	-118.77	73.584	5.467	1.62	0.075	5
SNP15x_XE	37.28	-118.6	69.732	5.222	1.763	0.099	4
SNP16x_XE	37.35	-118.26	67.5	5.517	1.425	0.075	2
SNP21x_XE	36.82	-119.51	78.994	3.562	1.517	0.13	3
SNP22x_XE	37.01	-119.36	87.601	8.1	1.388	0.166	4
SNP23x_XE	37.12	-119.21	89	13	1.15	0.38	1
SNP24x_XE	37.28	-118.97	64.898	8.602	1.413	0.097	4
SNP25x_XE	37.36	-118.7	67	3.003	1.475	0.025	2
SNP26x_XE	37.57	-118.49	68.757	7.153	1.41	0.108	5
SNP27x_XE	37.66	-118.35	66.67	5.324	1.9	0.301	3
SNP28x_XE	37.9	-118.16	73	5	1.15	0.23	1
SNP34x_XE	37.39	-119.06	77.014	5.204	1.092	0.061	6
SNP36x_XE	37.68	-118.65	34.612	8.425	1.317	0.06	3
SNP37x_XE	37.82	-118.55	63.384	27.076	1.062	0.094	4
SNP42x_XE	37.25	-119.58	83.5	6.528	1.375	0.075	2
SNP43x_XE	37.41	-119.48	79.122	11.716	1.29	0.13	5
SNP44x_XE	37.5	-119.28	81	14.295	1.225	0.375	2
SNP45x_XE	37.68	-119.08	65.996	3.746	1.4	0.087	3
SNP47x_XE	37.98	-118.73	77.29	7.969	1.3	0.029	3
SNP52x_XE	37.34	-119.81	89	11.5	1.5	0.45	1
SNP53x_XE	37.51	-119.67	82	5.5	1.7	0.25	1
SNP54x_XE	37.74	-119.51	60	9	1.8	0.6	1
SNP55x_XE	37.88	-119.33	57.164	2.673	1.25	0.073	6
SNP56x_XE	37.97	-119.17	61.003	2.83	1.317	0.142	3
SNP57x_XE	38.14	-118.97	61.681	4.793	1.483	0.093	3
SNP63x_XE	37.72	-119.81	63.367	4.639	1.294	0.065	8
SNP64x_XE	37.87	-119.65	66.333	4.113	1.422	0.025	9
SNP67x_XE	38.28	-119.15	61.751	3.494	1.45	0.084	4
SNP74x_XE	37.99	-119.93	72.5	0.5	1.45	0.45	2
SNP75x_XE	38.13	-119.7	61.566	9.813	1.783	0.217	3
SNP76x_XE	38.36	-119.51	67	8.053	1.85	0.05	2
SNP85x_XE	38.29	-119.95	67.059	8.49	1.475	0.183	4
SNP86x_XE	38.49	-119.81	73.749	4.331	1.512	0.055	4
SNP87x_XE	38.68	-119.61	65.299	12.95	1.1	0.069	7

SNP97x_XE	38.81	-119.81	69	1.5	1.25	0.13	1
SNPA7x_XE	39.01	-119.89	65.152	10.039	1.228	0.113	9
SNPA8x_XE	39.1	-119.6	57	6.022	1.15	0.25	2
SNPB9x_XE	39.36	-119.59	69	7.5	1.35	0.25	1
SOLxxx_AZ	32.84	-117.25	77.106	6.254	1.108	0.056	19
SPMNxx_TA	45.22	-92.8	37.06	17.471	1.071	0.042	56
SQMxxx_UW	48.07	-123.05	78.288	9.539	1.119	0.08	8
SQMxxx_UW	48.08	-123.05	78.288	9.539	1.119	0.08	8
SQRLxx_XL	32.7	-109.89	75	10	1.05	0.25	1
SRFxxx_XJ	36.94	-118.11	73.5	2.502	1.8	0.25	2
SRUxxx_UU	39.11	-110.52	-31.285	19.595	0.854	0.063	14
SSWxxx_UW	46.97	-123.44	57	5.5	1.4	0.33	1
STDxxx_CC	46.24	-122.22	-89.202	9.962	0.975	0.111	4
STGIxx_XN	36.03	-120.59	-54	7.5	1	0.15	1
STILxx_XC	47.7	-121.91	67	6	1.15	0.3	1
STORxx_UW	47.19	-121.99	75.102	4.465	1.205	0.047	10
SUSDxx_TA	44.44	-98.96	45.366	19.816	0.909	0.07	17
SUTBxx_TA	39.23	-121.79	80.5	4.509	1.95	0.3	2
SUTTxx_XT	40.58	-108.29	53	1	1.4	0.2	1
SVDxxx_CI	34.11	-117.1	87.787	9.762	1.31	0.048	49
SVDxxx_TS	34.1	-117.1	-88.667	2.869	1.233	0.224	3
SWF2xx_CC	46.18	-122.22	90	6	1.3	0.35	1
SWFLxx_CC	46.19	-122.2	-69.5	0.5	1.4	0.2	2
SWNBxx_CC	43.67	-121.36	63.941	7.151	1.405	0.044	10
SWSxxx_CI	32.95	-115.8	-61.5	25.064	1.325	0.125	2
T05Cxx_TA	36.9	-120.67	-84	6	1.95	0.35	1
T06Cxx_TA	37.01	-119.71	87.039	15	1.532	0.069	30
T11Axx_TA	37.24	-115.22	68.616	16.471	0.861	0.058	9
T12Axx_TA	36.73	-114.71	77.001	2.161	1.033	0.073	3
T13Axx_TA	37.02	-113.91	40.09	19.061	1.1	0.108	5
T14Axx_TA	37.06	-113.08	33.369	17.714	1.033	0.142	6
T15Axx_TA	37.02	-112.38	54	17	0.85	0.38	1
T16Axx_TA	36.98	-111.51	57.96	8.557	1.15	0.068	7
T17Axx_TA	37	-110.8	39.394	7.671	0.87	0.115	5
T18Axx_TA	37.14	-109.87	47.019	14.528	1.204	0.088	13
T19Axx_TA	36.83	-109.02	22.239	13.285	1.212	0.147	8
T21Axx_TA	36.99	-107.53	23.278	32.078	1.275	0.298	4
T23Axx_TA	37.04	-106.04	17.238	8.995	0.85	0.151	4
T25Axx_TA	37.14	-104.41	-1.494	20.192	1.148	0.066	26
T26Axx_TA	37.17	-103.59	12.3	11.769	0.864	0.052	11
T27Axx_TA	37.06	-102.72	-8.194	18.611	0.875	0.283	4

T28Axx_TA	37.12	-102.11	-54	7.5	0.95	0.18	1
T29Axx_TA	37.16	-101.29	10.425	15.485	0.717	0.09	6
T30Axx_TA	37.05	-100.53	24.951	10.878	0.743	0.103	7
T31Axx_TA	37.1	-99.68	63.009	3.537	0.863	0.037	4
T32Axx_TA	37.18	-98.92	58.489	33.646	0.788	0.031	4
T33Axx_TA	37.08	-98.24	74.151	10.803	0.808	0.104	6
T34Axx_TA	37.02	-97.19	81.037	6.397	0.8	0.144	3
T35Axx_TA	36.92	-96.51	79.807	13.771	0.533	0.044	3
T36Axx_TA	37.06	-95.88	71.345	4.927	0.567	0.077	6
T37Axx_TA	37.12	-94.92	63.942	8.396	0.762	0.126	8
T38Axx_TA	37.04	-94.29	69.5	10.621	0.85	0.05	2
T39Axx_TA	37.02	-93.38	68.5	2.502	0.75	0.05	2
T40Axx_TA	37.15	-92.52	59.174	11.233	0.917	0.117	9
T41Axx_TA	37.04	-91.76	65.516	12.356	0.625	0.097	4
T42Axx_TA	37.03	-91.09	32	1	0.85	0.2	2
T42Bxx_N4	37.03	-91.09	66	10.5	1.05	0.4	1
T43Axx_TA	37.08	-90.29	13	2.001	0.85	0.1	2
TAKOxx_UW	43.74	-124.08	67.578	7.957	1.267	0.068	15
TASNxx_TA	34.95	-106.46	43	5	2.5	0.48	1
TCBUxx_CC	44.24	-121.66	76.859	9.081	1.44	0.094	10
TCBUxx_CC	44.24	-122.66	76.859	9.081	1.44	0.094	10
TFRDxx_TA	33.49	-116.6	-83	5.013	1.725	0.025	2
TFRDxx_YN	33.49	-116.6	-89.971	18.951	1.283	0.183	3
TINxxx_CI	37.05	-118.23	70.64	6.429	1.565	0.053	17
TMBUxx_CC	43.6	-121.14	69.669	2.626	0.917	0.06	3
TOL0xx_XN	44.68	-124	77.5	0.5	1.35	0	2
TOLOxx_UW	44.62	-123.92	74.539	6.389	1.229	0.055	12
TOLTxx_UW	47.69	-121.69	69.275	10.638	1.25	0.05	23
TOVxxx_CI	34.16	-118.82	78.426	10.064	1.259	0.035	37
TPAWxx_IW	43.49	-110.95	46.127	10.351	1.372	0.097	16
TPFOxx_TA	33.61	-116.45	-83.636	14.115	1.414	0.097	11
TPHxxx_LB	38.08	-117.22	76.391	16.053	0.935	0.084	23
TPNVxx_US	36.95	-116.25	67.522	14.494	1.055	0.065	19
TROxxx_AZ	33.52	-116.43	-78.594	13.971	1.567	0.127	18
TTWxxx_UW	47.69	-121.69	66.601	11.48	1.258	0.052	25
TUCAxx_UW	46.51	-118.15	-70.725	11.592	1.114	0.135	11
TUCxxx_IU	32.31	-110.78	32.723	11.132	1.267	0.109	12
TUCxxx_US	32.31	-110.78	30.252	4.929	1.288	0.253	4
TUL1xx_TA	35.91	-95.79	74.832	7.098	0.956	0.06	18
TUQxxx_CI	35.44	-115.92	87.733	10.98	1.38	0.046	27
TWR2xx_XJ	36.35	-118.41	67	6.5	1.2	0.22	1

TX01xx_XM	31.42	-103.11	11.5	2.502	0.875	0.175	2
TX03xx_XM	31.62	-103.32	26	12.183	1.125	0.025	2
TX05xx_XM	31.88	-103.61	19	3	0.9	0.1	1
TX06xx_XM	31.97	-103.71	-9	17.543	0.875	0.075	2
TX31xx_IM	29.33	-103.67	-70.768	14.217	0.84	0.062	26
TX32xx_IM	29.33	-103.67	-75.581	14.156	0.76	0.043	36
U04Cxx_TA	36.36	-120.78	-86.822	8.929	2.09	0.143	5
U05Cxx_TA	36.34	-120.12	87.026	9.32	1.525	0.244	4
U10Axx_TA	36.42	-116.33	77.585	17.489	1.138	0.225	4
U11Axx_TA	36.42	-115.38	53.494	14.564	0.836	0.087	11
U12Axx_TA	36.43	-114.54	45.72	10.436	0.861	0.083	9
U13Axx_TA	36.42	-113.97	24.543	9.145	1.4	0.15	7
U14Axx_TA	36.42	-113.18	24.991	12.84	1.208	0.067	13
U15Axx_AE	36.43	-112.29	62	12	0.7	0.15	1
U15Axx_AR	36.43	-112.29	39	18.651	0.9	0.1	2
U15Axx_TA	36.43	-112.29	24.06	46.596	1.056	0.124	8
U16Axx_TA	36.14	-111.13	55.127	7.52	1.014	0.101	7
U17Axx_TA	36.6	-110.66	47.904	8.13	0.981	0.095	8
U18Axx_TA	36.42	-109.87	41.264	12.777	1.075	0.07	10
U19Axx_TA	36.29	-109.21	4	3.003	1.05	0.5	2
U20Axx_TA	36.38	-108.52	10.353	29.6	1.286	0.186	7
U21Axx_TA	36.43	-107.66	9.168	16.795	1.265	0.221	10
U22Axx_TA	36.38	-106.85	64	16	0.6	0.22	1
U23Axx_TA	36.33	-106.19	32.567	6.738	1.125	0.144	4
U24Axx_TA	36.41	-105.28	23	7.035	2	0.4	2
U25Axx_TA	36.4	-104.41	33.898	6.609	1.25	0.068	8
U26Axx_TA	36.39	-103.74	19.078	16.662	0.931	0.098	8
U27Axx_TA	36.42	-102.82	23.752	7.838	0.95	0.132	4
U28Axx_TA	36.38	-102.22	15.082	9.161	0.894	0.082	9
U29Axx_TA	36.45	-101.27	17.851	16.59	0.827	0.081	13
U30Axx_TA	36.53	-100.65	34.665	12.272	0.825	0.089	6
U32Axx_OK	36.38	-99	27.5	30.206	1.075	0.025	2
U32Axx_TA	36.38	-99	43	15.366	0.875	0.125	2
U33Axx_TA	36.43	-98.11	76.5	4.509	0.775	0.225	2
U34Axx_TA	36.44	-97.54	74.924	14.024	0.667	0.117	3
U35Axx_TA	36.37	-96.73	70.124	21.595	0.787	0.09	4
U36Axx_TA	36.39	-95.73	67.041	7.029	0.85	0.052	5
U37Axx_TA	36.41	-95.12	58.656	10.916	0.925	0.096	6
U38Axx_TA	36.44	-94.39	57.79	14.591	0.842	0.047	6
U38Bxx_N4	36.44	-94.39	50.5	6.528	1.125	0.175	2
U39Axx_TA	36.38	-93.48	47.751	12.45	0.863	0.101	4

U40Axx_TA	36.36	-92.85	52.639	16.133	0.941	0.044	28
U41Axx_TA	36.34	-91.92	48.776	26.042	0.822	0.089	9
U42Axx_TA	36.35	-91.24	38	7	0.65	0.17	1
U43Axx_TA	36.37	-90.41	54.567	21.919	0.9	0.097	6
UALRxx_NM	34.78	-92.34	55.109	11.52	1.262	0.108	25
UKHxxx_YC	45.16	-118.9	45	7.5	0.95	0.23	1
ULMxxx_CN	50.25	-95.88	57.822	15.781	1.348	0.037	68
UMATxx_UW	45.29	-118.96	-81.242	6.506	1.32	0.138	5
USCxxx_CI	34.02	-118.29	73.715	12.219	1.464	0.088	14
USCxxx_TS	34.02	-118.29	72	9.871	1.733	0.083	3
UT51xx_XM	37.07	-110	46.676	4.998	1.067	0.192	3
UT52xx_XM	37.23	-110.13	59	14.5	1.3	0.42	1
UT53xx_XM	37.35	-110.33	60.854	8.281	1.225	0.188	4
UT54xx_XM	37.42	-110.51	67.272	14	1.087	0.072	4
UT55xx_XK	37.61	-110.7	51.95	7.146	0.9	0.189	3
UT57xx_XK	37.74	-110.92	42.121	9.877	1.013	0.094	4
UT59xx_XK	37.98	-111.2	37.5	4.509	1.35	0.1	2
UT62xx_XK	38.37	-111.71	13.68	10.551	0.925	0.103	4
UT63xx_XK	38.35	-111.96	13	3.5	1.25	0.3	1
UT65xx_XK	38.58	-112.43	10.41	12.944	1	0.106	5
UT66xx_XK	38.68	-112.55	-18	7.5	1.55	0.37	1
UT67xx_XK	38.76	-112.74	0	4.007	1.375	0.275	2
UT68xx_XK	38.83	-112.87	-11.13	6.794	1.381	0.104	8
UT69xx_XK	38.91	-112.99	-4.778	6.089	1.25	0.117	5
UT70xx_XK	39.02	-113.26	-25.324	4.033	1.433	0.213	3
UT71xx_XK	39.09	-113.43	-29.665	2.496	1.65	0.161	3
UT72xx_XK	39.15	-113.56	-30	4.306	1.45	0.184	4
V03Cxx_TA	36.02	-121.24	88.445	6.447	1.5	0.118	5
V04Cxx_TA	35.64	-120.87	-72.862	17.703	1.35	0.172	5
V05Cxx_TA	35.87	-119.9	-73.5	12.707	1.55	0.45	2
V11Axx_TA	35.84	-115.43	84.195	22.947	1.087	0.159	8
V12Axx_TA	35.73	-114.85	65.592	19.852	1.35	0.112	7
V13Axx_TA	35.85	-113.98	34.194	7.635	1.17	0.115	10
V14Axx_TA	35.63	-113.11	25.243	15.931	1.42	0.107	15
V15Axx_TA	35.82	-112.17	39.77	10.494	1.163	0.074	16
V17Axx_TA	35.62	-110.79	34.316	12.915	1.3	0.477	3
V18Axx_TA	35.71	-109.93	26.053	11.515	1.112	0.23	4
V19Axx_TA	35.71	-109.05	14.027	10.101	1.106	0.148	8
V20Axx_TA	35.8	-108.47	31.013	5.879	1.42	0.121	5
V21Axx_TA	35.81	-107.64	53.673	7.796	0.967	0.192	3
V22Axx_TA	35.91	-106.91	45.858	33.51	0.69	0.037	5

V23Axx_TA	35.75	-106.18	29.5	8.564	1.775	0.675	2
V24Axx_TA	35.73	-105.27	44.796	16.406	1.31	0.177	5
V25Axx_TA	35.84	-104.62	42.131	5.016	1.138	0.088	8
V26Axx_TA	35.8	-103.79	28	4	1.2	0.18	1
V27Axx_TA	35.76	-102.84	19.884	10.758	1.04	0.051	5
V28Axx_TA	35.75	-102.22	4.651	9.857	0.875	0.092	4
V29Axx_TA	35.87	-101.52	28.5	4.509	0.9	0.3	2
V30Axx_TA	35.76	-100.69	3.559	10.08	0.744	0.071	9
V31Axx_TA	35.77	-99.84	64.5	2.502	0.65	0.05	2
V32Axx_TA	35.72	-99.04	43	10.5	0.6	0.15	1
V33Axx_TA	35.82	-98.29	-87.612	8.425	1	0.218	3
V34Axx_TA	35.83	-97.52	-81.933	22.513	1.31	0.193	5
V35Axx_TA	35.76	-96.84	71.392	7.593	0.907	0.093	7
V36Axx_TA	35.79	-95.94	68.557	5.98	0.867	0.064	9
V37Axx_TA	35.88	-95.14	74.976	8.017	1.01	0.071	10
V38Axx_TA	35.86	-94.41	75.434	22.298	0.989	0.087	9
V39Axx_TA	35.84	-93.64	62.654	5.92	1.069	0.067	13
V40Axx_TA	35.8	-92.82	65.543	9.36	1.05	0.069	14
V41Axx_TA	35.79	-92.16	76.424	9.338	0.971	0.057	7
V42Axx_TA	35.81	-91.39	55.475	29.096	1.05	0.072	5
V43Axx_TA	35.79	-90.54	79	15	0.45	0.1	1
VALTxx_CC	46.21	-122.19	-85.509	14.118	1.265	0.107	10
VBMSxx_US	32.22	-90.52	70.393	15.852	1.055	0.062	11
VCSxxx_CI	34.48	-118.12	-86.261	7.021	1.417	0.046	45
VESxxx_CI	35.84	-119.08	-84.5	10.215	1.188	0.043	4
VINExx_XN	35.95	-120.54	-75.5	4.509	1.3	0.5	2
VTVxxx_CI	34.56	-117.33	-77.356	9.697	1.208	0.058	20
VTVxxx_TS	34.57	-117.33	-80.506	11.077	1.232	0.103	11
W01xxx_ZG	44.92	-115.95	79.418	7.415	1.241	0.11	11
W020xx_XU	47.87	-122.95	80.358	4.506	1.397	0.054	15
W02xxx_ZG	44.93	-116.14	-87.739	7.044	1.087	0.347	4
W030xx_XU	47.81	-122.91	80.584	7.057	1.353	0.049	16
W03xxx_ZG	44.99	-116.4	79	9.076	1.25	0.15	2
W040xx_XU	47.6	-123.12	83.62	6.135	1.4	0.138	8
W05xxx_ZG	45.13	-116.84	43	17	0.9	0.4	1
W060xx_XU	47.32	-123.31	79.513	6.635	1.212	0.109	8
W070xx_XU	46.92	-123.23	72.604	8.721	1.11	0.121	5
W080xx_XU	46.72	-123.28	73.844	5.709	1.08	0.119	5
W08xxx_ZG	45.43	-117.36	83.5	3.504	1.075	0.025	2
W090xx_XU	46.6	-123.42	78	17	0.55	0.17	1
W09xxx_ZG	45.5	-117.81	63	0.01	0.75	0.15	2

W100xx_XU	46.41	-123.66	61.5	12.522	1.037	0.137	4
W10xxx_ZG	45.64	-117.68	70.817	4.07	1.36	0.134	5
W110xx_XU	46.2	-123.29	57	6.5	0.8	0.12	1
W11xxx_ZG	45.81	-117.55	81	9.5	1.15	0.23	1
W12Axx_TA	35.3	-114.87	71.251	2.818	1.163	0.058	8
W12xxx_ZG	45.95	-117.46	76.977	8.652	1.367	0.044	3
W13Axx_AE	35.1	-113.89	41.066	14.777	1.133	0.084	12
W13Axx_AR	35.1	-113.89	37.551	7.538	1.075	0.047	14
W13Axx_TA	35.1	-113.89	42.931	7.681	1.052	0.047	21
W13xxx_ZG	46.12	-117.38	77.587	5.289	1.29	0.102	5
W14Axx_TA	35.21	-113.08	43.865	10.462	1.095	0.068	11
W14xxx_ZG	46.27	-117.5	72.813	13.569	1.332	0.071	11
W15Axx_TA	35.18	-112.27	47.503	7.515	1.5	0.054	19
W15xxx_ZG	46.38	-117.55	77.413	7.831	1.2	0.148	5
W16Axx_TA	35.1	-111.53	71.325	10.049	1.125	0.13	6
W16xxx_ZG	46.51	-117.64	-77.534	12.382	1.075	0.12	10
W17Axx_TA	35.08	-110.71	39.568	13.612	1.16	0.103	5
W17xxx_ZG	46.62	-117.72	-87.284	17.954	0.91	0.066	5
W18Axx_TA	35.12	-109.74	7.663	10.902	0.863	0.022	34
W19Axx_TA	35.11	-109.39	16.5	5.517	0.9	0.1	2
W20Axx_TA	35.13	-108.5	52.214	17.437	0.783	0.145	3
W20xxx_ZG	44.54	-117.92	67.014	5.109	1.067	0.145	3
W21Axx_TA	35.12	-107.65	36.902	15.174	1.067	0.089	18
W21xxx_ZG	46.72	-117.38	73.081	8.691	1.1	0.153	3
W22Axx_TA	35.07	-106.87	48.637	5.922	1.5	0.278	3
W22xxx_ZG	46.79	-118.07	69	13.234	1	0.3	2
W23Axx_TA	35.16	-106.15	36.543	11.698	1.289	0.136	9
W23xxx_ZG	46.97	-117.76	78.5	6.528	1.05	0.2	2
W24Axx_TA	35.21	-105.41	37.938	13.006	1.047	0.085	17
W24xxx_ZG	45.54	-118.08	54	4	0.8	0.1	1
W25Axx_TA	35.22	-104.46	16.283	19.015	1	0.103	13
W26Axx_TA	35.09	-103.77	24	12.183	0.925	0.175	2
W27Axx_TA	35.06	-103.06	-7.358	11.684	0.875	0.145	4
W28Axx_TA	35.26	-102.21	45.5	2.502	0.775	0.125	2
W29Axx_TA	35.12	-101.65	-2.565	11.019	0.85	0.127	5
W30Axx_TA	35.18	-100.58	-61.669	49.789	0.688	0.136	4
W31Axx_TA	35.19	-99.94	77	2.5	0.95	0.07	1
W32Axx_TA	35.12	-99.25	-79.5	19.211	1.025	0.325	2
W33Axx_TA	35.15	-98.47	88.416	9.012	1.133	0.164	3
W34Axx_TA	35.24	-97.77	-88.354	9.883	0.667	0.159	3
W35Axx_TA	35.15	-96.87	84.006	4.553	0.55	0.058	3

W36Axx_TA	35.14	-96.23	72.956	11.491	0.867	0.065	6
W37Axx_TA	35.14	-95.43	72.561	11.735	0.967	0.073	3
W37Bxx_TA	35.14	-95.43	76.284	7.625	0.912	0.107	4
W38Axx_TA	35.07	-94.52	87.593	14.977	0.975	0.108	8
W39Axx_TA	35.2	-93.78	71.412	10.707	1.256	0.083	17
W40Axx_TA	35.19	-93.07	52.387	14.259	1.06	0.157	5
W41Axx_TA	35.17	-92.25	76	7	1.1	0.23	1
W41Bxx_TA	35.17	-92.25	63.07	25.223	1.093	0.08	15
W42Axx_TA	35.27	-91.52	62	10.104	0.7	0.1	2
W43Axx_TA	35.09	-90.71	-59	21	0.85	0.45	1
WALxxx_YC	45.55	-117.47	79.5	1.5	1.125	0.025	2
WCNxxx_NN	39.3	-119.76	64.144	17.438	1.6	0.267	4
WCPxxx_XH	40.52	-114.17	-36.325	7.176	0.983	0.087	6
WDCxxx_BK	40.58	-122.54	52.219	15.772	1.035	0.043	37
WDCxxx_US	40.58	-122.54	50.324	13.553	1.133	0.061	21
WENLxx_BK	37.62	-121.76	-81.331	2.626	2.417	0.117	3
WHA00x_YA	35.87	-117.73	-87	5	1.1	0.12	1
WHAS5x_YA	35.85	-117.74	-74	3.5	1.4	0.15	1
WHPxxx_XJ	36.59	-118.22	78.5	5.517	1.525	0.175	2
WHTXxx_TA	31.99	-97.46	12.555	17.094	0.741	0.046	28
WIFExx_CC	44.06	-121.82	62.112	6.097	1.469	0.055	21
WIGxxx_XG	40.33	-104.07	60	13.5	0.9	0.35	1
WISHxx_UW	47.12	-123.77	83.667	2.055	1.633	0.169	3
WMCxxx_AZ	33.57	-116.67	-85.42	9.618	1.323	0.058	51
WMOKxx_US	34.74	-98.78	-74.968	18.336	0.83	0.04	20
WMTxxx_XH	40.11	-112.84	-7	7.5	1.3	0.2	1
WOLLxx_UW	47.06	-118.92	88.005	11.574	1.306	0.086	25
WSHxxx_YC	46.11	-117.19	76	4.007	0.925	0.325	2
WUAZxx_US	35.52	-111.37	39.484	8.782	1.105	0.035	83
WVORxx_US	42.43	-118.64	81.786	5.397	1.866	0.051	51
X13Axx_TA	34.59	-113.83	47.532	11.12	0.967	0.126	6
X14Axx_TA	34.47	-112.89	57.095	10.158	1.214	0.054	18
X15Axx_TA	34.49	-112.24	39.799	9.274	1.262	0.072	17
X16Axx_AE	34.42	-111.44	42.262	9.516	1.45	0.092	9
X16Axx_AR	34.42	-111.44	46.636	9.518	1.515	0.094	10
X16Axx_TA	34.42	-111.44	49.027	8.745	1.614	0.076	11
X17Axx_TA	34.34	-110.81	64.399	9.806	1.013	0.086	8
X18Axx_AE	34.53	-109.95	34.456	21.231	0.967	0.262	3
X18Axx_AR	34.53	-109.95	8.5	26.303	0.725	0.175	2
X18Axx_TA	34.53	-109.95	24.614	9.857	1.025	0.18	4
X19Axx_TA	34.43	-109.29	43.731	13.002	0.893	0.08	7

X20Axx_TA	34.54	-108.5	37.317	22.322	0.82	0.049	5
X21Axx_TA	34.45	-107.79	38.853	10.5	1.132	0.101	11
X22Axx_TA	34.51	-107.01	-64	5.5	1.45	0.38	1
X23Axx_TA	34.58	-106.19	32.773	23.905	1.17	0.165	5
X24Axx_TA	34.56	-105.43	37.445	11.707	1.267	0.295	3
X25Axx_TA	34.53	-104.66	30.08	5.546	1.017	0.039	12
X27Axx_TA	34.65	-103.1	14	12.5	0.55	0.12	1
X28Axx_TA	34.52	-102.2	23.147	11.89	0.967	0.079	6
X29Axx_TA	34.45	-101.7	26.5	0.5	1.05	0.05	2
X30Axx_TA	34.45	-100.87	18	6.022	0.625	0.025	2
X31Axx_TA	34.63	-99.98	86.139	29.452	0.7	0.076	6
X32Axx_TA	34.42	-99.29	-87.326	11.032	0.9	0.11	5
X33Axx_TA	34.54	-98.5	-69.863	12.344	0.855	0.033	11
X34Axx_TA	34.6	-97.83	-54	2.001	0.95	0	2
X35Axx_TA	34.4	-96.97	76.233	10.157	0.683	0.017	3
X36Axx_TA	34.57	-96.35	-87.209	20.577	0.9	0.059	6
X37Axx_OK	34.59	-95.37	75.716	4.597	0.943	0.04	7
X37Axx_TA	34.59	-95.37	77.731	7.157	0.871	0.066	7
X38Axx_TA	34.67	-94.83	-77.307	15.23	1.123	0.074	11
X39Axx_TA	34.51	-94.11	-77.668	3.686	1.167	0.06	3
X40Axx_TA	34.49	-92.83	60.023	7.438	1.36	0.052	24
X41Axx_TA	34.49	-92.51	58.244	9.882	1.275	0.053	12
X42Axx_TA	34.55	-91.63	30.078	10.536	1.075	0.17	4
X43Axx_TA	34.52	-90.88	66.9	9.147	1.35	0.124	6
X44Axx_TA	34.5	-90.15	65.937	14.209	1.308	0.13	6
XPFOxx_II	33.61	-116.46	89	14	1.05	0.3	1
Y02xxx_XC	44.07	-112.64	44.05	14.071	1.288	0.212	4
Y03xxx_XC	43.81	-112.31	37.5	4.509	0.925	0.125	2
Y04xxx_XC	43.51	-111.9	64.501	2.18	1.462	0.123	4
Y05xxx_XC	43.19	-111.58	62.5	7.544	1.575	0.025	2
Y07xxx_XC	42.56	-110.89	56.143	12.378	1.112	0.152	4
Y12Cxx_TA	33.75	-114.52	73.612	6.793	1.117	0.079	12
Y12xxx_XC	45.6	-113.11	61.5	3.504	0.8	0.2	2
Y13Axx_TA	33.81	-113.83	60.522	12.356	1.292	0.112	12
Y13xxx_XC	45.27	-112.82	28.141	29.056	0.938	0.112	4
Y14Axx_AE	33.94	-113	60.694	3.742	1.37	0.059	10
Y14Axx_AR	33.94	-113	61.583	7.53	1.49	0.075	15
Y14Axx_TA	33.94	-113	60.46	9.649	1.35	0.054	32
Y14xxx_XC	44.99	-112.46	54	3.5	1.2	0.12	1
Y15Axx_TA	33.95	-112.33	58.178	9.779	1.492	0.081	13
Y15xxx_XC	44.58	-112.06	61.635	7.883	1.433	0.044	3

Y16Axx_TA	33.88	-111.48	55.377	6.867	1.527	0.107	11
Y16xxx_XC	44.4	-111.6	29	3.003	1.35	0.15	2
Y17Axx_TA	33.7	-110.84	35.78	8.752	1.417	0.079	12
Y17xxx_XC	44.1	-111.19	65.514	11.066	1.267	0.196	3
Y18Axx_TA	33.78	-110.03	35.293	8.092	1.478	0.055	16
Y18xxx_XC	43.75	-111.03	63.5	0.5	1.6	0.4	2
Y19Axx_TA	33.96	-109.25	34.275	8.938	1.422	0.056	9
Y19xxx_XC	43.62	-110.6	51.471	10.424	1.167	0.109	3
Y20Axx_TA	33.91	-108.38	50.248	3.964	1.213	0.101	4
Y20xxx_XC	43.17	-110	-82.5	27.571	1	0.05	2
Y21Axx_TA	34.01	-107.67	35.645	15.795	1.182	0.126	11
Y22Axx_SC	33.94	-106.97	45.51	8.702	1.247	0.062	16
Y22Axx_TA	33.94	-106.97	47.414	20.63	1.241	0.137	11
Y22Cxx_TA	34.07	-106.92	56.884	20.051	1.444	0.177	9
Y22Dxx_TA	34.07	-106.92	49.925	9.2	1.337	0.113	8
Y22Exx_TA	34.07	-106.92	55	3.5	1.45	0.15	1
Y22xxx_XC	42.59	-109.25	77	4.5	1.65	0.43	1
Y23Axx_TA	33.93	-106.05	47.994	4.553	1.1	0.104	3
Y23xxx_XC	46.28	-112.93	31.5	19.211	1.225	0.425	2
Y24Axx_TA	33.93	-105.44	39.24	11.73	1.057	0.103	15
Y24xxx_XC	45.98	-112.62	29.165	10.457	0.917	0.06	3
Y25Axx_TA	33.92	-104.69	12.029	19.984	0.923	0.085	11
Y25xxx_XC	45.71	-112.18	73	11.5	1	0.22	1
Y26Axx_TA	33.92	-103.82	10.708	4.898	1.007	0.046	7
Y26xxx_XC	45.45	-111.75	62.5	0.5	0.8	0.1	2
Y27Axx_TA	33.88	-103.16	7.189	23.17	1.007	0.103	7
Y28Axx_TA	33.91	-102.25	38.302	18.863	0.842	0.081	6
Y29Axx_TA	33.86	-101.67	21.104	12.071	0.5	0.132	4
Y30Axx_TA	33.88	-100.9	30.72	18.774	1.055	0.088	11
Y31Axx_TA	33.96	-100.26	43.53	23.421	1.078	0.078	9
Y32Axx_TA	34	-99.44	57.067	25.816	0.909	0.081	11
Y32xxx_XC	43.58	-109.45	67.528	10.3	1.475	0.166	4
Y33Axx_TA	34.01	-98.63	82.736	43.348	0.811	0.073	9
Y33xxx_XC	43.23	-108.98	87	11	0.8	0.17	1
Y34Axx_TA	33.96	-97.76	72.462	7.052	1.028	0.132	9
Y35Axx_TA	33.91	-97.04	61.472	4.929	1.038	0.099	4
Y35xxx_XC	42.57	-108.04	50	17.5	0.9	0.38	1
Y36Axx_TA	33.9	-96.28	76.986	5.109	1.1	0.05	3
Y37Axx_TA	33.98	-95.62	75.355	6.903	1.25	0.107	7
Y37xxx_XC	46.18	-112.03	30.916	24.65	1.013	0.062	4
Y38Axx_TA	33.93	-94.73	65.367	9.055	1.217	0.136	6

Y38xxx_XC	45.9	-111.61	-67	13.5	0.7	0.2	1
Y39Axx_TA	33.94	-94.09	66.597	7.948	1.443	0.072	15
Y39xxx_XC	45.59	-111.22	82.5	0.5	0.825	0.275	2
Y40Axx_TA	34.01	-93.28	82.588	4.031	0.88	0.046	5
Y40xxx_XC	45.35	-110.75	90	4	1.4	0.18	1
Y41Axx_TA	33.88	-92.61	67.87	5.461	1.117	0.093	6
Y42Axx_TA	33.84	-91.79	64.257	12.52	1.05	0.134	6
Y43Axx_TA	33.91	-90.93	51.511	12.155	1.175	0.209	4
Y44Axx_TA	33.96	-90.21	64.85	10.968	1.167	0.109	6
Y46xxx_XC	43.6	-108.2	72	2.5	1.3	0.15	1
Y47xxx_XC	45.99	-110.04	60.308	11.159	1.25	0.117	4
Y50xxx_XC	45.15	-108.97	41	17.543	0.925	0.075	2
Y51xxx_XC	44.77	-108.53	48	9	1.1	0.22	1
Y61xxx_XC	46.6	-111.03	58.5	13.763	1.55	0.4	2
Y62xxx_XC	46.17	-110.56	66	14.295	0.975	0.075	2
Y63xxx_XC	44.54	-107.92	55	10	0.65	0.1	1
Y64xxx_XC	44.11	-107.47	84.522	28.469	0.833	0.102	9
YACTxx_UW	45.93	-122.42	87.096	9.268	1.188	0.092	12
YAQxxx_AZ	33.17	-116.35	85.241	6.379	1.29	0.12	5
YBHxxx_BK	41.73	-122.71	62.8	13.17	1.279	0.04	21
YOS01x_XE	37.75	-119.78	69.892	9.779	1.35	0.065	4
YOS02x_XE	37.77	-119.76	74.579	12.873	1.267	0.088	3
YOS03x_XE	37.79	-119.73	73.279	7.753	1.367	0.174	3
YOS04x_XE	37.82	-119.71	59.621	10.837	1.48	0.122	5
YOS05x_XE	37.84	-119.69	80.001	2.161	1.25	0.15	3
YOS06x_XE	37.85	-119.61	68.658	6.571	1.367	0.088	3
YOS07x_XE	37.81	-119.58	64.249	3.494	1.388	0.125	4
YOS08x_XE	37.81	-119.55	62.75	1.921	1.287	0.094	4
YOS09x_XE	37.82	-119.5	64.272	6.278	1.388	0.175	4
YOS10x_XE	37.85	-119.44	56.524	9.847	1.5	0.179	4
YOS11x_XE	37.88	-119.4	49.062	10.864	1.55	0.151	4
YSCFxx_XT	40.43	-108.43	66	2	2.35	0.42	1
YUMxxx_XG	40.16	-102.78	27	16.448	0.8	0.15	2
Z13Axx_TA	33.2	-113.66	62.921	18.041	1.244	0.152	8
Z14Axx_AR	33.36	-112.95	62.546	4.302	1.317	0.111	9
Z14Axx_TA	33.36	-112.95	64.091	11.072	1.388	0.061	36
Z15Axx_TA	33.29	-112.16	64.037	6.928	1.007	0.077	7
Z16Axx_TA	33.34	-111.43	54.425	11.278	1.338	0.109	8
Z17Axx_TA	33.3	-110.47	22.594	13.895	1.243	0.084	7
Z18Axx_TA	33.09	-110.04	32.563	9.298	1.292	0.081	6
Z19Axx_TA	33.29	-109.27	45.501	3.002	1.337	0.084	8

Z20Axx_TA	33.11	-108.59	49.584	6.14	1.56	0.162	5
Z21Axx_TA	33.31	-107.67	32.728	19.077	1.246	0.118	14
Z22Axx_TA	33.26	-106.96	29.865	16.232	1.045	0.121	10
Z23Axx_TA	33.26	-106.23	-87	4.5	1.3	0.28	1
Z24Axx_TA	33.33	-105.36	38.599	15.944	0.997	0.045	16
Z25Axx_TA	33.28	-104.72	38.364	15.773	1.022	0.071	18
Z26Axx_TA	33.27	-103.98	17.276	8.127	1.11	0.121	5
Z27Axx_TA	33.31	-103.21	28.734	14.819	0.779	0.077	7
Z28Axx_TA	33.29	-102.39	41	2.001	0.775	0.025	2
Z29Axx_TA	33.26	-101.71	57	5.5	1.45	0.55	1
Z30Axx_TA	33.29	-101.13	15.58	28.937	0.795	0.07	11
Z31Axx_TA	33.32	-100.14	12.159	22.201	0.979	0.115	7
Z32Axx_TA	33.31	-99.48	30.896	17.385	0.7	0.124	8
Z33Axx_TA	33.29	-98.76	42.79	10.778	1.219	0.127	8
Z34Axx_TA	33.37	-97.92	39.37	7.576	0.961	0.115	9
Z35Axx_TA	33.33	-97.25	52	0.816	1.233	0.28	3
Z35Bxx_N4	33.33	-97.25	62.174	9.041	1.317	0.15	6
Z36Axx_TA	33.27	-96.43	61.5	8.564	1.05	0.1	2
Z37Axx_TA	33.2	-95.62	69.417	14.765	1.017	0.136	3
Z38Axx_TA	33.25	-94.99	60	3.5	1.15	0.1	1
Z38Bxx_N4	33.26	-94.99	58	2.001	1.025	0.025	2
Z39Axx_TA	33.24	-94.18	66.843	9.726	1.035	0.072	10
Z40Axx_TA	33.26	-93.4	57.144	11.931	1.113	0.131	8
Z41Axx_TA	33.26	-92.8	59.359	9.341	1.26	0.08	10
Z42Axx_TA	33.27	-91.95	67.416	16.483	1.135	0.104	10
Z43Axx_TA	33.21	-91.24	74.959	10.917	1.06	0.098	5
Z44Axx_TA	33.28	-90.43	64	3.003	1.325	0.025	2
ZIZZxx_XL	34.26	-109.72	41.669	16.371	0.95	0.126	3

Table S2. Averaged Splitting Parameters in 726 Overlapping Circles of 1º Radius.

C-lat	C-lon	PHI	PHI-STD	DT	DT-STD	N-meas
27	-115	96	0	1.55	0	1
27	-114	111.655	19.0582	1.1667	0.1236	6
27	-113	118.2756	25.7286	1.15	0.1118	7
27	-112	55.6443	35.8326	1.15	0.2473	6
27	-111	54	0	2.15	0	1
27	-110	75.4923	8.7047	1.262	0.0622	25
27	-109	75.4923	8.7047	1.262	0.0622	25
27	-108	78.2567	4.0268	1.2625	0.0625	4
27	-106	66	0	1.55	0	1
27	-105	66	0	1.55	0	1
27	-100	58.5104	22.2561	1.0618	0.0494	17
27	-99	48.6865	16.3989	1.1527	0.0364	56
27	-98	46.7333	13.6341	1.1727	0.0425	55
27	-97	46.4163	15.5968	1.3	0.2019	5
28	-115	81.5468	10.621	0.9833	0.306	3
28	-114	101.8189	23.7276	1.05	0.1243	8
28	-113	112.3836	18.4657	1.175	0.1289	6
28	-112	100	0	1.6	0	1
28	-110	71.9473	11.5367	1.2938	0.0959	16
28	-109	80.0123	4.2047	1.15	0.0837	6
28	-106	66	0	1.55	0	1
28	-105	66	0	1.55	0	1
28	-101	46.4709	15.1747	1.1846	0.1081	13
28	-100	71.7209	26.0009	1.1577	0.0313	71
28	-99	64.9887	22.9535	1.1907	0.0256	107
28	-98	54.9802	15.6974	1.264	0.0458	50
28	-97	51.497	14.9744	1.3417	0.1895	6
28	-96	54	0	1.35	0	1
29	-115	74.5	3.5044	0.7	0.2	2
29	-114	74.5	3.5044	0.7	0.2	2
29	-112	62	7.0353	1.05	0.2	2
29	-111	69.256	15.776	1.2976	0.0856	21
29	-110	69.4293	16.0625	1.295	0.0914	20
29	-109	69.2895	16.9263	1.2361	0.0808	18
29	-105	105.6709	12.1337	0.8333	0.0463	48
29	-104	106.0003	14.5778	0.825	0.0336	76
29	-103	109.2224	12.0157	0.835	0.0387	60
29	-102	10.0517	15.8858	0.97	0.0815	5

29	-101	41.6394	20.2906	1.175	0.0693	26
29	-100	65.6948	27.3911	1.1259	0.0336	87
29	-99	72.0129	18.8099	1.1863	0.0303	95
29	-98	69.728	14.9231	1.3675	0.038	80
29	-97	71.23	10.3776	1.5158	0.0386	57
29	-96	69.2064	8.2985	1.6781	0.0768	16
29	-95	71.321	9.5196	1.6813	0.1172	8
29	-91	70.2498	2.2788	1.5625	0.1434	4
29	-90	72.5	0.5	1.675	0.275	2
30	-117	76	0	1.6	0	1
30	-116	80.5769	22.4039	0.9875	0.1267	8
30	-115	81.5058	24.1433	0.9	0.1058	7
30	-113	48.1341	13.2836	0.9357	0.098	7
30	-112	50.8376	14.2894	0.925	0.0856	8
30	-111	62	7.0353	1.05	0.2	2
30	-110	71.6962	20.8732	1.205	0.1214	10
30	-109	58	0	0.75	0	1
30	-106	37.8225	11.1199	0.9071	0.0602	7
30	-105	48.8518	38.4081	0.8758	0.051	33
30	-104	102.5018	39.68	0.9042	0.0312	107
30	-103	52.5343	57.4016	1.0071	0.0398	56
30	-102	27.2727	15.8444	1.0948	0.0372	58
30	-101	32.6223	18.3191	1.0259	0.0387	79
30	-100	44.8984	26.8481	0.9692	0.0383	86
30	-99	72.0842	17.9991	1.0227	0.0383	66
30	-98	65.1917	18.4408	1.2431	0.0298	131
30	-97	67.062	13.1998	1.4411	0.0296	135
30	-96	68.8191	8.8837	1.6546	0.0322	87
30	-95	70.8305	6.7007	1.7563	0.0378	48
30	-94	73.0737	4.8315	1.7771	0.0621	24
30	-93	73.5153	6.107	1.5588	0.0656	17
30	-92	81.39	15.8907	1.4353	0.0711	17
30	-91	80.2904	16.1241	1.3146	0.0596	24
30	-90	73.4173	15.3571	1.425	0.0964	10
31	-117	89.8226	19.9749	1.5778	0.1532	9
31	-116	82.7679	18.334	1.266	0.0991	25
31	-115	88.535	11.7815	0.75	0.057	5
31	-113	49.2051	12.6745	0.9562	0.0873	8
31	-112	52.2339	13.298	1.0654	0.1116	13
31	-111	57.775	7.7065	1.4	0.1085	15
31	-110	47.1107	8.0386	1.2068	0.0354	103

31	-109	47.6114	10.0643	1.1657	0.034	102
31	-108	35.1712	22.0633	1.025	0.0743	10
31	-107	15.552	10.9745	1.4286	0.0712	28
31	-106	26.9363	13.2072	1.1079	0.0338	108
31	-105	26.8354	13.5249	1.079	0.0241	162
31	-104	16.8012	16.3629	1.0918	0.0297	104
31	-103	14.3888	15.0709	1.006	0.0249	108
31	-102	21.1613	19.1958	1.0167	0.0271	111
31	-101	33.8583	21.4651	0.9433	0.0286	112
31	-100	47.3516	23.5847	0.9239	0.0266	113
31	-99	55.7125	21.8107	0.9318	0.0262	118
31	-98	53.6007	20.8843	1.1347	0.0281	147
31	-97	55.356	18.4072	1.3054	0.0313	147
31	-96	62.0032	14.7506	1.4395	0.0359	114
31	-95	65.9306	11.1849	1.4389	0.0441	90
31	-94	71.0944	8.2061	1.4482	0.0388	85
31	-93	74.31	8.4186	1.494	0.0348	84
31	-92	75.7373	12.0861	1.3588	0.0402	68
31	-91	75.8458	14.5114	1.2551	0.0377	59
31	-90	75.591	12.2246	1.2189	0.043	37
32	-120	98	0	1.25	0	1
32	-118	77.6461	12.0225	1.1453	0.0444	32
32	-117	73.3805	14.4649	1.1959	0.0338	135
32	-116	87.9777	26.7614	1.257	0.0611	43
32	-115	118.4633	17.6918	0.9811	0.0411	53
32	-114	81.6716	19.6576	1.0603	0.0394	58
32	-113	61.7257	16.4249	1.127	0.0608	37
32	-112	51.4571	16.7331	1.2147	0.0434	68
32	-111	46.8617	14.4758	1.207	0.0457	64
32	-110	48.5635	10.7481	1.2316	0.0299	144
32	-109	39.1461	17.679	1.18	0.0249	180
32	-108	22.5693	19.687	1.1935	0.0356	107
32	-107	17.7665	17.4298	1.2936	0.0458	78
32	-106	25.2388	17.1073	1.1291	0.0236	239
32	-105	28.3905	17.2195	1.0767	0.0187	305
32	-104	22.0247	19.6944	1.0326	0.0237	184
32	-103	12.7278	16.4096	0.954	0.0234	136
32	-102	19.1313	19.1508	0.9179	0.0256	106
32	-101	37.1907	21.6564	0.9328	0.0321	87
32	-100	48.6722	17.5352	0.9634	0.0279	119
32	-99	50.2716	17.2538	0.9738	0.0242	147

32	-98	41.2665	24.0083	0.9616	0.0276	160
32	-97	39.6491	24.9213	1.055	0.0337	151
32	-96	52.9904	19.7901	1.1639	0.0397	97
32	-95	64.0352	15.5411	1.2061	0.0287	107
32	-94	71.3304	12.4014	1.3136	0.0311	118
32	-93	74.2475	11.3298	1.38	0.0322	100
32	-92	76.4115	14.7534	1.3156	0.0462	77
32	-91	71.0105	13.7133	1.1802	0.0439	63
32	-90	73.3255	12.754	1.1822	0.0392	45
33	-121	98	0	1.25	0	1
33	-120	92.2147	7.6437	1.4763	0.0695	19
33	-119	89.293	11.7265	1.3734	0.021	160
33	-118	87.1626	15.4803	1.2029	0.0116	787
33	-117	89.6226	14.4792	1.3042	0.0101	1325
33	-116	93.4329	18.5275	1.2253	0.0147	651
33	-115	93.9043	24.7311	1.2395	0.0283	181
33	-114	73.5499	17.6542	1.296	0.0289	149
33	-113	66.2356	14.0246	1.2732	0.026	166
33	-112	48.0362	15.389	1.2663	0.0366	83
33	-111	37.6666	14.2937	1.3006	0.0359	79
33	-110	41.0133	14.8835	1.3301	0.0311	73
33	-109	32.1003	20.4666	1.2832	0.0317	110
33	-108	27.4057	19.7443	1.226	0.0322	123
33	-107	33.4705	22.5815	1.2504	0.0319	137
33	-106	31.5273	20.9213	1.1749	0.0222	229
33	-105	30.2229	21.2515	1.1184	0.0187	313
33	-104	28.6114	24.744	1.0808	0.0261	185
33	-103	17.2713	30.3795	1.0162	0.0341	105
33	-102	26.8992	27.685	1.045	0.0385	70
33	-101	30.8262	32.3322	1.0682	0.036	88
33	-100	50.3355	24.8524	1.1559	0.0307	111
33	-99	55.1804	18.3901	1.158	0.0301	112
33	-98	54.7635	25.1277	1.1043	0.0316	117
33	-97	58.8346	27.0005	1.1423	0.0391	84
33	-96	62.8574	21.5042	1.1873	0.0474	51
33	-95	69.3206	12.1602	1.184	0.0358	72
33	-94	68.6958	14.0106	1.2443	0.0304	79
33	-93	71.4005	19.0448	1.2853	0.0345	68
33	-92	71.5456	18.33	1.2045	0.0408	66
33	-91	70.1462	14.9593	1.1277	0.0327	56
33	-90	68.8927	13.0724	1.1812	0.0478	24

34	-121	96.5696	18.7687	1.3188	0.0568	24
34	-120	85.3678	17.6834	1.3669	0.024	145
34	-119	84.6004	13.4124	1.377	0.0116	662
34	-118	88.2793	12.8529	1.3683	0.0088	1383
34	-117	91.898	12.9383	1.3199	0.0095	1465
34	-116	91.1471	13.1272	1.393	0.0126	876
34	-115	76.2271	21.9042	1.1646	0.0237	253
34	-114	63.4844	12.7016	1.3064	0.0238	181
34	-113	58.9575	11.7314	1.3412	0.0239	176
34	-112	50.7522	12.9374	1.37	0.0304	120
34	-111	44.0108	16.6787	1.393	0.0323	100
34	-110	38.7261	15.7999	1.2515	0.0378	66
34	-109	42.7063	15.73	1.2458	0.0419	59
34	-108	42.6431	17.6767	1.2711	0.0308	135
34	-107	43.3469	17.9564	1.2866	0.025	186
34	-106	35.5423	20.239	1.2053	0.0262	187
34	-105	29.1578	19.216	1.0997	0.023	195
34	-104	16.0036	24.9971	1.0062	0.0219	170
34	-103	10.3865	31.9191	1.0053	0.0335	95
34	-102	12.5469	31.1611	1.0271	0.0348	96
34	-101	40.7519	30.5781	1.075	0.0492	46
34	-100	77.3767	34.4142	1.069	0.0363	79
34	-99	81.7687	31.6911	1.046	0.0343	87
34	-98	76.6927	28.1003	1.0795	0.0462	56
34	-97	72.1537	17.7875	1.1329	0.0621	41
34	-96	79.7903	18.2795	1.0344	0.0327	45
34	-95	75.9302	17.9294	1.1536	0.0348	70
34	-94	71.5111	18.0404	1.1975	0.0296	101
34	-93	66.8629	15.7504	1.2055	0.0268	109
34	-92	62.0381	17.541	1.1638	0.0335	69
34	-91	66.151	10.897	1.2286	0.0457	42
34	-90	62.479	12.2876	1.1955	0.0608	22
35	-122	101.3061	19.4568	1.29	0.1298	5
35	-121	116.7437	19.8493	1.1881	0.0363	67
35	-120	92.8969	18.7591	1.4395	0.0291	147
35	-119	84.3718	14.326	1.3819	0.0129	589
35	-118	88.3114	13.8192	1.3183	0.0113	790
35	-117	93.8026	12.2374	1.2399	0.0138	525
35	-116	85.3479	19.0639	1.1527	0.0168	413
35	-115	67.7601	22.8871	1.0917	0.019	294
35	-114	51.2697	17.963	1.0766	0.0217	207

35	-113	48.105	16.0161	1.3115	0.0265	148
35	-112	44.209	12.6753	1.2378	0.025	189
35	-111	37.9195	20.4364	1.152	0.0266	175
35	-110	21.2536	24.5663	1.0279	0.0353	70
35	-109	28.3116	23.5805	1.1133	0.0305	124
35	-108	41.1756	19.9865	1.225	0.026	158
35	-107	42.1024	19.205	1.318	0.0258	217
35	-106	42.1186	18.1607	1.319	0.0238	231
35	-105	37.767	18.4179	1.2	0.0288	142
35	-104	15.7184	26.3434	1.0758	0.0616	31
35	-103	4.3328	28.4621	0.9897	0.0324	58
35	-102	11.7825	32.5339	1.0354	0.0476	48
35	-101	19.4034	44.4733	1.0581	0.0529	43
35	-100	87.1392	27.3733	0.996	0.0404	50
35	-99	94.8681	21.6648	0.954	0.0322	62
35	-98	91.0486	21.2443	0.9942	0.0462	43
35	-97	76.8319	16.8225	1.0148	0.0598	27
35	-96	82.194	16.6658	1.075	0.0391	62
35	-95	79.3909	17.9124	1.1548	0.0348	84
35	-94	72.6244	18.5493	1.2198	0.0297	121
35	-93	65.9796	18.1534	1.2067	0.0287	150
35	-92	60.208	17.2379	1.2464	0.0366	97
35	-91	57.9695	24.275	1.3263	0.0681	38
35	-90	66.2833	16.7931	1.2868	0.0681	19
36	-123	98.5	1.5003	2.025	0.075	2
36	-122	106.3191	15.8001	1.656	0.0449	124
36	-121	105.3608	17.3689	1.6041	0.0431	134
36	-120	99.1489	19.3379	1.5213	0.0396	157
36	-119	86.4312	13.5516	1.4189	0.0277	180
36	-118	88.6904	12.0045	1.3518	0.0184	307
36	-117	89.4131	15.1849	1.216	0.019	287
36	-116	79.9236	18.9369	1.2027	0.0326	129
36	-115	59.5749	23.4004	1.186	0.0376	100
36	-114	36.4205	15.3386	1.1794	0.0311	114
36	-113	36.443	17.2847	1.2747	0.0349	99
36	-112	42.8697	14.9938	1.1503	0.0276	147
36	-111	40.7531	14.3829	1.1023	0.0274	133
36	-110	28.528	22.5582	1.112	0.0291	142
36	-109	32.9426	26.5187	1.1837	0.039	98
36	-108	38.4853	25.8706	1.2386	0.0435	92
36	-107	45.2236	23.2332	1.3733	0.0424	105

36	-106	41.1294	17.9813	1.3403	0.0272	176
36	-105	36.7379	19.6234	1.235	0.0274	143
36	-104	31.9308	22.503	1.1333	0.0456	48
36	-103	17.1246	22.4708	1.0382	0.0566	34
36	-102	18.6943	30.1201	1.025	0.0452	50
36	-101	28.7645	43.4849	1.1125	0.0692	40
36	-100	61.2089	36.9018	1.0571	0.1131	14
36	-99	78.8534	27.0387	1.3029	0.0999	17
36	-98	84.3885	20.3071	1.1926	0.068	27
36	-97	76.5974	15.1499	1.1122	0.0503	45
36	-96	73.2471	10.6224	1.0493	0.0373	68
36	-95	70.3763	12.771	1.0813	0.0326	91
36	-94	63.778	16.266	1.0688	0.0301	93
36	-93	62.9996	16.6146	1.0217	0.0255	99
36	-92	62.0197	19.5663	1.1195	0.0437	77
36	-91	65.7979	31.5952	1.0705	0.0672	22
36	-90	59.9876	35.1481	1.0773	0.0832	11
37	-124	138	2.0008	0.975	0.075	2
37	-123	123.4831	18.2607	1.4015	0.08	34
37	-122	110.0595	17.5623	1.6186	0.0507	86
37	-121	93.6225	17.9139	1.6733	0.0273	232
37	-120	74.6618	14.4665	1.4595	0.0206	273
37	-119	76.6734	17.1516	1.4426	0.0195	290
37	-118	83.615	13.8231	1.442	0.0227	243
37	-117	84.2922	16.9949	1.2875	0.0303	148
37	-116	66.5717	19.8491	1.0764	0.0379	72
37	-115	55.124	20.1741	1.1015	0.0475	65
37	-114	38.3259	21.819	1.1313	0.0433	56
37	-113	37.0636	27.5919	1.1478	0.0435	45
37	-112	50.2918	27.0477	1.0964	0.041	56
37	-111	44.6561	20.1818	1.148	0.0283	125
37	-110	38.3212	22.8653	1.1735	0.0271	162
37	-109	32.9577	22.7985	1.1944	0.0321	144
37	-108	21.7974	23.9494	1.2806	0.0504	80
37	-107	24.1854	22.6547	1.1991	0.0525	58
37	-106	22.8845	21.5454	1.1655	0.0418	74
37	-105	19.438	25.7889	1.1773	0.0345	99
37	-104	7.4879	27.1013	1.1693	0.0356	75
37	-103	9.9538	32.2094	1.1085	0.058	47
37	-102	25.8014	40.0403	1.1837	0.0634	49
37	-101	46.4396	37.9809	1.1846	0.063	52

37	-100	60.4164	31.2825	1.2243	0.0867	35
37	-99	70.8282	25.1705	1.1688	0.0972	24
37	-98	72.0182	18.1928	1.1414	0.0866	29
37	-97	81.5498	16.3193	1.2583	0.0784	36
37	-96	73.7365	15.6347	1.193	0.0552	64
37	-95	68.98	16.3822	1.1	0.0537	57
37	-94	63.5424	19.9687	0.9551	0.04	69
37	-93	60.7706	21.7637	1.059	0.0377	105
37	-92	54.179	24.2798	1.0844	0.0463	80
37	-91	33.3017	26.8738	1.0888	0.0632	40
37	-90	34.1666	30.4584	1.0471	0.0898	17
38	-124	127.0464	15.1391	1.4684	0.1188	19
38	-123	126.4636	18.1686	1.4159	0.0716	44
38	-122	100.3325	25.0516	1.5658	0.0466	95
38	-121	80.4588	15.0892	1.6337	0.0221	297
38	-120	73.5548	15.3827	1.5402	0.0171	442
38	-119	67.7675	14.8293	1.4078	0.0173	321
38	-118	71.7809	18.2641	1.3603	0.0254	219
38	-117	73.9832	26.3916	1.1688	0.0476	77
38	-116	51.5413	26.0504	1.2073	0.0656	41
38	-115	50.2163	20.1235	1.167	0.0575	50
38	-114	47.3084	32.1355	1.2462	0.0675	40
38	-113	1.5966	31.0482	1.3096	0.0461	57
38	-112	18.8001	33.902	1.1628	0.0356	78
38	-111	39.193	34.8666	1.1153	0.0384	75
38	-110	48.2572	30.4049	1.2	0.049	70
38	-109	32.664	32.5042	1.2432	0.0505	73
38	-108	21.4786	27.7048	1.289	0.0435	86
38	-107	22.7758	29.2304	1.2024	0.0391	84
38	-106	21.8951	35.3891	1.1537	0.0429	80
38	-105	10.2231	35.5545	1.1848	0.0423	69
38	-104	172.7515	38.1981	1.2119	0.0489	63
38	-103	169.2923	45.321	1.2	0.0579	50
38	-102	68.1433	46.0573	1.4385	0.101	26
38	-101	50.1903	38.0199	1.3314	0.0868	43
38	-100	53.941	33.819	1.2283	0.0816	46
38	-99	60.7487	21.6151	1.0019	0.0866	27
38	-98	65.6643	19.0913	1.0048	0.0771	31
38	-97	73.1594	20.3331	1.1804	0.1025	28
38	-96	71.1802	21.5088	1.3394	0.087	33
38	-95	67.1336	19.5636	1.1288	0.0857	33

38	-94	83.821	22.682	0.9775	0.0662	40
38	-93	75.988	28.182	1.1149	0.0517	77
38	-92	46.3677	26.1806	1.1236	0.0337	161
38	-91	41.0507	23.5421	1.0805	0.0318	149
38	-90	51.7193	21.8622	1.0302	0.0443	63
39	-125	124	0	0.95	0	1
39	-124	124.1006	20.4346	1.4368	0.1066	19
39	-123	131.4121	27.5508	1.3667	0.0626	42
39	-122	88.545	35.0281	1.4035	0.054	57
39	-121	79.2267	16.6174	1.6278	0.0311	203
39	-120	73.4196	19.3349	1.4759	0.0323	164
39	-119	70.9845	17.8001	1.3771	0.0327	131
39	-118	76.6884	19.8955	1.352	0.0446	98
39	-117	80.8569	27.6941	1.273	0.0708	37
39	-116	112.0627	52.8672	1.3583	0.0756	30
39	-115	142.1703	48.4869	1.2459	0.0667	37
39	-114	158.9222	27.1004	1.3042	0.0365	96
39	-113	161.4983	18.126	1.3695	0.0298	128
39	-112	169.1043	23.0196	1.1786	0.0377	96
39	-111	164.8118	36.6684	1.1185	0.065	54
39	-110	115.6104	62.7904	1.194	0.0762	50
39	-109	69.8648	44.8915	1.2864	0.0624	55
39	-108	43.4665	48.652	1.2777	0.0483	74
39	-107	13.064	62.5995	1.1765	0.0323	113
39	-106	172.0245	53.5093	1.1455	0.0398	78
39	-105	15.6936	46.6363	1.1402	0.0612	46
39	-104	68.3449	59.586	1.1768	0.0753	41
39	-103	66.9032	35.168	1.2292	0.0572	65
39	-102	70.2591	26.3162	1.1962	0.0579	65
39	-101	73.6468	30.3939	1.243	0.0532	79
39	-100	71.2945	30.9816	1.2541	0.0477	86
39	-99	68.7229	26.6282	1.1458	0.0429	96
39	-98	57.1615	17.5529	1.0796	0.0468	71
39	-97	57.0124	22.1935	1.1331	0.0459	74
39	-96	57.6449	26.9561	1.1819	0.0686	47
39	-95	61.3358	21.0152	1.2739	0.0767	44
39	-94	76.986	34.6463	1.1787	0.0574	61
39	-93	95.0089	33.0319	1.252	0.0651	50
39	-92	47.5553	28.4594	1.1549	0.038	122
39	-91	45.4389	20.3606	1.112	0.0313	158
39	-90	51.5168	16.2204	1.0826	0.0424	66

40	-125	67.5	15.9052	1.325	0.475	2
40	-124	51.3626	36.2008	1.1672	0.0396	58
40	-123	55.2141	34.3851	1.1354	0.0252	151
40	-122	64.7453	26.9544	1.2385	0.0246	205
40	-121	75.4487	19.2995	1.2899	0.0291	153
40	-120	78.9123	19.0401	1.3122	0.0362	98
40	-119	83.8156	15.1432	1.3122	0.057	49
40	-118	86.3928	8.7867	1.2842	0.0301	152
40	-117	90.2408	16.3454	1.2618	0.0269	182
40	-116	101.8148	20.6906	1.1835	0.0297	127
40	-115	116.5845	28.4676	1.1257	0.0288	136
40	-114	150.7428	16.842	1.2607	0.0279	177
40	-113	153.7076	16.3393	1.2784	0.0274	169
40	-112	149.9308	19.2904	1.3102	0.0333	118
40	-111	143.8896	29.788	1.1614	0.081	35
40	-110	86.9112	49.0971	1.1197	0.0914	33
40	-109	74.079	33.1002	1.2333	0.0466	90
40	-108	72.482	29.6275	1.1945	0.0313	136
40	-107	66.4373	34.8849	1.1367	0.0238	177
40	-106	64.8128	37.2309	1.1434	0.0264	160
40	-105	55.2191	30.2558	1.1819	0.0417	80
40	-104	51.831	32.8813	1.1319	0.0617	36
40	-103	57.4755	25.9012	1.1188	0.0471	64
40	-102	73.5035	26.8275	1.1654	0.0456	91
40	-101	75.5099	25.1967	1.1693	0.0533	75
40	-100	81.4438	23.7953	1.219	0.0441	100
40	-99	74.8288	22.1833	1.172	0.0413	118
40	-98	62.5733	19.0949	1.0966	0.0331	132
40	-97	55.0122	21.5169	1.126	0.0391	104
40	-96	53.4391	29.4773	1.2088	0.0527	68
40	-95	54.229	25.3944	1.153	0.0546	67
40	-94	62.8469	27.0549	1.1418	0.0531	73
40	-93	75.0855	31.6328	1.1267	0.0501	73
40	-92	70.7503	33.291	1.1755	0.0649	49
40	-91	56.0249	23.1644	1.1576	0.0533	59
40	-90	52.6255	19.8901	1.141	0.0601	39
41	-125	62.9486	27.3727	1.0556	0.1257	9
41	-124	61.4853	21.1669	1.1371	0.0219	167
41	-123	61.8541	21.6349	1.1851	0.0171	278
41	-122	64.3199	19.9442	1.2398	0.0177	310
41	-121	72.2747	15.5615	1.359	0.0241	173

41	-120	81.3331	14.2378	1.582	0.0303	153
41	-119	87.9292	10.6521	1.6972	0.0287	176
41	-118	90.7145	11.1224	1.4641	0.0258	251
41	-117	90.7318	11.3317	1.3899	0.0215	278
41	-116	100.4287	14.823	1.2471	0.0209	243
41	-115	109.5751	22.2584	1.1744	0.0236	195
41	-114	143.1569	24.9943	1.0772	0.031	103
41	-113	147.4687	30.9315	1.121	0.0335	124
41	-112	124.6468	43.9754	1.1951	0.0461	72
41	-111	102.6118	26.3173	1.1342	0.0636	38
41	-110	147.0665	51.059	1.1156	0.0722	32
41	-109	73.5452	37.9992	1.2386	0.0501	79
41	-108	81.4015	35.2241	1.1497	0.03	161
41	-107	88.5113	35.1208	1.1044	0.0202	248
41	-106	78.4897	31.7508	1.1237	0.0186	270
41	-105	77.7319	27.7311	1.1466	0.0243	179
41	-104	71.3185	18.2954	1.2175	0.0529	60
41	-103	75.9477	23.8461	1.1651	0.0457	73
41	-102	74.89	29.6861	1.1926	0.0569	61
41	-101	77.4777	27.4513	1.1696	0.0627	51
41	-100	76.1226	30.4972	1.1797	0.0831	32
41	-99	75.6995	18.4312	1.1599	0.0472	101
41	-98	75.0756	17.5649	1.1353	0.0372	153
41	-97	71.3261	18.7346	1.0781	0.031	135
41	-96	68.7989	17.3957	1.0644	0.0269	125
41	-95	65.1888	19.4602	1.0622	0.0293	123
41	-94	61.074	17.7843	1.0786	0.0313	131
41	-93	67.6331	21.7806	1.0663	0.0381	101
41	-92	70.1258	22.2622	1.0877	0.0462	77
41	-91	66.9496	21.3464	1.0969	0.0524	65
41	-90	67.3217	16.6827	1.075	0.0685	30
42	-125	60.7642	14.851	1.4195	0.0564	41
42	-124	61.5423	10.7943	1.5511	0.0248	263
42	-123	64.0001	12.4872	1.4986	0.0215	349
42	-122	67.3696	14.0471	1.4002	0.0206	222
42	-121	72.2861	13.7532	1.5134	0.0348	127
42	-120	84.3246	9.7101	1.7893	0.021	275
42	-119	87.121	8.5077	1.8202	0.0175	354
42	-118	92.0602	10.8807	1.7303	0.0163	471
42	-117	98.5662	9.5707	1.6169	0.0136	646
42	-116	101.0613	10.5084	1.5482	0.0152	550

42	-115	111.0021	14.7855	1.2622	0.0226	196
42	-114	114.6527	19.7956	1.13	0.0298	100
42	-113	98.2719	36.8629	1.144	0.0387	83
42	-112	77.1673	33.6566	1.1926	0.041	88
42	-111	78.8729	28.2309	1.1797	0.0392	79
42	-110	96.5441	50.1213	1.1618	0.0478	51
42	-109	101.6546	32.1996	1.2029	0.0388	85
42	-108	95.056	27.2225	1.1645	0.0326	141
42	-107	93.3983	28.3512	1.1485	0.0223	236
42	-106	87.2053	29.6049	1.1273	0.0201	247
42	-105	72.0901	20.4179	1.1388	0.0249	143
42	-104	79.8935	21.0935	1.1892	0.0483	74
42	-103	83.7544	21.8924	1.1802	0.043	91
42	-102	81.9873	25.398	1.1171	0.0478	70
42	-101	90.7068	28.6513	1.1052	0.0565	48
42	-100	78.6731	25.2163	1.1881	0.0622	42
42	-99	84.2186	17.1431	1.2975	0.0523	99
42	-98	85.276	17.5594	1.2144	0.0408	149
42	-97	78.3872	16.5648	1.1199	0.0313	163
42	-96	70.5631	17.5186	1.0812	0.0274	149
42	-95	60.4418	20.1381	1.0929	0.0275	140
42	-94	58.2931	18.444	1.1247	0.0272	160
42	-93	58.171	18.6312	1.1187	0.0302	126
42	-92	64.6288	21.7873	1.0741	0.0393	87
42	-91	64.5984	25.8395	1.1229	0.0516	59
42	-90	59.2011	33.34	1.1241	0.0598	27
43	-125	59.7632	10.5407	1.6505	0.0339	94
43	-124	60.7933	8.9805	1.676	0.019	340
43	-123	61.6152	9.7174	1.6494	0.0166	420
43	-122	68.7216	12.8529	1.5929	0.022	303
43	-121	79.8692	14.0333	1.5538	0.0236	290
43	-120	85.3563	9.7913	1.7525	0.0259	306
43	-119	84.3528	9.8378	1.8142	0.0204	395
43	-118	86.9124	12.1388	1.8255	0.0179	466
43	-117	94.3934	11.1693	1.741	0.0142	695
43	-116	95.4998	9.839	1.6785	0.0144	646
43	-115	88.873	14.9136	1.6727	0.0188	471
43	-114	85.2244	17.331	1.6239	0.024	324
43	-113	75.8818	21.7588	1.3301	0.0462	68
43	-112	58.8715	17.378	1.2595	0.026	185
43	-111	58.3474	15.6442	1.2761	0.0231	259

43	-110	68.1774	24.8483	1.1786	0.0285	168
43	-109	82.0352	22.7888	1.2193	0.0357	135
43	-108	88.1214	18.4082	1.2351	0.0329	194
43	-107	86.7931	16.1097	1.1937	0.0305	215
43	-106	85.4509	18.4997	1.1792	0.0349	166
43	-105	77.7673	21.0672	1.1228	0.049	81
43	-104	91.0773	25.8684	1.1644	0.044	108
43	-103	100.6273	23.2246	1.0914	0.0285	152
43	-102	102.1183	20.4469	1.1261	0.0369	134
43	-101	101.4851	23.4345	1.2306	0.0431	134
43	-100	89.8398	24.0371	1.2951	0.0601	92
43	-99	95.6623	28.8339	1.196	0.0466	100
43	-98	95.391	25.0723	1.1703	0.0413	118
43	-97	89.5669	28.2043	1.1185	0.0376	135
43	-96	73.0911	22.1297	1.1205	0.0396	129
43	-95	67.5598	22.4055	1.1272	0.038	123
43	-94	62.5756	23.6271	1.1226	0.031	126
43	-93	60.5182	29.5878	1.1445	0.0392	100
43	-92	73.3985	34.6299	1.176	0.06	52
43	-91	67.3763	36.2084	1.1959	0.0786	49
43	-90	53.3584	31.2125	1.1111	0.1403	18
44	-125	68.7177	11.5183	1.4883	0.0284	128
44	-124	67.0811	11.2475	1.5552	0.0136	552
44	-123	67.3954	10.5272	1.5822	0.0118	707
44	-122	69.8198	12.0245	1.5757	0.0137	567
44	-121	79.0813	15.9639	1.4685	0.0188	375
44	-120	83.2333	14.6232	1.4541	0.0254	255
44	-119	79.3412	12.1215	1.5822	0.0305	242
44	-118	76.0936	10.7798	1.7153	0.0359	183
44	-117	84.7379	11.4484	1.7957	0.0301	199
44	-116	83.4337	9.9962	1.7708	0.0252	303
44	-115	80.2244	13.2454	1.7055	0.0204	411
44	-114	76.8732	15.6249	1.6613	0.0221	337
44	-113	63.1501	17.451	1.3859	0.0367	96
44	-112	59.0028	16.2889	1.318	0.0195	322
44	-111	59.8548	17.9212	1.3282	0.0199	323
44	-110	62.4809	18.5078	1.2979	0.0223	285
44	-109	77.5462	16.0408	1.2356	0.0286	222
44	-108	80.9058	16.323	1.2003	0.0214	379
44	-107	83.218	16.7404	1.163	0.0246	289
44	-106	79.6746	19.5225	1.1598	0.0369	107

44	-105	68.9795	31.1886	1.1857	0.0495	63
44	-104	95.8962	35.8143	1.1372	0.0358	109
44	-103	99.3657	29.9205	1.0972	0.0297	159
44	-102	100.7951	25.1651	1.0704	0.0262	174
44	-101	89.4965	32.0534	1.1177	0.0332	147
44	-100	75.4593	31.0425	1.1386	0.0455	105
44	-99	69.7762	33.8911	1.1707	0.0419	92
44	-98	72.1015	37.9806	1.171	0.0438	88
44	-97	71.2364	32.2813	1.0936	0.0457	70
44	-96	74.1279	30.7435	1.1222	0.0445	79
44	-95	74.832	27.9162	1.0372	0.0363	86
44	-94	73.8629	31.2187	0.991	0.0341	78
44	-93	75.1369	26.7449	1.0561	0.0413	74
44	-92	94.526	31.8907	1.063	0.053	50
44	-91	84.0505	35.8204	0.9888	0.0574	40
44	-90	83.2069	33.7906	0.9603	0.0643	29
45	-125	78.5391	10.0294	1.4051	0.028	107
45	-124	73.3193	11.1109	1.4694	0.015	470
45	-123	73.2979	10.6009	1.5156	0.0126	721
45	-122	74.9567	14.4025	1.4973	0.0151	538
45	-121	83.6238	18.8743	1.3916	0.0214	285
45	-120	95.407	27.0621	1.2473	0.0335	111
45	-119	80.6368	17.9484	1.2849	0.0276	126
45	-118	83.0491	17.3202	1.2235	0.0297	119
45	-117	85.0474	15.6318	1.2411	0.0318	118
45	-116	75.7486	20.0529	1.2267	0.0344	116
45	-115	71.0585	18.6343	1.2314	0.0327	118
45	-114	62.1927	18.1047	1.1981	0.0287	161
45	-113	55.1051	19.95	1.158	0.0321	137
45	-112	59.5111	24.3421	1.2316	0.0302	179
45	-111	67.2866	22.7353	1.325	0.0328	140
45	-110	74.1055	23.582	1.2258	0.0352	120
45	-109	74.5727	19.4083	1.1811	0.0203	314
45	-108	75.525	19.1911	1.1609	0.0189	358
45	-107	77.8572	19.8509	1.1507	0.0209	272
45	-106	72.2458	27.6801	1.1287	0.0376	87
45	-105	72.2059	32.4321	1.116	0.0428	81
45	-104	71.6321	25.5693	1.1348	0.041	89
45	-103	74.6953	21.6104	1.1258	0.0406	99
45	-102	73.4444	17.23	1.1117	0.0359	124
45	-101	64.786	19.5641	1.0705	0.0313	134

45	-100	61.5338	18.1626	1.1289	0.0297	152
45	-99	58.6394	14.1955	1.1866	0.0343	112
45	-98	55.4581	14.111	1.0771	0.0312	94
45	-97	51.3289	18.7929	1.091	0.0378	83
45	-96	49.8526	24.3514	1.094	0.0384	83
45	-95	59.0016	31.3156	1.0925	0.0474	60
45	-94	53.8844	31.8774	1.1042	0.0378	83
45	-93	55.2924	26.4891	1.129	0.0345	105
45	-92	54.3786	26.7402	1.1514	0.0372	107
45	-91	61.8564	20.7653	1.1204	0.0427	71
45	-90	58.3654	19.6909	1.0593	0.0459	43
46	-125	67.0915	16.2013	1.3024	0.0374	63
46	-124	76.5142	13.3175	1.2616	0.0188	254
46	-123	77.7685	13.56	1.2676	0.0159	391
46	-122	82.0689	13.2132	1.2722	0.0185	338
46	-121	92.4448	21.0618	1.2047	0.026	212
46	-120	107.0249	18.2315	1.2214	0.0244	201
46	-119	99.0241	20.0731	1.2093	0.022	258
46	-118	86.4734	19.114	1.1986	0.0266	181
46	-117	83.4509	18.7168	1.1751	0.0262	177
46	-116	80.4415	25.7486	1.1701	0.0405	82
46	-115	87.3628	27.5722	1.1146	0.0333	106
46	-114	79.7417	23.308	1.1573	0.0265	193
46	-113	61.184	22.2426	1.1538	0.0276	185
46	-112	60.2248	20.3808	1.1635	0.0313	159
46	-111	65.8498	20.5317	1.2164	0.0365	107
46	-110	64.4853	18.4827	1.1432	0.0282	170
46	-109	60.5688	19.4301	1.1045	0.0244	202
46	-108	59.6691	21.4629	1.1084	0.0297	143
46	-107	73.0288	31.0721	1.0869	0.0423	84
46	-106	78.0586	31.6792	1.0695	0.0428	82
46	-105	75.4269	28.0623	1.0561	0.0405	74
46	-104	66.5849	25.1303	1.0856	0.0431	59
46	-103	67.302	20.7445	1.1314	0.0351	86
46	-102	61.9336	20.0405	1.142	0.0297	113
46	-101	56.7505	18.0832	1.1374	0.0236	151
46	-100	51.4817	16.4911	1.1533	0.0249	137
46	-99	52.7316	17.2608	1.0466	0.0302	103
46	-98	49.4308	20.9055	1.0277	0.0376	92
46	-97	40.4413	17.0537	1.0069	0.0322	87
46	-96	43.8958	20.3573	1.0942	0.0341	103

46	-95	51.7764	23.2583	1.0825	0.0366	80
46	-94	54.4637	20.3107	1.1175	0.0328	100
46	-93	49.9019	19.2193	1.1531	0.0283	131
46	-92	57.8472	14.4336	1.1478	0.0322	115
46	-91	60.9884	12.5008	1.1691	0.035	89
46	-90	61.7714	11.0268	1.1138	0.0332	58
47	-125	74.0145	15.1634	1.24	0.0261	110
47	-124	76.0017	12.7724	1.2571	0.0161	361
47	-123	77.5107	12.0579	1.2699	0.0133	560
47	-122	78.6524	14.3927	1.2664	0.0176	439
47	-121	86.8931	19.9173	1.2843	0.0216	302
47	-120	100.2693	17.0195	1.273	0.0219	278
47	-119	96.8395	19.6063	1.3176	0.0203	309
47	-118	89.4571	17.6033	1.2804	0.0217	278
47	-117	82.854	17.8145	1.2411	0.0279	168
47	-116	84.1731	18.4055	1.2517	0.0391	89
47	-115	89.4959	16.7581	1.3003	0.03	185
47	-114	83.4298	20.0885	1.3075	0.028	207
47	-113	78.1458	23.9754	1.3199	0.0278	211
47	-112	54.2114	17.5846	1.3198	0.0405	86
47	-111	55.7064	16.984	1.3196	0.0447	74
47	-110	55.0991	17.3441	1.1778	0.0365	97
47	-109	54.0175	17.1838	1.0792	0.0349	108
47	-108	55.8556	25.1624	1.0965	0.0381	101
47	-107	65.1167	27.4871	1.186	0.0499	68
47	-106	66.0847	28.4837	1.1545	0.0483	66
47	-105	62.9133	28.4763	1.119	0.0598	50
47	-104	63.0249	33.6785	1.1731	0.0604	39
47	-103	60.7545	30.3827	1.1346	0.0416	68
47	-102	49.7234	24.3847	1.1495	0.0329	100
47	-101	39.5376	21.9118	1.2093	0.0301	124
47	-100	40.8905	18.3672	1.1663	0.0245	150
47	-99	42.0114	19.8828	1.095	0.0273	129
47	-98	44.8952	16.5758	1.0754	0.0289	122
47	-97	39.1373	17.609	1.1171	0.032	120
47	-96	39.5832	15.7548	1.1603	0.0279	121
47	-95	44.4782	18.8902	1.1891	0.0294	119
47	-94	45.189	17.8334	1.1785	0.0237	130
47	-93	45.1665	17.7502	1.1829	0.0253	129
47	-92	52.112	14.9296	1.3668	0.0299	134
47	-91	59.9133	14.8195	1.1344	0.046	45

47	-90	63.2639	12.2116	1.1313	0.061	24
48	-125	81.1944	10.7271	1.2715	0.0341	79
48	-124	79.3971	10.8212	1.2968	0.0163	358
48	-123	77.3029	11.6032	1.2776	0.012	597
48	-122	76.5157	12.4012	1.3124	0.0132	592
48	-121	75.1757	13.6465	1.3223	0.0178	356
48	-120	75.5215	17.0644	1.506	0.0218	252
48	-119	76.901	18.1011	1.4667	0.0195	263
48	-118	76.8877	15.1081	1.3571	0.0174	330
48	-117	74.7269	11.0232	1.3398	0.0194	260
48	-116	74.3142	15.2512	1.3419	0.0242	203
48	-115	66.2286	19.9445	1.3358	0.0332	116
48	-114	67.7394	17.9854	1.3861	0.0331	133
48	-113	60.3592	16.6257	1.3965	0.0384	100
48	-112	59.7868	20.2673	1.2786	0.035	98
48	-111	60.4351	19.8	1.2264	0.034	125
48	-110	57.7708	17.4728	1.2004	0.0336	115
48	-109	56.4143	20.4113	1.1607	0.0366	98
48	-108	23.745	33.4896	1.2099	0.034	86
48	-107	22.9771	35.8611	1.2218	0.0324	103
48	-106	37.6268	33.2031	1.2	0.0368	84
48	-105	52.4036	22.9584	1.1802	0.0429	58
48	-104	60.9733	22.6979	1.1121	0.0425	62
48	-103	67.4939	27.3454	1.143	0.0525	57
48	-102	58.7204	28.9528	1.1592	0.0451	87
48	-101	49.1394	24.6401	1.122	0.027	152
48	-100	47.6933	19.3956	1.1358	0.025	155
48	-99	46.0121	14.3989	1.1341	0.0182	173
48	-98	46.8792	15.9869	1.1374	0.021	151
48	-97	41.7802	15.7427	1.1798	0.02	225
48	-96	42.6107	15.94	1.1887	0.0204	235
48	-95	45.8771	16.4447	1.1998	0.022	203
48	-94	52.2248	15.9919	1.243	0.0281	100
48	-93	54.8297	12.9578	1.3593	0.0213	227
48	-92	58.6904	11.0196	1.3887	0.0219	203
48	-91	59.3776	10.4412	1.3955	0.025	178
48	-90	64.1267	12.1109	1.15	0.0555	26
49	-125	68.6661	1.7001	1.3167	0.2167	3
49	-124	76.9832	9.2014	1.2433	0.0274	82
49	-123	78.1268	12.6148	1.2947	0.0177	208
49	-122	75.7823	13.4269	1.2639	0.0183	183

49	-121	71.2238	14.2471	1.2958	0.0222	156
49	-120	60.361	13.6751	1.4179	0.0349	95
49	-119	56.8916	14.4228	1.4739	0.0295	117
49	-118	64.1145	13.8988	1.367	0.0224	171
49	-117	64.4236	14.0256	1.3959	0.0224	195
49	-116	60.4519	12.9435	1.4277	0.0233	179
49	-115	54.9497	14.2243	1.4285	0.0297	130
49	-114	56.184	14.7083	1.3077	0.0337	97
49	-113	60.8007	23.6454	1.3062	0.0488	65
49	-112	60.0787	24.8808	1.279	0.0479	62
49	-111	53.5318	22.6675	1.3309	0.0436	76
49	-110	57.8212	17.3002	1.2174	0.0396	92
49	-109	50.3357	20.1816	1.2708	0.0518	48
49	-108	7.8921	29.4013	1.2067	0.0379	60
49	-107	18.0911	30.5503	1.233	0.0359	88
49	-106	30.8316	33.9974	1.1823	0.0396	79
49	-105	49.2677	23.3554	1.1729	0.0466	70
49	-104	55.8468	18.4542	1.1241	0.0445	54
49	-103	61.4163	21.3508	1.1621	0.0458	66
49	-102	61.9158	21.0718	1.1543	0.0415	81
49	-101	61.2771	16.5712	1.2029	0.0362	104
49	-100	56.1254	15.1297	1.1683	0.0258	139
49	-99	54.7677	13.7617	1.2063	0.0261	127
49	-98	57.314	13.5106	1.2025	0.0245	119
49	-97	51.1385	17.5204	1.23	0.0219	210
49	-96	49.8684	18.0509	1.209	0.0219	205
49	-95	59.0497	12.8201	1.2342	0.0301	111
49	-94	63.555	11.1172	1.2726	0.0484	42
49	-93	63.4566	8.894	1.3161	0.0486	28
49	-92	63.604	8.8162	1.3162	0.029	99
49	-91	64.9532	9.1139	1.2969	0.0367	81
49	-90	59.928	10.804	0.8	0.0764	3

SECTION

2. CONCLUSIONS

In this study, we analyzed over 4000 shear wave splitting parameters with unprecedented spatial resolution are observed on the northern Great Plains of North America. Although lithospheric contributions to the observed anisotropy cannot be completely ruled out especially beneath the Superior province, depth estimates using spatial coherency of the splitting parameters and the dominantly APM-parallel fast orientations imply that coupling between the lithosphere and the asthenosphere is the most likely cause of the observed anisotropy. Along the northern boundary of the Yavapai province, beneath which a zone of thinned lithosphere is revealed by seismic tomography, a double-layer anisotropy model can satisfactorily explain the azimuthal dependence of the splitting parameters. An edge-parallel flow system is proposed to be driven by the southwestward movement of the bottom of the continental lithosphere, which gradually deepens toward the interior of the North American continent. We propose that shear strain associated with partial coupling between the lithosphere and the asthenosphere contributes to the bulk of the observed anisotropy on plates with a significant differential movement relative to the underlying asthenosphere.

We have also produced a new version of a uniformly created shear wave splitting (SWS) database for the western and central United States using broadband seismic data recorded before the end of 2014, for the purpose of updating a previous version that used data recorded prior to the end of 2012. The resulting uniform SWS database contains a total of 23448 pairs of well-defined and manually-checked XKS splitting parameters. Relative to the previous version of the database, the additional measurements significantly

improved the spatial and azimuthal coverages of the measurements, providing an excellent dataset for constraining geodynamic models related to lithospheric deformation and asthenospheric flow, as well as for complex anisotropy recognition and characterization.

3. BIBLIOGRAPHY

Balch, R. S., H. E. Hartse, A. R. Sanford, and K. W. Lin (1997), A new map of the geographic extent of the Socorro mid-crustal magma body, Bull. Seismol. Soc. Am., 87, 174–182.

Baldridge, W. S., F. V. Perry, D. T. Vaniman, L. D. Nealey, B. D. Leavy, A. W. Laughlin, P. R. Kyle, Y. Bartov, G. Steintz, and E. S. Gladney (1991), Middle to late Cenozoic magmatism of the southeastern Colorado Plateau and central Rio Grande rift (New Mexico and Arizona, USA): A model for continental rifting, Tectonophysics, 197, 327–354.

Barruol, G., G. Helffrich, and A. Vauchez (1997a), Shear wave splitting around the northern Atlantic, frozen Pangaean lithospheric anisotropy, Tectonophysics, 279(1-4), 135–148.

Barruol, G., P. G. Silver, and A. Vauchez (1997b), Seismic anisotropy in the eastern United States: Deep structure of complex continental plate, J. Geophys. Res., 102, 8329–8348, doi:10.1029/96JB03800.

Becker, T. W., V. Schulte-Pelkum, D. K. Blackman, J. B. Kellogg, and R. J. O'Connell (2006), Mantle flow under the Western United States from shear wave splitting, Earth Planet. Sci. Lett., 247, 235–251.

Bedle, H., and S. van der Lee (2009), S velocity variations beneath North America, J. Geophys. Res., 114, B07308, doi:10.1029/2008JB005949.

Bird, P., Z. Liu, and W. K. Rucker (2008). Stress that drive the plates from below: definitions, computational path, model optimization, and error analysis, J. Geophys. Res. 113, B11406.

Bormann, P., G. Grunthal, R. Kind, and H. Montag (1996), Upper mantle anisotropy beneath Central Europe from SKS wave splitting: Effects of absolute plate motion and lithosphere-asthenosphere boundary topography?, J. Geodyn., 22, 11–32.

Burdick, S., R. D. Van Der Hilst, F. L. Vernon, V. Martynov, T. Cox, J. Eakins, G. H. Karasu, J. Tylell, L. Astiz, and G. L. Pavlis (2012), Model update March 2011: Upper mantle heterogeneity beneath North America from traveltime tomography with global and USArray transportable array data, Seismol. Res. Lett., 83, 23–28, doi:10.1785/gssrl.83.1.23.

Burdick, S., R. D. Van Der Hilst, F. L. Vernon, V. Martynov, T. Cox, J. Eakins, G. H. Karasu, J. Tylell, L. Astiz, and G. L. Pavlis (2014), Model update January 2013: Upper mantle heterogeneity beneath North America from travel-time tomography with global and USArray transportable array data, Seismol. Res. Lett., 85, 77–81, doi:10.1785/0220130098.

Conrad, C. P., and M. D. Behn (2010), Constraints on lithosphere net rotation and asthenospheric viscosity from global mantle flow models and seismic anisotropy, Geochem. Geophys. Geosyst., 11, Q05W05, doi:10.1029/2009GC002970.

Coward, M. P., R. W. H. Butler, M. A. Khan, and R. J. Knipe (1987), The tectonic history of Kohistan and its implications for Himalayan structure, J. Geol. Soc., London, 144, 377–391.

Darbyshire, F. A., D. W. Eaton, A. W. Frederiksen, and L. Ertolahti (2007), New insights into the lithosphere beneath the Superior Province from Rayleigh wave dispersion and receiver function analysis, Geophys. J. Int., 169, 1043–1068, doi:10.1111/j.1365-246X.2006.03259.x.

Darbyshire, F. A., and S. Lebedev (2009), Rayleigh wave phase-velocity heterogeneity and multilayered azimuthal anisotropy of the Superior Craton, Ontario, Geophys. J. Int., 176, 215–234.

Davidson, A. (1995), A review of the Grenville orogen in its North American type area, J. Austra. Geol. Geophys., 16, 3–24.

Doglioni, C., A. Ismail-Zadeh, G. Panza, and F. Riguzzi (2011), Lithosphere-asthenosphere viscosity contrast and decoupling, Phys. Earth Planet. Inter., 189, 1–8.

Forte, A. M., J. X. Mitrovica, R. Moucha, N. A. Simmons, and S. P. Grand (2007), Descent of the ancient Farallon slab drives localized mantle flow below the New Madrid seismic zone, Geophys. Res. Lett., 34, L04308, doi:10.1029/2006GL027895.

Fouch, M. J., and S. Rondenay (2006), Seismic anisotropy beneath stable continental interiors, Phys. Earth Planet. Inter., 158, 292–320, doi:10.1016/j.pepi.2006.01.022.

Frederiksen, A. W., T. Bollmann, F. Darbyshire, and S. van der Lee (2013a), Modification of continental lithosphere by tectonic processes:

A tomographic image of central North America, J. Geophys. Res. Solid Earth, 18, 1051–1066, doi:10.1002/jgrb.50060.

Frederiksen, A. W., I. Deniset, O. Ola, and D. Toni (2013b), Lithospheric fabric variations in central North America: Influence of rifting and Archean tectonic styles, Geophys. Res. Lett., 40, 4583–4587, doi:10.1002/grl.50879.

Frederiksen, A. W., S. K. Miong, F. A. Darbyshire, D. W. Eaton, S. Rondenay, and S. Sol (2007), Lithospheric variations across the superior Province, Ontario, Canada: Evidence from tomography and shear-wave splitting, J. Geophys. Res., 112, B07318, doi:10.1029/2006JB004861.

Gao, S. S., P. M. Davis, K. H. Liu, P. D. Slack, A. W. Rigor, Y. A. Zorin, V. V. Mordvinova, V. M. Kozhevnikov, and N. A. Logatchev (1997), SKS splitting beneath continental rift zones, J. Geophys. Res., 102, 22,781–22,797.

Gao, S. S., and K. H. Liu (2009), Significant seismic anisotropy beneath the southern Lhasa Terrane, Tibetan Plateau, Geochem. Geophys. Geosyst., 10, Q02008, doi:10.1029/2008GC002227.

Gao, S. S., and K. H. Liu (2012), AnisDep: A FORTRAN program for the estimation of the depth of anisotropy using spatial coherency of shear-wave splitting parameters, Comput. Geosci., 49, 330–333, doi:10.1016/j.cageo.2012.01.020.

Gao, S. S., K. H. Liu, and M. G. Abdelsalam (2010), Seismic anisotropy beneath the Afar Depression and adjacent areas: Implications for mantle flow, J. Geophys. Res., 115, B12330, doi:10.1029/2009JB007141.

Grand, S. P., and D. V. Helmberger (1984), Upper mantle shear structure beneath the northwest Atlantic Ocean, J. Geophys. Res., 89, 11,465–11,475.

Gripp, A. E., and R. G. Gordon (2002), Young tracks of hotspots and current plate velocities, Geophys. J. Int., 150, 321–361.

Hoffman, P. F. (1988), United plates of America, the birth of a craton: Early Proterozoic assembly and growth in Laurentia, Annu. Rev. Earth Planet. Sci., 16, 543–603.

Hoffman, P. F. (1989), Precambrian geology and tectonic history of North America, in The Geology of North America—An Overview, edited by A. W. Bally and A. R. Palmer, pp. 447–512, Geol. Soc. Amer., Boulder, Colo.

Holm, D. (1999), A geodynamic model for Paleoproterozoic post-tectonic magma genesis in the southern Trans-Hudson and Penokean orogens, Rocky Mt Geol., 34, 183–194, doi:10.2113/34.2.183.

Huang, Z., L. Wang, D. Zhao, N. Mi, and M. Xu (2011), Seismic anisotropy and mantle dynamics beneath China, Earth Planet. Sci. Lett., 306, 105–117.

Karlstrom, K. E., and S. A. Bowring (1988), Early Proterozoic assembly of tectono-stratigraphic terranes in southwestern North America, J. Geol., 96, 561–576.

Kay, I., S. Sol, J.-M. Kendall, C. Thomson, D. White, I. Asudeh, B. Roberts, and D. Francis (1999), Shear wave splitting observations in the Archean Craton of Western Superior, Geophys. Res. Lett., 26, 2669–2672.

Kendall, J.-M., G. W. Stuart, C. Ebinger, I. D. Bastow, and D. Keir (2005), Magma-assisted rifting in Ethiopia, Nature, 433, 146–148.

Kong, F. S., S. S. Gao, and K. H. Liu (2015a). On the applicability of the multiple-event stacking technique for shear wave splitting analysis, Bull. Seism. Soc. Am. 105(6).

Kong, F. S., S. S. Gao, and K. H. Liu (2015b). A systematic comparison of the transverse energy minimization and splitting intensity techniques for measuring shear wave splitting parameters, Bull. Seism. Soc. Am. 105, 230-239, doi:10.1785/0120140108.

Kreemer, C. (2009), Absolute plate motions constrained by shear wave splitting orientations with implications for hotspot motions and mantle flow, J. Geophys. Res., 114, B10405, doi:10.1029/2009JB006416.

Lay, T., Q. Williams, and E. Garnero (1998). The core-mantle boundary layer and deep Earth dynamics, Nature 392, 461-468.

Lawton, T. F., and N. J. McMillan (1999), Arc abandonment as a cause for passive continental rifting: Comparison of the Jurassic Mexican Borderland rift and the Cenozoic Rio Grande rift, Geology, 27, 779–782.

Li, Y., Q. Wu, F. Zhang, Q. Feng, and R. Zhang (2011), Seismic anisotropy of the northeastern Tibetan Plateau from shear wave splitting analysis, Earth Planet. Sci. Lett., 304, 147–157, doi:10.1016/j.epsl.2011.01.026.

Liu, K. H. (2009), NA-SWS-1.1: A uniform database of teleseismic shear-wave splitting measurements for North America, Geochem. Geophys. Geosyst., 10, Q05011, doi:10.1029/2009GC002440.

Liu, K. H., A. Elsheikh, A. Lemnifi, U. Purevsuren, M. Ray, H. Refayee, B. Yang, Y. Yu, and S. S. Gao (2014). A uniform database of teleseismic shear wave splitting measurements for the western and central United States, Geochem. Geophys. Geosyst. 15, 2075-2085, doi: 10.1002/2014GC005267.

Liu, K. H., and S. S. Gao (2011), Estimation of the depth of anisotropy using spatial coherency of shear-wave splitting parameters, Bull. Seismol. Soc. Am., 101, 2153–2161.

Liu, K. H., and S. S. Gao (2013), Making reliable shear-wave splitting measurements, Bull. Seismol. Soc. Am., 103, 2680–2693, doi:10.1785/0120120355.

Liu, K. H., S. S. Gao, Y. Gao, and J. Wu (2008), Shear wave splitting and mantle flow associated with the deflected slab beneath northeast Asia, J. Geophys. Res., 113, B01305, doi:10.1029/2007JB005178.

Long, M. D., and P. G. Silver (2009), Shear wave splitting anisotropy: Measurements, interpretation, and new directions, Surv. Geophys., 30, 407–461.

Mardia, K. V., and P. Jupp (2000). Directional Statistics, John Wiley and Sons Ltd., 2nd edition.

Mainprice, D., G. Barruol, and W. Ben Ismail (2000), The seismic anisotropy of the Earth's mantle: From single crystal to polycrystal, in Earth's Deep Interior: Mineral Physics and Tomography From the Atomic to the Global Scale, edited by S. I. Karato, pp. 237–264, AGU, Washington, D. C..

Marone, F., and B. Romano (2007), The depth distribution of azimuthal anisotropy in the continental upper mantle, Nature, 447, 198–201.

Maupin, V., E. J. Garnero, T. Lay, and M. J. Fouch (2005), Azimuthal anisotropy in the D layer beneath the Caribbean, J. Geophys. Res., 110, B08301, doi:10.1029/2004JB003506.

McMillan, J., A. P. Dickin, and D. Haag (2000), Evolution of magma source regions in the Rio Grande rift, southern New Mexico, Geol. Soc. Am. Bull., 112, 1582–1593.

Morgan, P., W. R. Seager, and M. P. Golombek (1986), Cenozoic thermal mechanical and tectonic evolution of the Rio Grande rift, J. Geophys. Res., 91, 6262–6276.

Mosher, S. (1998), Tectonic evolution of the southern Laurentian Grenville orogenies belt, Geol. Soc. Am. Bull., 110, 1357–1375.

Refayee, H. A., B. B. Yang, K. H. Liu, and S. S. Gao (2013), Mantle flow and lithosphere-asthenosphere coupling beneath the southwestern edge of the North American craton: Constrains from shear-wave splitting measurements, Earth Planet. Sci. Lett., doi:10.1016/j.epsl.2013.01.031i.

Sandvol, E., and J. Ni (1994), Mapping seismic azimuthal anisotropy in the United States from LRSM short period data, Eos Trans. AGU, 75, 481.

Satsukawa, T., K. Michibayashi, E. Y. Anthony, R. J. Stern, S. S. Gao, and K. H. Liu (2011), Seismic anisotropy of the uppermost mantle beneath the Rio Grande rift: Evidence from Kilbourne Hole peridotite xenoliths, New Mexico, Earth Planet. Sci. Lett., 311, 172–181.

Savage, M. K. (1999), Seismic anisotropy and mantle deformation: What have we learned from shear wave splitting?, Rev. Geophys., 37, 65–106.

Savage, M. K., A. F. Sheehan, and A. Lerner-Lam (1996), Shear wave splitting across the Rocky Mountain Front, Geophys. Res. Lett., 23, 2267–2270.

Silver, P. G. (1996), Seismic anisotropy beneath the continents: Probing the depths of geology, Annu. Rev. Earth Planet. Sci., 24, 385–432.

Silver, P. G., and W. W. Chan (1991), Shear wave splitting and subcontinental mantle deformation, J. Geophys. Res., 96, 16,429–16,454.

Silver, P. G., and W. E. Holt (2002), The mantle flow field beneath western North America, Science, 295, 1054–1057, doi:10.1126/science. 1066878.

Silver, P. G., and S. Kaneshima (1993), Constraints on mantle anisotropy beneath Precambrian North America from a transportable teleseismic experiment, Geophys. Res. Lett., 20, 1127–1130.

Silver, P. G., and M. Savage (1994), The interpretation of shear-wave splitting parameters in the presence of two anisotropic layers, Geophys. J. Int., 119, 949–963, doi:10.1111/j.1365-246X.1994.tb04027.x.

Tommasi, A., A. Vauchez, and R. Russo (1996), Seismic anisotropy in oceanic basins: Resistive drag of the sublithospheric mantle?, Geophys. Res. Lett., 23, 2991–2994.

van der Lee, S., and A. Frederiksen (2005), Surface wave tomography applied to the North American upper mantle, in Seismic Data Analysis and Imaging With Global and Local Arrays, vol. 157, edited by G. Nolet and A. Levander, pp. 67–80, Amer. Geophys. Union Monograph, Washington, D. C.

van der Lee, S., and G. Nolet (1997), Upper mantle S velocity structure of North America, J. Geophys. Res., 102, 22,815–22,838, doi:10.1029/97JB01168.

Vecsey, L., J. Plomerova, and V. Babuska (2008). Shear-wave splitting measurements-Problems and solutions, Tectonophys. 462, 178-196.

Vinnik, L. P., L. J. Makeyeva, A. Milev, and A. Y. Usenko (1992), Global patterns of azimuthal anisotropy and deformations in the continental mantle, Geophys. J. Int., 111, 433–447.

Whitmeyer, S. J., and K. E. Karlstrom (2007), Tectonic model for the Proterozoic growth of North America, Geosphere, 3, 220–259.

Wilson, D., R. Aster, W. West, J. Ni, S. Grand, W. Gao, W. S. Baldridge, and P. Patel (2005), Lithospheric structure of the Rio Grande rift, Nature, 433, 851–855.

Wolfe, C. J., and P. G. Silver (1998). Seismic anisotropy of oceanic upper mantle: Shear-wave splitting methodologies and observations, J. Geophys. Res. 103, 749-771.

Wustefeld, A., G. H. R. Bokelmann, G. Barruol, and J. P. Montagner (2009). Identifying global seismic anisotropy patterns by correlating shear-wave splitting and surface waves data, Phys. Earth Planet. Int. 176(3-4), 198-212.

Yang, B. B., S. S. Gao, K. H. Liu, A. A. Elsheikh, A. A. Lemnifi, H. A. Refayee, and Y. Yu (2014). Seismic anisotropy and mantle flow beneath the northern Great Plains of North America, J. Geophys. Res. 119, doi:10.1002/2013JB010561.

Yuan, H., and B. Romanowicz (2010), Lithospheric layering in the North American craton, Nature, 466, 1063–1069.

Zhao, G. C., P. A. Cawood, S. A. Wilde, and M. Sun (2002), Review of global 2.1-1.8 Ga orogens: Implications for a pre-Rodinia supercontinent, Earth Sci. Rev., 59, 125–162.

4. VITA

Bin Yang was born in the city of Dongying, China. He received his Bachelor's and Master's degree in Applied Geophysics from China University of Petroleum (East China). He joined the PhD program in Geology and Geophysics at Missouri University of Science and Technology (Missouri S&T) in August, 2011.

During his graduate studies, he was actively involved in various academic activities. He was an active member in the American Geophysical Union (AGU), Society of Exploration Geophysics (SEG), American Association of Petroleum Geologist (AAPG), and Geologic Society of America (GSA). He served as the treasure and vice president of the Missouri S&T chapter in 2014, 2015 and 2016. He presented his research works at the AGU annual meeting in 2013, 2014, 2015 and 2016. His research focuses on the seismic anisotropy and mantle dynamics beneath the United States. He was one of the five Missouri S&T team members to participate in the AAPG Imperial Barrel Award Program in 2013 and awarded as honorable mention. He also got several scholarships from the SEG foundation for the support of his PhD study.

He received his Doctor of Philosophy degree in Geology and Geophysics from Missouri University of Science and Technology in July, 2016.